Developing models to study the mechanisms of weakness and myotonia in Periodic Paralysis

By Neta Bat-El Amior

This thesis is submitted for consideration as a degree of Doctor of Philosophy from the department of Cell and Developmental Biology and the Institute of Neurology at University College London

May 2017

I, Neta Bat-El Amior confirm that the work presented in this thesis is my own. Where information has been derived from other sources, I confirm that this has been indicated in the thesis.

ACKNOWLEDGMENTS

First and foremost I would like to thank my supervisors. I would like to thank Professor Michael Duchen for supporting me throughout my project, for teaching me the art of confocal microscopy and for encouraging me to think critically about my work. I would also like to thank my second supervisor Professor Mike Hanna for his optimism and for giving me the opportunity to meet patients and to work with patient skin biopsies.

I'd like to thank all of the members of the Duchen lab for making the lab a wonderful place to work in. In particular I'd like to thank Laura Osellame for introducing me to benchwork, Jose Vicencio for teaching me about flow cytometry, Thomas Blacker for explaining Fourier transform to me and Sam Ranasinghe for confocal support and for help with the FLIPR investigations. I'd like to thank several other members of the UCL scientific community – James Dick for teaching me *in vivo* techniques, James Burge for teaching me single fibre isolation, Professor Alasdair Gibb for teaching me whole cell patch clamping and Michael Thor for help with sharp electrode patch clamping.

ABSTRACT

Periodic paralysis (PP) is a disorder characterised by episodic attacks of paralysis, caused by mutations of skeletal muscle voltage gated ion channels. Although episodes eventually subside, patients develop progressive muscle weakness and frequently, myopathy. The relationship between this progression and the associated mutations is not understood. I propose that the longer term defect might result from disordered calcium signalling secondary to altered excitability, and its impact on mitochondrial function. I sought models where these aspects of muscle signalling could be studied. These were:

A genetic model derived from patients: patient derived fibroblasts were virally transduced with MyoD to generate myoblasts, which were differentiated into myotubes with patient specific gene mutations.

A pharmacological model: generated by treating neonatal rat myotube cultures with barium (an inhibitor of potassium channels) and low extracellular potassium to simulate attacks of PP. Treated cultures displayed more frequent spontaneous calcium fluctuations. Mitochondrial membrane potential was not affected by the treatment, but expression of TFAM (mitochondrial transcription factor A; a regulator of mitochondrial transcription and biogenesis) was upregulated, suggesting activation of retrograde signalling pathways.

A mouse model: collaborators at MRC Harwell generated mice carrying a mutation (c.1744A>G; p.Ile582Val) equivalent to a novel point mutation in *SCN4A,* one of the ion channel genes associated with PP. Measurements *in vivo* established that affected mice show muscle weakness and delayed fatigue during tetanic responses. Calcium handling and mitochondrial function were analysed in single isolated myofibres. Calcium handling was not affected, however mitochondrial membrane potential was reduced in fibres from the PP mice and distribution was also affected, with fewer intermyofibrillar mitochondria, indicating altered mitochondrial bioenergetics.

Thus I describe several approaches to investigate mechanisms that cause progressive weakness and myopathy in PP, and assess the relative merits of each approach. Furthermore, results suggest that a shift toward a more oxidative phenotype is taking place.

TABLE OF CONTENTS

LIST OF FIGURES, TABLES AND EQUATIONS

LIST OF ABREVIATIONS

AMPK – AMP-activated protein kinase

AraC – cytosine beta-D-arabinofuramoside

ATP – adenosine triphosphate

AV – adenovirus

BSA – bovine serum albumin

CaV1.1 – Skeletal muscle voltage gated calcium channel

CCD – central core disease

CEE – chick embryo extract

Dgn – Draggen mouse model as described

DMEM – Dulbecco's modified eagle medium

DMSO – dimethyl sulfoxide

DNA – deoxyribonucleic acid

EDL – extensor digitorum longus

EGF – epidermal growth factor

EPP – end plate potential

ETC – electron transport chain

ETS – electron transport system

FACS – fluorescence activated cell sorting

FBS – fetal bovine serum

FCCP – carbonyl cyanide 4-(trifluoromethoxy)phenylhydrazone

FDB – flexor digitorum brevis

FGF – fibroblast growth factor

FLIPR – fluorescence imagine plate reader

FSL – forward scattered light

GAPDH - glyceraldehyde 3-phosphate dehydrogenase

HBS – Hank’s balanced salt solution

HCX – proton calcium exchanger

HGF – hepatocyte growth factor

HS – horse serum

HyperPP - hyperkalaemic periodic paralysis

HypoPP – hypokalaemic periodic paralysis

IGF – insulin like growth factor

IMDM – Iscove's modified Dulbecco's media

IP_3R – inositol triphosphate receptor

IRK2.1 – inwardly rectifying potassium channel

LV - lentivirus

MCU – mitochondrial calcium uniporter

MEF-2 – myocyte enhancer factor-2

MH – malignant hyperthermia

MPTP – mitochondrial permeability transition pore

Mrf4 – myogenic regulatory factor 4

mtDNA – mitochondrial DNA

Myf5 – myogenic determination factor 5

MyoD – myogenic differentiation factor D

NaV1.4 – skeletal muscle voltage gated sodium channels

NCX – sodium calcium exchanger

NRF-1 – nuclear restriction factor-1

NRF-2 – nuclear restriction factor-2

Pax3 – paired box protein 3

P/S – penicillin/streptomycin

PBS – phosphate buffered saline

PGC-1α – peroxisome proliferator-activated receptor gamma coactivator 1-alpha

PGC-1β – peroxisome proliferator-activated receptor gamma coactivator 1-beta

PI – propidium iodide

PMSF – phenylmethylsulfonyl fluoride, a protease inhibitor

PMT – photomultiplier tube

PP – periodic paralysis

PVDF (Immobilon-P Membrane**,** IPVH00010 EMD MILLIPORE)

RIPA lysis and extraction buffer (Thermo Scientific, 89900)

ROS – reactive oxygen species

RyR – ryanodine receptor

SERCA – sarcoplasmic endoplasmic reticulum calcium ATPase

SR – sarcoplasmic reticulum

SSL – side scattered light

SupM – supplemented media

TA – tibialis anterior

TFAM – mitochondrial transcription factor A

TGF-β – transformin growth factor - beta

TMRM – tetramethylrhodamine

T-tubule – transverse tubule

VDAC – voltage dependant anion channel

WT – wild type

1. INTRODUCTION

Muscle disease is a major cause of disability. There are a number of hereditary muscle diseases where a genetic cause has been identified but the pathophysiological mechanisms that underlie the progression of the disease are not clear. This limits the development of suitable treatments and disease management strategies and such development may be facilitated by the use of appropriate experimental models. Periodic Paralysis (PP) is a genetic muscle disease resulting from mutations of the skeletal muscle cation channels. Patient's quality of life is severely impaired by episodic attacks of paralysis which can last from minutes to days, while intermittent muscle strength is maintained. Attacks of paralysis typically present in the first decade of life and reduce in frequency after the fifth when progressive weakness and in some cases also myopathy begin to develop. A suitable model is sought for investigating the pathophysiology leading to weakness and myopathy in PP.

1.1 PERIODIC PARALYSIS

1.1.1 The periodic paralysis mutations and classification

Periodic Paralysis (PP) results from mutations in skeletal muscle voltage gated ion channels. Disorders originating in ion channel dysfunction are known as channelopathies and result from dysfunction of ion channels either on the membranes of cells or organelles, ranging from congenital to autoimmune disorders. PP is an autosomal dominant congenital disorder resulting from mutations in the voltage gated sodium channels (NaV1.4; Rojas et al., 1991), voltage gated calcium channels (CaV1.1; Jurkat-Rott et al., 1994) or voltage gated potassium channels.

There are several different subcategories of PP which display distinct characteristics. Mutations in the potassium channel are associated with Anderson Tawil Syndrome and those in CaV1.1 channels with HypoPP. Mutations in NaV1.1 channels can be associated with paramyotonia congenita (PMC), HyperPP or HypoPP, depending on which residues of the channel protein have been affected.

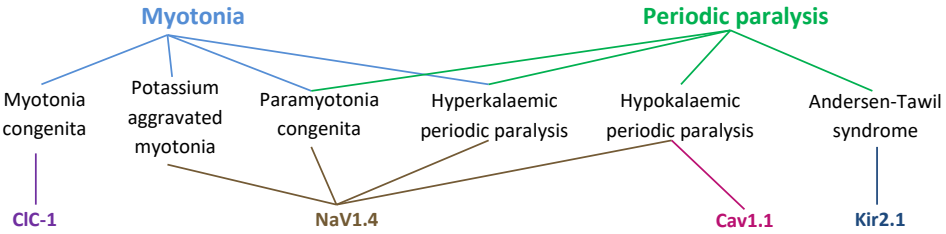

Figure 1: Clinical spectrum of periodic paralysis and myotonia. *Clinical spectrum of PP and myotonia indicating which channels are associated with each condition, adapted from a review by Cannon (Cannon, 2006).*

As the figure above demonstrates, a range of conditions come under the general definition of PP. In this thesis I focus on HyperPP and HypoPP, nevertheless much of the methodology should be applicable to paramyotonia congenita and Anderson Tawil syndrome, and likewise to other muscle diseases.

1.1.2 HyperPP and HypoPP mutations and classification

HyperPP mutations occur at different locations of the NaV1.4 alpha subunit (Rojas et al, 1991; Ptacek et al., 1991), whereas most known HypoPP mutations occur at a highly conserved region of the S4 segment of the alpha subunit of either NaV1.4 or CaV1.1 channels (Grosson et al, 1996; Bulman et al, 1999). This is despite their distinct roles in cell signalling. NaV1.4 allows the passage of sodium ions into excitable cells, and thereby allows for the propagation of action potentials. CaV1.1 associates with RyRs to facilitate the release of calcium from intracellular stores during excitation contraction coupling as demonstrated in figure 6. Both NaV1.4 and CaV1.1 feature positively charged arginine residues in the conserved S4 segment of the alpha subunit (see figure 2), which encodes the voltage sensor of the channel. Loss of positive charge in the voltage sensor leads to formation of an aberrant proton pore in the channel as described in section 1.1.4 (Matthews et al, 2009).

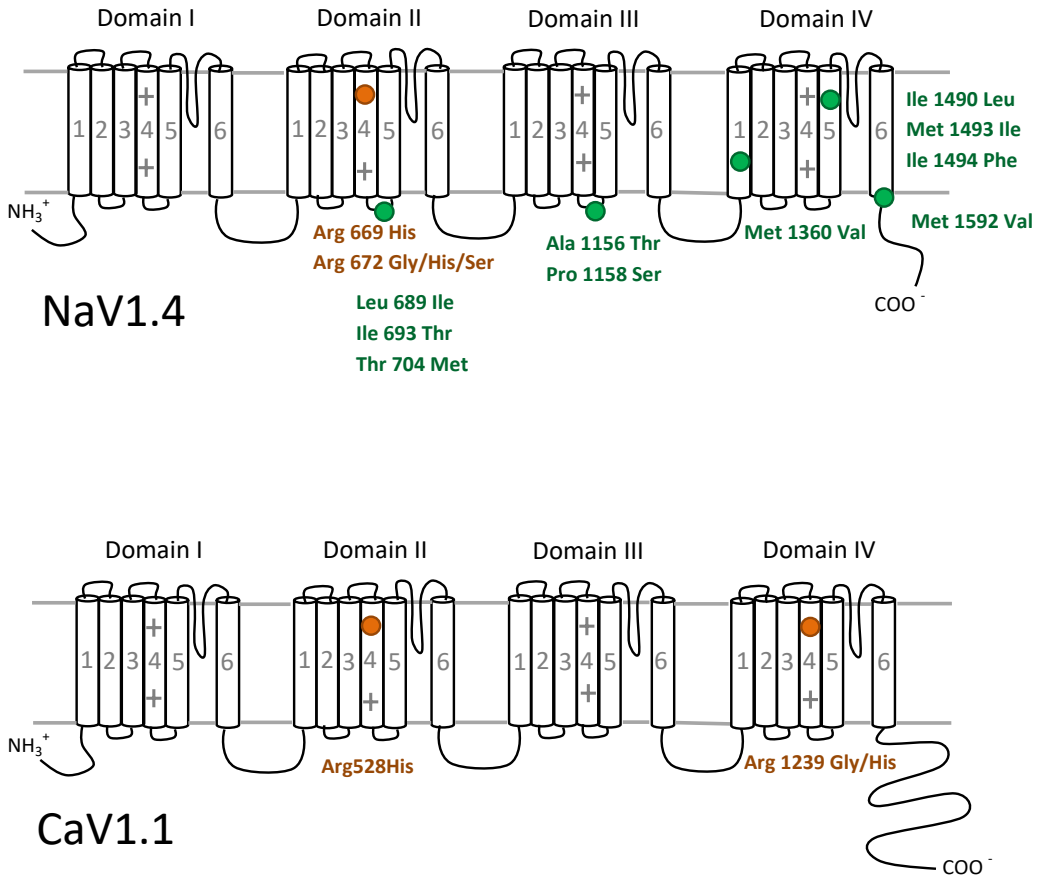

Figure 2: The periodic paralysis mutations in NaV1.4 and CaV1.1. *Diagram showing the location of PP mutations in the alpha subunit of NaV1.4 and CaV1.1 (Cannon, 2006; Sternberg et al, 2001). Orange circles indicate the locations of HypoPP mutations, and green circles indicate the locations of HyperPP mutations.*

HyperPP and HypoPP are subcategorised according to the level of serum potassium present during attacks. In cases where attacks occur during periods of high serum potassium, the disease is referred to as HyperPP (Gamstorp 1956; Gamstorp et al., 1957), whereas individuals with HypoPP typically experience attacks when their serum potassium levels are low (Aitken et al., 1937; Talbott, 1941; McArdle, 1956; Conn & Streeten, 1960).

1.1.3 The direct effects of HyperPP mutations

The HyperPP mutations are considered “gain-of-function” mutations, as they increase the probability of the sodium channel being open. This subsequently promotes depolarisation. In HyperPP, depolarisation can result from defective NaV1.4 slow inactivation (Bendahhou et al, 2002; Cannon et al., 1991; Silva & Goldstein, 2013) or from activation at more hyperpolarised conditions (Cummins et al., 1993). A study on a HyperPP patient with an L689I point mutation in domain II of the S4-S5 linker, for example, indicates that slow inactivation is associated with immobilisation of the voltage sensor in domains I, II and III (Silva & Goldstein, 2013). This study shows that the onset of slow inactivation is most influenced by immobilisation of domains I and II, whereas domain III is more associated with recovery from slow inactivation (Silva & Goldstein, 2013).

Overall, such gain-of-function alterations in sodium channel gating mode are promoted by elevated extracellular potassium levels. Increases in extracellular potassium levels thus promote depolarisation and are associated with attacks of paralysis in HyperPP (Cannon et al, 1999).

1.1.4 The direct effects of HypoPP mutations

Excitable cells have a bi-stable relationship with extracellular potassium concentration, whereby reducing potassium levels leads to two different ranges of V-rest values. One is linked to the potassium equilibrium potential and the other occurs between -50 and -60 millivolts (see figure 3b below). Consequently, although reducing extracellular potassium initially hyperpolarises cells, further reduction of the potassium concentration can result in depolarisation. This second depolarisation is thus considered to be paradoxical. Mutations associated with HypoPP result in the formation of an aberrant cation pore distinct from the voltage sensor areas of CaV1.1 and NaV1.4 channels (Tombola et al., 2005). The threshold for paradoxical depolarisation is potentiated by this aberrant gating pore (Struyk et al, 2007). In unaffected cells a reduction in extracellular potassium concentration only promotes depolarisation if it reaches below 2mM and not under normal physiological conditions. The addition of the proton current, however, allows for the second stable condition to occur at more physiological potassium concentrations. Consequently small

drops in potassium concentration can lead to paradoxical depolarisation and thereby to attacks of paralysis.

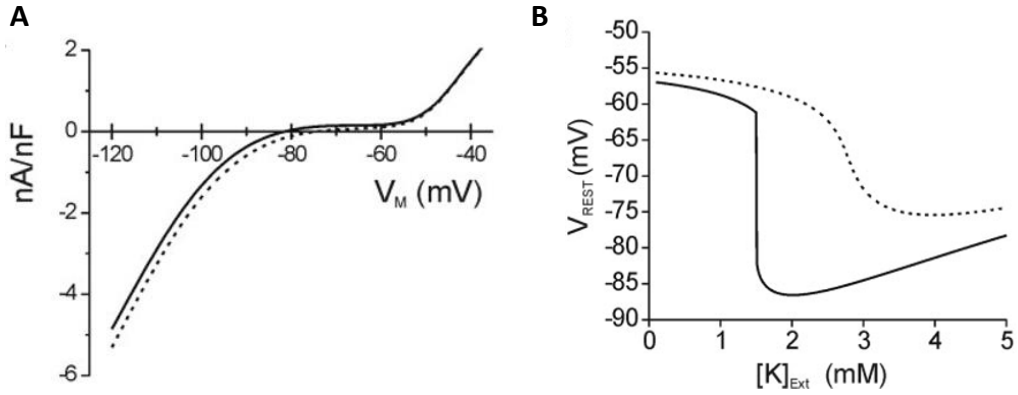

Figure 3: The cation leak in HypoPP. *(**A**) The I-V relationship of mutant (dotted line) compared to control (solid line) channels. From Struyk (Struyk et al, 2007) where a computer simulation of responses is used to predict the consequences of the cation leak in HypoPP. (**B**) The potassium dependence of V-rest in cells with a HypoPP mutation (dotted line) compared to controls (solid line). This figure demonstrates that small changes in the current voltage relationship can lead to large effects on the depolarisation threshold. From Struyk (Struyk et al, 2007) where a computer simulation of responses is used to predict the consequences of the cation leak in HypoPP.*

1.2 MUSCLE STRUCTURE AND PHYSIOLOGY

1.2.1 Muscle structure

Muscles are composed of long tubular multinucleated cells called muscle fibres which are formed by fusion of myoblasts. The fibres have a diameter of 50-100µm. During differentiation distinct stages of recognition and adhesion allow for the myoblasts to align whereupon they withdraw from the cell cycle and fuse to form the muscle fibres (Knudsen & Horwitz, 1978; Knudsen et al, 1989). Individual muscle fibres are bound by connective tissue called endomysium and the resultant groups of fibres (muscle fascicules) are further bound together by connective tissue called perimysium. A final coat of connective tissue called the epimysium binds the whole muscle together. Fibroblasts that lie between the muscle fibres are responsible for secreting these connective tissues.

Muscle fibres are composed of long structures called myofibrils which align along the fibre, each approximately 1µm in diameter. Many repeating units called sarcomeres attach end to end to make up these myofibrils. The characteristic striated appearance of skeletal muscle (see for example figure 35, page 114) results from alignment of these sarcomeres in adjacent myofibrils, as each sarcomere contains distinct bands of proteins. These bands are referred to as A-bands and I-bands. I-bands are composed of thin filaments in which actin protein is assembled along with troponin and tropomyosin. Within each I-band a line can be seen called a Z-line, adjacent Z-lines are held together by desmin and the region between two such Z-lines is defined as a single sarcomere. A-bands are composed of thick filaments in which myosin proteins are assembled. The myosin proteins are the most abundant proteins in muscle. Each myosin protein contains two myosin heavy chains (MHC) with a tail region and globular heads that are each associated with two light chains. A hinge region at the junction between the tail region and the globular myosin heads allows for thick filaments to shift relative to thin filaments and thereby facilitates muscle contraction (Hynes *et al,* 1987; Spudich, 2001).

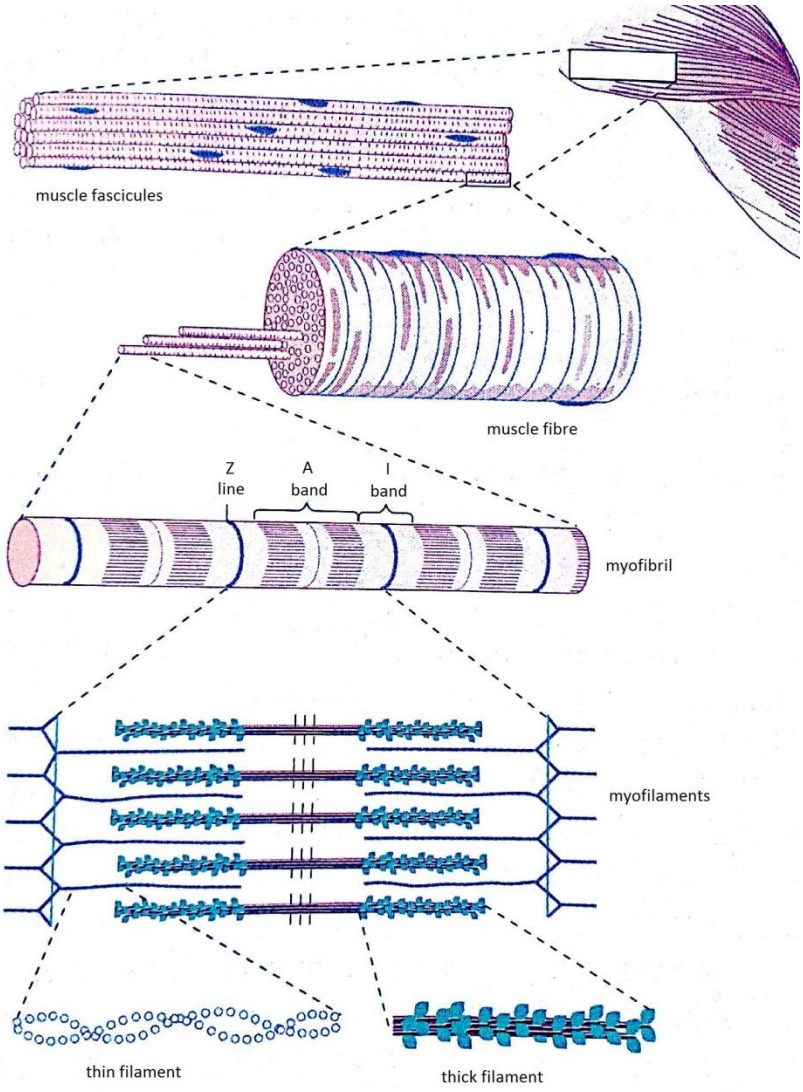

Figure 4: Muscle structure. *The organisation of skeletal muscle at various degrees of magnification, adapted from figure 7.2 in Pocock and Richards, 2006. The figure includes a whole muscle, a muscle fascicule, a muscle fibre, a myofibril and the organisation of thin and thick filaments in myofilaments.*

Each muscle fibre is bounded with a sarcolemma which has small indentations along its surface allowing it to stretch and contract, as well as deeper narrow indentations called transverse (T)-tubules which associate with the sarcoplasmic reticulum to form a complex known as a triad junction. CaV1.1 channels can be found along these T-tubules, where they sense voltage changes resulting from end-plate potentials. Within the triad junction, Cav1.1 channels on the T-tubules associate with Ryanodine receptors (RyR) on the sarcoplasmic reticulum. RyR are intracellular calcium conducting receptors. Activation of CaV1.1 leads to allosteric changes in RyRs which then facilitate calcium release from intracellular stores.

Many mitochondria lie beneath the sarcolemma along with the fibre nuclei, providing the muscle with ATP and proteins.

1.2.2 Ionic influences on the resting membrane potential of a cell

Cell function is largely influenced by the flow of sodium, potassium, calcium and chloride ions across the cell membrane. The flow of each ion across the plasma membrane is governed by its electrochemical gradient and the potential at which ion flow across the membrane is balanced, is called the equilibrium potential. The equilibrium potential of each ion can be predicted using the Nernst equation.

$$E = \frac{RT}{F} ln \frac{[C]_o}{[C]_i}$$

Equation 1: The Nernst equation. *The Nernst equation, where E is the equilibrium potential, R, T and F are physical constants (gas, absolute temperature and Faraday constants respectively). Ln is the natural logarithm (log_e) and $[C]_o$ and $[C]_i$ are the extracellular and intracellular concentrations of the ion.*

However the equilibrium potentials of each of the ions also influence each other, and thus the resting membrane potential of the cell. The resting membrane potential of a muscle cell typically lies close to the potassium equilibrium potential, but is also influenced by sodium and chloride ions. The potassium equilibrium potential provides a measure of the net flow of potassium ions into or out of a cell across the plasma membrane. The potassium equilibrium potential is governed by the high concentration of potassium inside the cell (approximately 140mM) relative to the outside (approximately 5mM) as well as by the negative membrane potential inside skeletal muscle relative to outside it (approximately -90mV). Potassium ions leave the cell down their concentration gradient, and enter the cell down their electrical gradient as each potassium ion carries a single positive change.
The relationship between potassium, sodium and chloride ions in a cell can be described by the Goldman equation, a modified version of the Nernst equation. The Goldman equation accounts for influences of multiple ion channels on the cell and predicts the membrane potential.

$$E = \frac{RT}{F} ln \frac{P_{Na}[Na^+]_o + P_K[K^+]_o + P_{Cl}[Cl^-]_i}{P_{Na}[Na^+]_i + P_K[K^+]_i + P_{Cl}[Cl^-]_o}$$

Equation 2: The Goldman equation. *The Goldman equation, where E is the membrane potential, R, T and F are physical constants (gas, absolute temperature and Faraday constants respectively). Ln is the natural logarithm (log_e). P_{Na}, P_k and P_{Cl} are permeability coefficients of the membrane potential to sodium, potassium and chloride ions. $[Na^+]_o$ and $[Na^+]_i$ are extracellular and intracellular sodium concentrations, $[K^+]_o$ and $[K^+]_i$ are the same for potassium concentrations and $[Cl^+]_o$ and $[Cl^+]_i$ for chloride ion concentrations.*

1.2.3 Excitation-contraction coupling

The direct effects of PP mutations have been shown to disrupt excitation-contraction coupling. This is the process by which excitation of a muscle fibre leads to its contraction (Sandow, 1952). Action potentials travel along motoneuron axons towards muscle fibres, leading to the depolarisation of muscle cells. Muscle cell depolarisation involves the opening and closing of voltage gated sodium and potassium ions, as demonstrated in figure 5 below. Within skeletal muscle these neurons branch out to supply single muscle fibres, the area where the muscle fibre and the neuron interact is called an end plate, and the space between them is the synaptic cleft.

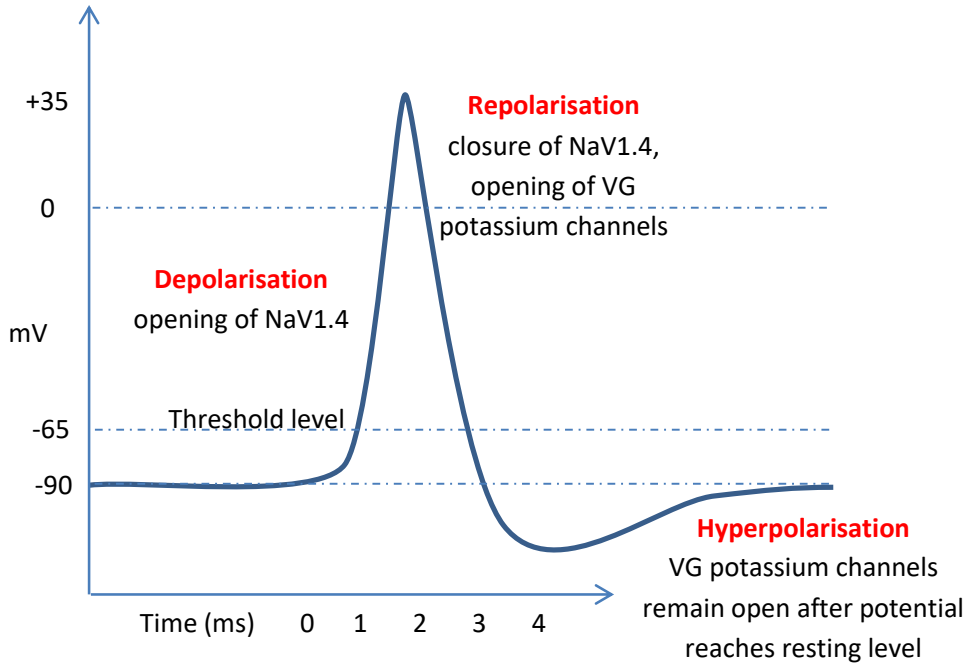

Figure 5: Action potential dynamics. *Upon depolarisation of a muscle cell, sodium channels open allowing the inward passage of positive sodium ions. This depolarises the cell from approximately -90mV to approximately +35mV. Closure of the sodium channels and opening of voltage gated potassium ion channels results in efflux of positive potassium ions, leading to recovery of the depolarised state. The potassium channels remain open and the membrane potential briefly becomes hyperpolarised before returning to the resting membrane potential.*

At rest the sarcolemma has a voltage across it called the resting membrane potential. This is determined by concentration gradients of ions across the membrane and by membrane permeability to the ions through ion channels. Concentration gradients for sodium and potassium are established by the sodium-potassium ATPase. The membrane is more permeable to potassium than to sodium and the selective passage of potassium ions across the membrane drives the resting membrane potential toward the potassium equilibrium potential. Chloride ion permeability also contributes to the skeletal muscle resting membrane potential. Muscle contraction can lead to leakage of potassium ions and repeated stimulation can dissipate the potassium concentration gradient. The chloride permeability helps to maintain muscle activity during repeated stimulation (Hopkins, 2006). Arrival of an action potential at the axon terminal causes exocytosis of acetylcholine from the neuron end plate. The acetylcholine binds to acetylcholine receptors on the

postsynaptic muscle fibre membrane, causing cation influx into the cell. This response is graded, whereby release of a single vesicle containing acetylcholine will produce a miniature end plate potential, and the release of many vesicles will produce an end plate potential (EPP). If an EPP depolarises the postsynaptic membrane to a threshold level, voltage gated sodium channels on the membrane open generating a regenerative sodium current across the fibre membrane, and causing a rapid membrane depolarisation and the initiation of an action potential. The voltage gated potassium channels open more slowly, allowing for the membrane potential to peak before the positive ions begin to leave the cell down their electrochemical gradient. Following the action potential, the voltage gated ion channels become inactivated. The sodium channels become inactivated faster, such that for a short period there is a net efflux of potassium ions which leads to hyperpolarisation of the membrane, toward the potassium ion resting potential of approximately -100mV.

During an action potential, the postsynaptic membrane is not responsive to further stimulation; a phase known as the absolute refractory period. During hyperpolarisation on the other hand, further action potentials can be induced, albeit with a greater level of activation. This phase is thus known as the relative refractory period. Following an action potential acetylcholine is removed from the synaptic cleft by the enzyme acetylcholine esterase to avoid repeated initiation of EPPs.

Chloride ions also contribute to the regulation of muscle cell function; increased permeability to the ions leads to influx down their electrochemical gradient. This hyperpolarises the cell and makes depolarisation less likely to occur.

The muscle cell membrane has indentations known as T-tubules which allow for depolarisation to spread along the membrane toward the centre of the cell. The T-tubules contain many CaV1.1s which come into direct contact with RyR on the sarcoplasmic reticulum (SR). Calcium ion uptake into the SR is mediated by sarcoplasmic/endoplasmic reticulum ATPases (SERCAs). Calcium is stored in the SR where it binds calcium binding proteins, primarily calsequestrin (Royer & Ríos, 2009). This lowers the free luminal calcium concentration and facilitates further calcium uptake through SERCAs. Calsequestrin binds with high capacity but low affinity; it thus enables the storage of large amounts of calcium as well as rapid calcium release from the SR upon stimulation. Calsequestrin is also involved

in regulating calcium release from the SR by sensing the SR calcium concentration (Györke et al, 2009). This calcium is released from the SR in response to membrane depolarisation which activates CaV1.1. Conformational changes in these channels promote the allosteric activation of RyR which open to mediate calcium release from the SR to the sarcoplasm (Proenza et al, 2002). The calcium binds to a calcium sensitive contractile protein known as troponin, which in turn initiates a conformational change in tropomyosin. This conformational change exposes myosin binding sites on actin, allowing myosin proteins in the fibres to interact with actin in a manner described by the sliding-filament theory.

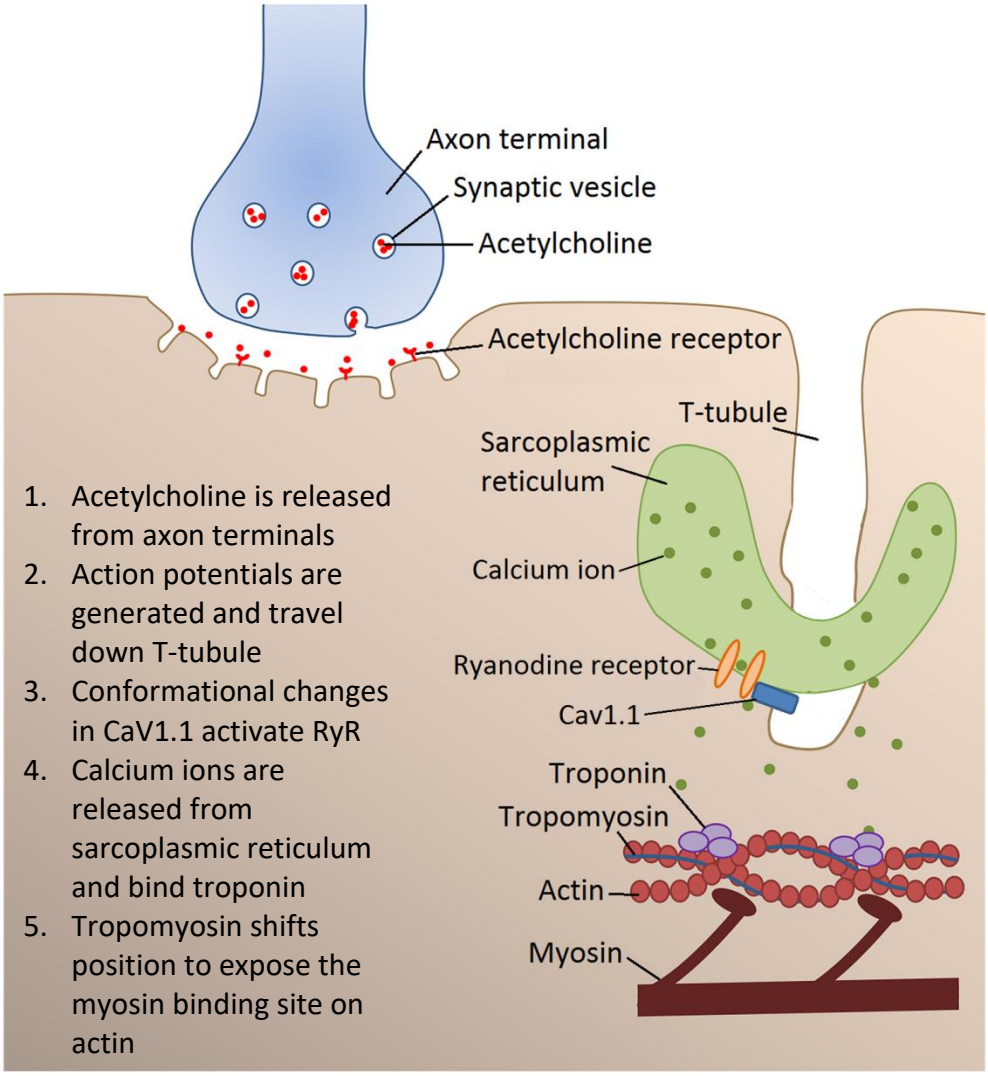

Figure 6: The sliding filament theory. *The sliding filament theory involves acetylcholine release from the axon terminal, the generation and propagation of action potentials down T-tubules, the release of calcium ions into the cytoplasm and the binding of these ions to troponin leading to exposure of myosin.*

The sliding filament theory describes how movement of actin filaments relative to myosin filaments can generate muscle tension (Figure 6; Huxley & Niedergerke, 1954; Huxley & Hanson 1954). Myosin moves forward to bind actin forming a cross bridge between the thick and thin filaments. The hinge region of the myosin then contracts making the myosin head shift. This movement of the myosin head is referred to as a power stroke. During a power stroke the thick filament stays in place and pulls the thin filament along approximately 10 nanometres. ATP hydrolysis to ADP and phosphate then provides energy

for myosin to release actin and re-establish its original conformation, ready to bind to actin again and produce a further power stroke.

Following muscle contraction, calcium dissociates from Troponin. ADP is released and a further ATP molecule attaches allowing for actin and myosin to dissociate and resume their original positions. Calcium is pumped back into the SR by the sarco/endoplasmic reticulum calcium-ATPase (SERCA), ready for the next action potential to arrive. Sodium-calcium exchangers (NCX) are also involved in the removal of calcium from the sarcoplasm following an action potential. NCXs can be found on the plasma membrane, mitochondria and SR of excitable cells, and extrude one calcium ion in exchange for three sodium ions. As with calsequestrin, it has both a low affinity and a high capacity, exchanging the ions when sarcoplasmic calcium or extracellular sodium concentrations are sufficiently elevated, such as after an action potential (Blaustein & Lederer, 1999).

1.3 ALTERATIONS OF SKELETAL MUSCLE IN DISEASE AND WITH AGING

1.3.1 Symptoms and progression of periodic paralysis

Patients of PP experience periods of intense muscle weakness which can last for hours to days. Ke et al showed that there is greater penetrance of hypokalaemic periodic paralysis (HyperPP) in males (100%) than in females (less than 30%), and that attack frequency is greater in males than females (2013). Such an association has not been found in HyperPP (Neki et al, 2013). Attacks of paralysis occur sporadically, but certain factors including exercise and potassium ingestion are known to influence their occurrence (Hoskins et al., 1975). Whereas in HyperPP attacks begin in early childhood, HypoPP attacks may begin at any age, but typically in the second decade of life (Harirchian et al., 2003). Patients of both HyperPP and HypoPP experience a reduction in attack frequency around middle age. Although initially patients of both HyperPP and HypoPP are unaffected between attacks, this second phase of disease progression is typically accompanied by the development of muscle weakness (Walter et al., 1990). In patients of HyperPP this weakness is frequently coupled with myotonia, whereas in HypoPP presentation with myotonia is rare (see figure 1 for a schematic of the clinical overlap between conditions of myotonia and PP). Myotonia is the inability to relax voluntary muscle after strong exertion. The levels of weakness and

myotonia vary and may be unrelated to attack frequency or severity (Links, 1990; Buruma & Bots, 1978).

	HypoPP	**HyperPP**
Prevalence in England	0.13/100, 000	0.17/100, 000
Age at onset	1st or 2nd decade	1st decade
Reduction in attack frequency	From ~ age 35	From ~ age 50
Duration of attacks	Hours to days	Hours
Usual triggers	Rest after exercise (~67%), rest after large carbohydrate meal (~45%), cold (~24%), stress (~12%), salt (~11%)	Cold (~76%), rest after exercise (~67%), stress or fatigue (~47%), K-rich foods (~35%), pregnancy (~28% females)
Ictal K	↓	↑ or normal
Interictal muscle strength	Normal	Normal, mild myotonia in face and hands
Response to potassium	Improves weakness	Triggers weakness
Mutations	*CACNA1S* (~60%), SCN4A (~20%)	*SCN4A* (~50%)

Table 1. Clinical features of HyperPP and HypoPP*. Adapted from Venance et al (2006) with additional information on prevalence (Horga et al, 2013) and on triggers (Weber et al, 2016) (Charles et al, 2013)*

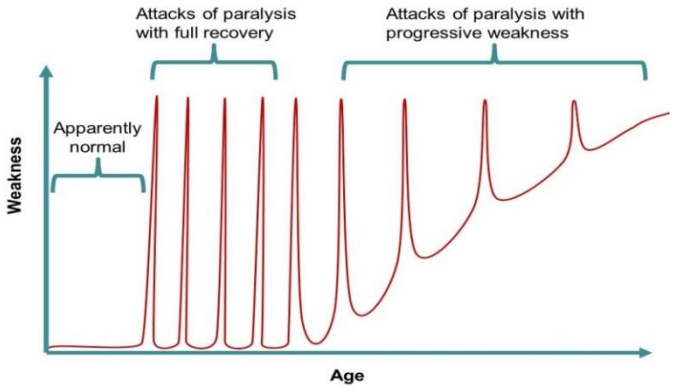

Figure 7: Progression of Periodic Paralysis. Patients of PP initially do not experience attacks of paralysis and weakness. During childhood or adolescence they begin experiencing sporadic attacks of paralysis with full recovery in between. Later in life these sporadic attacks reduce in frequency and patients develop progressive muscle weakness.

1.3.2 Histological changes in periodic paralysis

Histological changes that have been observed in muscle from patients of HypoPP include the formation of tubular aggregates and vacuoles and the centralisation of nuclei (Links et al, 1990). Central nuclei and the formation of tubular aggregates and vacuoles have also been reported to in HyperPP (Bradley et al, 1990).

1.3.3 Sarcopenia and periodic paralysis

Sarcopenia refers to the decline in skeletal muscle mass, strength and function associated with normal muscle ageing. As with PP, a reduction in type II fibres is a key feature of sarcopenia, with greater levels of atrophy of type IIb than of type IIa (Narici & Maffulli, 2010). This and several other common features such as the development of tubular aggregates (Chevessier et al, 2004) in both sarcopenia and PP have led to the speculation that the PP mutations may accelerate the development of a sarcopenia phenotype. As such it may be instructive to relate progressive features of PP to those of sarcopenia and to employ similar treatment strategies. Regular mild exercise, for example, can serve as a preventative measure in both sarcopenia and PP.

1.3.4 Fibre type switching and oxygen consumption

Muscle is composed of muscle fibres, as described in section 1.2.1. Myosin is the most abundant protein in these fibres, and variation in myosin contractile force means that

different isoforms of the myosin protein are associated with different muscle types (Bottinelli & Reggiani, 2000). Fibres within skeletal muscle are broadly categorised as slow twitch (type I) and fast twitch (type II). Muscle fibres rich in the slower MHC I isotype of myosin are considered slow twitch fibres and are referred to as type I fibres. Similarly, fibres rich in the fast MHC-IIa and -IIb isotypes of myosin are considered fast twitch fibres and are referred to as type IIa and IIb fibres, respectively. Type IIa fibres are more oxidative and type IIb are more glycolytic. Muscles typically contain a mixture of fibres types, and myosin contractile properties can adapt without a shift in isotype (Bottinelli, 2001), nevertheless, muscle is considered as "slow" if it predominantly contains type I fibres and as "fast" if type II fibres predominate.

Mitochondria have distinct features in different fibre types, and fibre type switching may be implicated during aging, under pathological conditions and in response to chronic changes in contractile demands. Different fibre types have varying metabolic demands, and synthesise distinct contractile and metabolic and regulatory proteins in order to meet those energy demands (Booth & Thomason, 1991). Skeletal muscle fibres contain many mitochondria in order to provide sufficient ATP for muscle contraction.

Type I fibres are more oxidative – they contain more mitochondria and promote the phosphorylation of greater quantities of ADP. This also makes type I fibres more resistant to muscle fatigue, as they have a larger supply of ATP required for muscle contraction. In addition, type IIb fibres are more susceptible to fatigue due to their glycolytic metabolism which acidifies the muscle upon repeated stimulation.

Changes in muscle activity can promote a shift in fibre type to meet the energy demands of the fibres, for example increased muscle activity can lead to increased mitochondrial biogenesis and thus to a shift toward a more oxidative (type I) fibre phenotype. Indeed fibre type switching may be promoted as a preventative measure in certain diseases linked to inactivity such as type 2 diabetes (Schiaffino and Reggiani, 2011).

Fibre type switching from a fast to a slow fibre phenotype is associated with an increase in action potential frequency and the resultant increase in muscle activity. Slow fibres contain more intracellular free calcium than fast fibres due to more frequent neural stimulation. The

pathway linking calcium levels to fibre type involves calcineurin (a calcium dependent protein phosphatase), which up-regulates slow fibre specific gene expression (Chin et al, 1998; Naya et al, 2000) and helps to prevent the atrophy of these fibres. Rhythmic muscle contractions activate calcineurin, leading to dephosphorylation and activation of NFAT (nuclear factor of activated T-cells). NFAT in turn promotes the expression of slow twitch muscle genes and inhibits the atrophy of slow oxidative fibres (Wang & Pessin, 2013). Indeed deletion or inhibition of the calcineurin/NFAT pathway can lead to a reduction in the number of type I fibres and impairs fast to slow fibre type transformation (Oh et al, 2005; Parsons et al, 2004).

Conversely overexpression of calcineurin in skeletal muscle increases the number of slow twitch fibres and the expression of PGC-1α (Naya et al, 2000). PGC-1α co-activates MEF2 transcriptional factors and promotes the expression of type I fibre proteins leading to an increase in slow twitch muscle fibres (Lin et al, 2002b). PGC-1α also prevents the atrophy of slow oxidative fibres and promotes mitochondrial biogenesis (Handschin et al, 2007; Lin et al, 2002b; Wu et al, 1999).

The relative expression of type I, type IIa and type IIb fibres is indicated in table 2, below, for several different muscles. TA, EDL and FDB are fast twitch muscles with a high abundance of type II fibres, whereas the soleus muscle is slow, with more type I fibres (Wei-LaPierre et al, 2013, Delp and Daun, 1996). Due to its role in promoting type one fibre expression, PGC-1 is likewise more abundant in the soleus and less so in type II rich fibres such as the EDL, TA and FDB (Lin et al, 2002a). This effect is not observed for the homologue PGC-1β (Lin et al, 2002b).

	I	IIa	IIb
TA	2%	39%	59%
EDL	2%	29%	69%
Sol	69%	29%	2%
FDB	8%	88%	4%

Table 2: Fibre type distribution. *The percentage of fibre type expressed in four hind limb muscles; tibialis anterior (TA), extensor digitorum longus (EDL), soleus (Sol) and flexor digitorum brevis (FDB). Proportions of type I fibres, type IIa and type IIb fibres are expressed as percentage of total fibre content (created using values from Delp and Daun, 1996, Lucas et al, 2014 and Wei-LaPierre et al, 2013).*

Fibre type switching has also been observed in the hind limb muscles of mouse models of PP. The EDL and soleus muscles of M1592V mice for example, typically shift from type IIb rich fibres to the more oxidative type IIa rich fibres (Hayward et al, 2008; Khogali et al, 2015). The M1592V mutation is equivalent to a human HyperPP associated mutation and the M1592V mice display characteristics of HyperPP as described in section 1.5.1(III). An equivalent shift has been described in TA muscles of mice with another HyperPP-associated sodium channel mutation (I588V; Corrochano et al, 2014). A further study on the M1592V mice indicated that such a shift in fibre type composition did not occur in the flexor digitorum brevis muscle (FDB) during the first 12 months of age (Lucas et al, 2014). Perhaps in FDB there is less pressure to shift from type IIb to type IIa muscle fibres because FDB already has a high proportion of type IIa fibres.

1.4 MANAGEMENT AND TREATMENT OF PEERIODIC PARALYSIS

1.4.1 Lifestyle changes

For many patients attacks of paralysis can be largely avoided by making appropriate lifestyle choices and avoiding triggers of paralytic attacks. Both HyperPP and HypoPP attacks can be triggered by rest after intense exercise, by stress and by cold. HyperPP attacks can also be

triggered by ingestion of potassium rich foods such as bananas and potatoes. Attacks of paralysis in HyperPP are associated with high serum potassium levels which promote opening of voltage gated sodium channels leading to the depolarisation of muscle fibres as described in section 1.1.3. Ingestion of potassium rich foods increases serum potassium levels and thereby makes patients of HyperPP more susceptible to attacks of paralysis. Carbohydrate ingestion, on the other hand, can trigger attacks of paralysis in HypoPP patients, where episodes of paralysis are associated with low serum potassium levels. The ingestion of carbohydrates stimulates the release of insulin. Insulin activates sodium-potassium ATPases causing potassium ions to enter cells and thereby reduces serum potassium levels. The carbohydrate ingestion thus lowers serum potassium levels, promoting paradoxical depolarisation in the patient's skeletal muscle fibres.

1.4.2 Drug treatment of PP

In many cases, such life-style choices are combined with treatments in order to ameliorate attacks and improve inter-attack strength as the disease progresses. Both HyperPP and HypoPP are primarily treated with drugs that counter the elevated or reduced potassium levels associated with attacks of paralysis. Severity and frequency of attacks of paralysis in HypoPP patients can be reduced by potassium ingestion or by the use of drugs that increase serum potassium levels. Conversely, a reduction in serum potassium levels can ameliorate attacks of paralysis in HyperPP patients. This can be achieved by reducing potassium intake or through the use of drugs. Diuretics and carbonic anhydrase inhibitors are used in the treatment of PP; thiazide diuretics for HyperPP patients (Links 1994) and carbonic anhydrase inhibitors for both HyperPP and HypoPP patients (McArdle, 1956; Resnick et al. 1968). A loop diuretic is currently also being assessed for efficacy in HypoPP patients (ClinicalTrials.gov identifier: NCT02582476).

I. Thiazide diuretics

Thiazide diuretics act by reducing serum potassium levels associated with attacks of paralysis in HyperPP patients. Diuretics act on the kidneys and are traditionally used to lower blood pressure by increasing excretion of urine. Thiazide diuretics inhibit the action of sodium-chloride transporters in the distal tubule of the renal system. Reduced blood volume and the increased levels of sodium in the distal tubule

stimulate reabsorption of sodium in exchange for potassium and hydrogen ions which are then lost in the urine. The loss of hydrogen ions can lead to metabolic alkalosis while potassium loss can lead to hypokalaemia.

II. Loop diuretics

Loop diuretics also promote accumulation of sodium ions in collecting ducts of the distal tubule, and the subsequent loss of potassium and hydrogen ions. These may likewise be associated with hypokalaemia and metabolic alkalosis. Nevertheless loop diuretics can protect against symptoms of HypoPP. In particular, the loop diuretic bumetanide has been found to ameliorate weakness and loss of excitability associated with HypoPP. The drug inhibits a co-transporter of sodium, potassium and two chloride ions, preventing the accumulation of chloride in skeletal muscle (Russell, 2000). This is thought to improve the condition, because high concentrations of chloride ions promote depolarisation when potassium concentration is low (Foppen et al, 2002). The efficacy of Bumetanide has been demonstrated in two murine models of HypoPP – one with a NaV1.4 mutation (R669H; Wu et al, 2013) and one with a CaV1.1 mutation (R528H; Wu & Cannon, 2013). The use of Bumetanide is currently being assessed in a clinical trial on 12 patients with HypoPP mutations (ClinicalTrials.gov identifier: NCT02582476).

III. Carbonic anhydrase inhibitors

Carbonic anhydrase inhibitors are used to treat a number of different conditions including glaucoma and to control seizures in epilepsy. Acetazolamide and dichlorphenamide are two carbonic anhydrase inhibitors that are used to reduce attack frequency in PP patients. According to a study by Tawil (Tawil et al, 2000) dichlorphenamide is more efficacious than acetazolamide. However a systematic review of these treatments suggests that it is unclear which has higher efficacy or fewer side effects (Sansone et al, 2008). A more recent study indicates that dichlorphenamide improves attack frequency and severity in hypokalaemia, but such effects on hyperkalaemic patients are as yet inconclusive (Burge et al, 2016).

IV. Acetazolamide

Acetazolamide has been used since 1956, and it was thought to work by reducing the elevated potassium levels (McArdle, 1956). However, acetazolamide has also been used to prevent paralytic attacks in HypoPP where attacks typically occur when serum potassium levels are reduced (Resnick et al. 1968). This suggests that another mechanism of action may be responsible for the therapeutic effects of acetazolamide in HypoPP patients. It has been suggested that metabolic acidosis induced by the drug reduces entry of potassium ions into muscle and thus reduces serum potassium concentration and the consequent paralysis (Vroom et al, 1975). However, this may not be the primary mechanism of action, as diuretics which cause alkalosis have also been found to ameliorate symptoms of the disease. Another proposed mechanism of action in HypoPP is that acetazolamide activates calcium activated potassium channels. Paralytic attacks in HypoPP are associated with a low level of potassium, however if serum potassium is increased when calcium levels are abnormally elevated, the firing of action potentials can be regulated (Tricarico et al., 2006).

Although acetazolamide has been found to reduce events in patients of HypoPP, approximately 50% of patients do not respond to the treatment. Those patients with mutations affecting the calcium channel are more likely to respond to treatment than those with sodium channel mutations according to a study investigating acetazolamide efficacy. The study found that 31 of 55 patients with calcium channel mutations responded to treatment, compared to only 3 of 19 patients with sodium channel mutations (Matthews et al, 2011). Furthermore, acetazolamide can cause an increase in attack frequency and severity (Torres et al, 1981), and long term use of acetazolamide can result in gastrointestinal disturbances, drowsiness and electrolyte imbalance (Sansone et al, 2008).

V. Coenzyme Q10

A more recent study of two patients with PP suggests that Coenzyme Q10 can also be used to successfully treat patients (Da et al, 2016). This enzyme is involved in a variety of processes in cell metabolism which may contribute to its therapeutic

effect. It promotes energy synthesis and antioxidant activity, and it regulates changes in fibre type and changes in gene expression.

1.4.3 The choice of treatment

There are currently no set guidelines regarding choice of medication for HyperPP and HypoPP (Sansone et al, 2008). While dichlorphenamide has been shown to be effective in patients of both HyperPP and HypoPP, there is variation in patient responses to the different therapies (Tawil et al, 2000). Such variations may be dependent on patient genotype. One study found that acetazolamide was a more effective treatment for HypoPP patients with mutations in the CaV1.1 channel than those where the NaV1.4 channel was affected (Matthews et al, 2014). This evidence that patients with the same mutations respond to the same treatments indicates that routine genotyping may help doctors prescribe more effective medication and thus improve treatment outcomes.

1.5 METHODS OF INVESTIGATING MUSCLE DISEASE

1.5.1 Current methods of investigating periodic paralysis

Many initial investigations focussed on locating genes associated with PP (Ptácek et al., 1991), and such investigations continue today due to the frequent discovery of novel mutations (see for example Zheng et al, 2016; Maggi et al., 2014). PP has been extensively investigated in simple cell models in order to observe direct effects of mutations on cell signalling. Patient observation has allowed for the identification of appropriate management of PP, and investigations performed on animals with equivalent mutations have helped to understand the relationship between PP-associated mutations and disease symptoms.

I. Observation of patients with periodic paralysis

Patient observation has contributed much to the understanding of PP. Features such as triggers of attacks and patterns of disease progression can be recorded in detail and help to understand key features of the disease. In addition, genome wide analysis of patients has helped to identify genes that are associated with the disease (for example Cheung et al, 2012). Clinical trials have improved the advice that can be given to PP patients and have helped to identify effective therapies. For example

efficacy of dichlorphenamide was demonstrated in randomised trials with PP patients (Tawil et al, 2000).

II. Expression of periodic paralysis mutations in HEK and oocyte models

Heterologous expression systems have been widely used in the investigation of PP. Mutant channels have been expressed in oocytes, human embryonic kidney cells (Struyk et al, 2000) and myotubes (Lehmann-Horn, 1995) in order to determine direct electrophysiological consequences of the mutations. One such study investigated the direct effects of expressing the M1592V mutation in oocytes, by recording sodium currents using two-electrode and cut-open oocyte voltage-clamp techniques (Rojas et al, 1999). The M1592V mutation is a mutation found in a mouse model of HyperPP, described below in section (III).

Such studies provide valuable information relating to how ion currents are affected by ion channel mutations. However expression of human mutations in different species can have different functional consequences, for example due to the presence of different accessory subunits or due to altered post translational modifications. Co-expression of both NaV1.4 and CaV1.1 channels with auxiliary subunits can make current recordings through these channels more representative of the currents in their native environments. Co-expression of NaV1.4 with its subsidiary β subunit, for example, impedes slow inactivation of the channels (Webb et al, 2009). In CaV1.1 expression systems, such co-expression is further complicated because a high level of diversity of the subunit isoforms contributes to functional diversity of the channels (Campiglio & Flucher, 2015).

Investigations on the effect of the mutations using heterologous expression systems must be limited to a direct effect on the current, as downstream effects in muscle tissue will depend on the presence of muscle specific cell content and structure. Heterologous expression studies are therefore frequently studied and interpreted alongside more physiological whole animal approaches, for example Struyk & Cannon (2007) and Wu et al (2011).

Investigations involving the expression of PP mutations in other cell types were of seminal importance in previous studies. They helped to clarify how the PP mutations can lead to abnormal activation patterns and thus to paralysis (Struyk & Cannon, 2007). These studies are still valuable for characterising novel mutations (for example see Fan et al, 2017), but are less valuable in broadening our understanding of disease progression.

III. Animal models of periodic paralysis

Several horse and mouse models of PP are available. HyperPP has become a growing problem in quarter horses (a breed of race horses) descending from a particular sire (Nayler, 1994). Four knock in mouse models of PP have also been developed.
The HyperPP mutation in horses is autosomal dominant and occurs in the NaV1.4 channels, as with the human disease (Rudolph et al 1992). The horses experience episodic attacks of muscle tremors, weakness and paralysis. Attacks are associated with eating potassium rich food, fasting and stress (Steiss & Naylor 1986; Spier et al, 1990).

The first mouse model to be characterised with PP has a methionine (M) substituted for valine (V) at a chromosome position which is equivalent to the human chromosome position 1592. Chromosomal position 1592 corresponds to a position in domain IV of the NaV1.4 alpha subunit, and the M to V substitution results in HyperPP. M1592V mice exhibit myotonia at rest and potassium sensitive paralysis, they also have a more oxidative phenotype compared to controls (Hayward et al., 2008).

Two further mouse models of PP that have been characterised lead to a HypoPP phenotype. Both involve an arginine to histidine substitution; one (R669H; Wu et al, 2011) at domain II of the NaV1.4 alpha subunit and one (R528H; Wu et al, 2012) at the same position in the CaV1.1 alpha subunit. These substitutions both lead to a loss of positive charge in the S4 segment of domain II of the affected channel. As with HypoPP mutations in patients (see section 1.1.4), the result is increased passage of cations through an aberrant pore in the channel. Consequently both of these mouse models have similar characteristics despite involving different ion channels.

Challenging either R669H or R528H mice with low extracellular potassium leads to reduced muscle excitability and to muscle weakness.

Although these three mouse models exhibit features of PP progression, they have not been observed to suffer spontaneous attacks of paralysis, such as those that characterise PP patients. This may support the hypothesis that the long term muscle degeneration experienced in patients of PP is not directly linked to the frequency or intensity of paralytic attacks that they experience earlier in their life. However these mice were not monitored continuously and it is also possible that attacks of paralysis occurred but were not observed.

The fourth mouse model was developed at Harwell (Corrochano et al, 2014) and is referred to as the Draggen (Dgn) model. The model was identified in an *N*-ethyl-*N*-nitrosurea mutagenesis screen (Nolan *et al*, 2002; Acevedo-Arozena *et al*, 2008). This Dgn model has an isoleucine (I) to valine (V) substitution at a chromosome position which is equivalent to the human chromosome position 588. Chromosomal position 588 corresponds to a position in domain II of the NaV1.4 alpha subunit, which has also been identified in one patient presenting with myotonia and PP.

While the other mouse models show similar progression to patients, the Dgn mice also exhibit attacks of paralysis similar to those that characterise the human disease. I contribute to the experiments performed at Harwell where we confirm that the mutation leads to some aspects of the PP phenotype. I elaborate on these investigations in the results section (section 4.2.1). Potassium levels seem normal between attacks, but have not been measured during attacks, and as a result, it is not clear if the phenotype is one of HyperPP or HypoPP. In addition, the nuclei of Dgn muscle fibres are typically found in the centre of fibres rather than the periphery. This can be taken as an indicator of increased muscle repair in the mutants. Central nuclei are also a common feature of both HyperPP and HypoPP (Links et al, 1990; Fouad et al, 1997; Bradley et al, 1990). Such nuclear positioning may also contribute to the development of muscle weakness, for example by disrupting muscle fibre contractions (Folker & Baylies, 2013).

Species	Mutation	Substitution	HyperPP/ HypoPP	Channel	Segment, domain, subunit	Clinical features	paper
Mouse	M1592V	M to V	HyperPP	NaV1.4	S6, IV, α	Myotonia at rest, K-sensitive paralysis	Hayward et al, 2008
	R669H	R to H	HypoPP	NaV1.4	S4, II, α	K-sensitive paralysis	Wu et al, 2011
	R528H	R to H	HypoPP	CaV1.1	S4, II, α	K-sensitive paralysis	Wu et al, 2012
	I588V	I to V	HyperPP	NaV1.4	S4, II, α	Episodic weakness, K-sensitive paralysis	Corrochano et al, 2014
Horse	E-HPP	F to L	HyperPP	NaV1.4	S4, III, α	K-sensitive paralysis	Cannon et al, 1995

Table 3: Animal models of HyperPP and HypoPP*. Summary of the mutations affecting different animal models of HyperPP and HypoPP, including key clinical features.*

IV. Drug induced periodic paralysis in rodents

The low potassium responsible for attacks of paralysis in HypoPP can be simulated in animals by modifying their diet. This has been achieved in rats by feeding them a potassium deficient diet and giving them insulin which further depletes potassium. This produced some aspects of the PP phenotype including weakness and muscle paralysis. However this model is not ideal, as potassium levels remain normal in HypoPP in between attacks, and reduce only during attacks. The continued depletion of potassium in this model of HypoPP affects levels of other ions such as sodium and calcium in the skeletal muscle cells (Dengler et al, 1979).

Barium has also been used to simulate HypoPP (Gallant, 1983). Extracellular barium acts by blocking the Kir2.1 channels (Gallant, 1983; Shieh et al, 1998). A reduction in the inwardly rectifying potassium conductance can potentiate the depolarisation threshold, so that challenge with low extracellular potassium is more likely to lead to depolarisation. In this manner blockade of the Kir2.1 channels can simulate the potentiation of paradoxical depolarisation observed in HypoPP.

The sodium ionophore gramicidin has been used to simulate the cation leak present in HypoPP. Gramicidin forms a beta helix in the cell membrane and dimerises to span the membrane, providing a channel for the passage of monovalent cations. The passage of monovalent cations is further facilitated by two cation binding sites.

Divalent cations, on the other hand, block the channel (Hladky & Haydon, 1972). As with leaks presented by HypoPP mutations, the aberrant leak current created by addition of gramicidin potentiates the threshold for depolarisation in response to reduced extracellular potassium concentration (Jurkat-Rott et al, 2009). These drugs can be used to replicate features of PP in muscle models, allowing for muscle specific downstream effects to be monitored.

V. Cultured cells from patient biopsies

The Institute of Neurology (UCL, London) is a referral centre for patients with PP and is thus visited by an exceptional number of individuals suffering from genetic muscle diseases including PP. Muscle cell cultures derived from human tissue can facilitate the expression of appropriate accessory subunits along with the channels, and allow for relevant post translational modifications to occur. Furthermore, myoblast cultures derived from skeletal muscle of patients have the advantage that they carry the exact mutations of the patients. Such cultures can be derived either directly from muscle biopsies (see section 1.5.2 (II)), or by growing fibroblasts or induced pluripotent stem cells and converting these to myocytes (see section 1.5.2 (III)). Under appropriate cultures conditions, myocytes then undergo a process of myogenesis (see section 1.5.2) whereby they fuse to form a syncytium of muscle cells (a myotube). The effects of specific mutations can then be investigated in the myotubes.

1.5.2 Myogenesis

Myogenesis is the formation of muscle tissue from mono-nucleated cells, either *in vivo* or in a laboratory context. *In vivo*, myogenesis is comprised of several steps involving exit from the cell cycle, alignment of mono-nucleated cells and fusion of the aligned cells (see table 4 below). This process can also be observed in myoblast cultured in vitro. Furthermore, factors that are known to promote myogenesis can be used *in vitro* to artificially induce myogenesis in non-myogenic cells. This allows for experimental muscle models to be created from non-myogenic tissue such as human skin biopsies.

I. Myogenesis *in vivo*

The initial stages of myogenesis *in vivo* are referred to as delamination and migration. Delamination involves segmentation of the paraxial mesoderm into somites, whereas migration involves the movement of these somites to the limb bud. Delamination and migration both occur in the presence of c-met, a tyrosine kinase receptor. Mutations in c-met, in its transcription factor (paired box protein 3; Pax3), or in its ligand (hepatocyte growth factor; HGF), result in the absence of limb muscles (Bladt et al, 1995; Maroto et al, 1997; Tajbakhsh et al, 1997).

Upon arrival at the limb bud, cells begin to proliferate, and this proliferation is partly maintained by continued expression of the transcription factor Pax3. The subsequent commitment and differentiation of cells to a myogenic phenotype involves the expression of a variety of factors. Four prominent factors in this process are members of the myogenic basic helix-loop-helix transcription factor family. These factors are myogenic determination factor 5 (Myf5), myogenic differentiation factor D (MyoD), myogenic regulatory factor 4 (Mrf4) and myogenin. Myf5, MyoD, Mrf4 and myogenin have overlapping roles during commitment and terminal differentiation (Rawls et al, 1998). Myf5 and MyoD are primarily involved in the commitment of multipotential somite cells to myogenic lineage (Maroto et al, 1997). Mrf4 is also transiently expressed during this determination phase of myogenesis. Mrf4 and MyoD are expressed again during differentiation. Together with myogenin they promote the terminal differentiation of committed muscle progenitor cells. Mrf4 continues to be expressed during postnatal development where it is thought to regulate muscle growth (Moretti et al, 2016).

A study in mice showed that Myf5 is activated in somites earlier than MyoD (in day 8 embryos rather than day 10 embryos; Cossu et al, 1996). Furthermore, this study showed that expression of Myf5 was induced in progenitors of epaxial muscles and that expression of MyoD initially occurred in progenitors of hypaxial muscle. Hypaxial muscles are those that lie ventral to the septum of the

vertebrae whereas epaxial muscles lie dorsal to the septum. Progenitors of both epaxial and hypaxial cells eventually expressed both the Myf5 and the MyoD genes (Cossu et al, 1996). At this stage Myf5 and MyoD compensate for one another, such that a mutation or knock out of either gene does not prevent muscle differentiation (Rudnicki et al, 1993; Braun et al, 1994). Knockout of Myf5 does however delay differentiation of epaxial muscles, because Myf5 is normally expressed earlier than MyoD. Differentiation is delayed until MyoD is expressed and can compensate for the lack of Myf5 (Braun et al, 1994). Knockout of both the Myf5 and the MyoD does, on the other hand prevent the development of skeletal muscle (Rudnicki et al, 1993).

Stage of cell cycle	MPC	MPC	myoblast	myocyte	myotube	Myofibre
Stage of myogenesis	Delamination	Migration	Proliferation	Commitment	Differentiation	Maturation
bHLH transcription factors				Myf5 (+) MyoD (+) Mrf4 (+)	Mrf4 (+) MyoD (+) Myogenin (+)	MHC (+) Mrf4 (+)
Other signalling molecules	c-met (+)	c-met (+) Pax3 (+)	Pax3 (+) Pax7 (+) Myostatin (-)	Wnt (+)	IGF2 (+)	

Table 4: Regulation of myogenesis*. Embryonic myogenesis involves the highly orchestrated expression of numerous molecules with overlapping periods of expression. These molecules include kinases, growth factors and transcription factors. This table indicates some of the key signalling molecules involved in the different stages of myogenesis. A plus sign (+) indicates that the molecule promotes the correlating stage of myogenesis, and a minus sign (-) indicates negative regulation. MPC – myogenic precursor cell; bHLH – basic helix loop helix; Myf5 – myogenic determination factor 5; MyoD – myogenic differentiation factor D; Mrf4 – myogenic regulatory factor 4; MHC – myosin heavy chain ; c-met – a receptor tyrosine kinase; pax3/7 – paired box protein 3/7; Wnt – wingless related integration site glycoproteins; IGF2 – insulin like growth factor 2. Summary of the above text with additional information (Olguín & Pisconti, 2012; Susuki et al, 2015)*

II. Myogenesis *in vitro* using cultured myoblasts

As with myogenesis *in vivo*, myogenesis *in vitro* involves the expression of myogenic factors (Rajan et al, 2011). Furthermore, the expression pattern of these factors in cell lines can be similar to that observed *in vivo*. Due to the

overlapping roles of the myogenic factors, only a subset is expressed in many skeletal muscle cells line. Typically either MyoD or myf5 is expressed constitutively whereas myogenin expression is initially repressed, and begins to be expressed during differentiation (Olson, 1990). MRF-4 on the other hand, is typically not expressed in muscle cell lines as it is more involved in muscle growth.

III. Myogenesis *in vitro* using non-myogenic cells

MyoD can be used to convert non myogenic cells such as fibroblasts, chondroblasts and retinal cells to myotubes (Choi et al, 1990). In this study I focus on the conversion of fibroblasts, because I have access to skin biopsies of PP patients.

Forming myotubes from fibroblasts involves two separate stages; the conversion of the fibroblasts into myoblasts and the fusion and differentiation of myoblasts into multinucleated myotubes. The fibroblast to myoblast conversion can be triggered in culture by viral delivery of MyoD to the nucleus of the cell. MyoD coordinates the expression of muscle specific proteins and thereby promotes the differentiation of muscle (Lattanzi et al, 1998). Following expression of MyoD, cells withdraw from the cell cycle and their original differentiation programme is downregulated, allowing for myogenic differentiation to occur. Such differentiation includes the initiation of desmin synthesis (Choi et al, 1990). Once a myoblast culture is achieved and confluent enough for contact between cells to occur, the process of cell fusion can begin (Tanaka et al, 2011).

IV. Factors that support differentiation *in vitro*

As well as the involvement of the basic helix-loop-helix factors in myogenesis, myoblast adhesion and fusion are guided by a range of factors *in vivo*. Indeed, supplementing media with appropriate factors, rather than with serum, encourages differentiation to occur in culture (St Clair et al., 1992). Factors of particular importance in this regard include insulin, creatine, and epidermal growth factor (EGF). These factors can be added to the culture medium when differentiating cells, in combination with bovine serum albumin (BSA). The

albumin functions as a carrier protein; it transports growth factors and facilitates their steady supply to the cells (Francis, 2010).

Insulin accelerates spontaneous myogenesis by induction of NF-kappaB (Conejo et al, 2001). Creatine enhances differentiation of myoblasts by promoting the phosphorylation of proteins including mitogen activated protein kinases and protein kinase B (Deldicque et al, 2007). EGF is typically included in culture to aid cell proliferation, however at low concentrations EGF can promote differentiation.

V. Myogenesis and therapeutic approaches

As well as being an integral part of muscle growth, myogenesis is important for the repair of injured muscle *in vivo*. This ability of muscle to regenerate can also be used therapeutically. Tissue from patients suffering from genetic muscle disease can be removed and converted into induced pluripotent stem (iPS) cells. Mutations in these iPS cell cultures can be corrected before converting them into myogenic progenitor cells and reintroducing the cells to the patients (reviewed in Tedesco et al, 2010). Although this line of investigation has not yet been explored for PP, it appears to have great potential in the treatment of other genetic muscle diseases including Duchenne muscular dystrophy (Maffioletti et al, 2015). In a study on dystrophic mice lacking α-sarcoglycan, for example, fibroblasts and myoblasts were reprogrammed to iPS cells which were then converted to mesoangioblasts-like cells. Viral introduction of the α-sarcoglycan gene to these mesangioblast-like cells meant that α-sarcoglycan expressing cells could be reintroduced into the α-sarcoglycan null mice. In these mice α-sarcoglycan was expressed and the dystrophic phenotype ameliorated (Tedesco et al, 2012).

1.6 CALCIUM HANDLING AND MITOCHONDRIAL FUNCTION IN SKELETAL MUSCLE

1.6.1 Calcium handling

Calcium ions are vital second messengers, required for the regulation of a wide range of functions, including contraction, cell survival and cell death. The PP mutations interfere with normal propagation of action potentials, causing excessive cell depolarisation, which in turn results in excessive calcium fluctuations in the cell. Due to its seminal role in regulating cell

function, and in particular muscle cell function, intracellular calcium concentration is both dynamic and tightly regulated. Transport across the plasma membrane and across membranes of intracellular storage compartments is achieved by several regulated channels and pumps while intracellular calcium stores provide a means of rapid release and rapid sequestration of calcium.

Disruption of calcium handling is consequently going to be a key consideration when searching for mechanisms involved in PP progression. In particular, it may be that the multiple periods of muscle over-activation and calcium accumulation experienced by patients lead to up or down regulation of ions, ion channels or organelle function (Green, 1997). Indeed such relationships have been observed in other muscle diseases. Mutations in skeletal RyR associated with malignant hyperthermia (MH) and central core disease (CCD), for example, result in increased cytosolic calcium levels (McCarthy et al, 2000). In MH such rises in calcium concentration are acute and lead to muscle rigidity whereas in CCD they are chronic and are associated with mitochondrial damage and disorganisation of myofibrils. Given the wide range of effects that changes in calcium handling can have, investigations on calcium handling will also consider downstream consequences on organelle function and on the expression of other skeletal ion channels.

1.6.2 Caffeine

Caffeine is a pharmacological agonist which selectively binds to and opens RyR. RyRs mediate the release of calcium from SR to the cytosol of muscle cells. Caffeine is therefore a useful tool for the investigation of calcium handling in muscle.

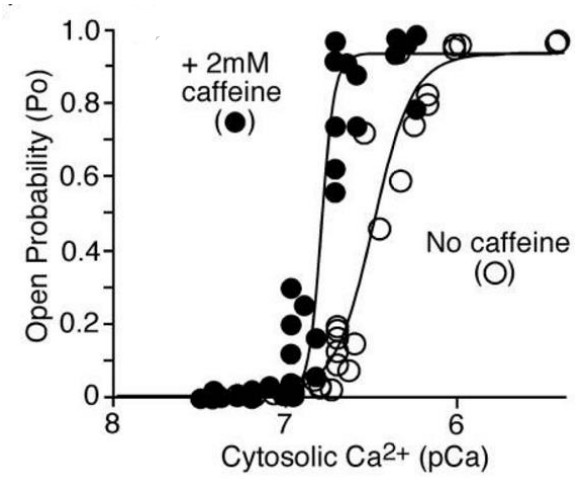

Figure 8: RyR open probability. *Analysis of the open probability (P_O) of RyRs in HEK293 cells (Kong et al, 2008). The relationship between Po and cytosolic Ca^{2+} concentration is plotted in the presence and absence of caffeine. Data points were individual measurements obtained from 7 RyR2 channels in the presence of 2mM caffeine (solid circles) and 5 RyR2 channels in the absence of caffeine. The average recording time was 93 seconds.*

Concentrations of less than 2mM caffeine sensitise RyR to cytosolic calcium by increasing the frequency of channel opening. In contrast, higher concentrations of caffeine act by increasing the open time of the receptors (Porta et al, 2011). Low concentrations of caffeine are only effective in the presence of activating levels of cytosolic calcium (0.1 and 10μM), whereas more than 5mM caffeine is required to increase the open probability of the RyR at sub-activating concentrations of cytosolic calcium. Indeed low caffeine concentrations (less than 1mM) act by sensitising the RyR to cytosolic calcium, whereas higher concentrations (2.5mM caffeine or more) increase the sensitivity of the receptors to luminal calcium (Porta et al, 2011).

1.6.3 Mitochondrial biogenesis

The main function of mitochondria in a cell is to synthesise ATP by oxidative phosphorylation. It is also involved in the biosynthesis of various metabolites involved in oxidative phosphorylation. Levels of mitochondrial activity must therefore be regulated according to energy demands of the cell. Indeed greater levels of mitochondrial biogenesis occur in tissue with greater energy demands. Mitochondrial biogenesis is defined as the growth in mitochondrial size and mass as well as mitochondrial division and it depends on transcription of both mitochondrial and nuclear DNA. Each mitochondrion contains circular double stranded mitochondrial DNA (mtDNA). Single molecules of mtDNA are packaged by proteins, primarily TFAM (mitochondrial transcription factor A), into mitochondrial nucleoids which are approximately 100nm long in mammals. TFAM is a regulator of mitochondrial transcription and biogenesis. Nucleoids frequently contain only one copy of mtDNA, with an average of 1.4 mtDNA molecules per nucleoid (Kukat et al, 2011). MtDNA encodes only 13 respiratory subunits and mitochondrial biogenesis relies primarily on nuclear gene products.

Two classes of transcriptional regulators of mitochondrial biogenesis are encoded in the nucleus; DNA binding (such as NRF-1 and 2) and non DNA binding transcriptional regulators. Non DNA binding regulators include peroxisome proliferator-activated receptor gamma coactivator-1 α and β (PGC-1α and PGC-1β); these interact with DNA bound transcriptional factors to co-activate the expression of genes. PGC-1α promotes the expression of nuclear gene products involved in oxidative phosphorylation including

NRF-1 and 2 and TFAM (Puigserver & Spiegelman, 2003). NRF-1 and 2 regulate transcription of nuclear genes associated with oxidative phosphorylation whereas TFAM regulates the transcription and replication of such genes encoded in the mitochondrial genome (Virbasius & Scarpulla, 1994). In addition TFAM maintains normal levels of mtDNA and regulates its aggregation and packaging (Ekstrand et al, 2004). TFAM contains consensus binding sites for NRF-1 and 2 and thus allows for the transcription of mtDNA and nuclear DNA encoded genes to be co-ordinated during mitochondrial biogenesis (Virbasius & Scarpulla, 1994). Furthermore TFAM expression is promoted by reactive oxygen species (ROS) which are a bi-product of respiration allowing for TFAM to respond to energy demands of the cell (Miranda et al, 1999). Indeed small increases in ROS may promote expression of genes involved in energy metabolism in order to rescue the affected cell. In this manner, ROS act as signalling molecules at non-toxic levels. Increased calcium levels activate ROS generating enzymes and the formation of free radicals (Gordeeva et al, 2003). Under oxidative stress, for example in pathology or during aging, larger increases in ROS can damage mtDNA and promote apoptosis by activating the mitochondrial permeability transition pore and by release of pro-apoptotic proteins.

Increased levels of mtDNA copy number per cell are associated with increased levels of oxidative stress in aged human skeletal muscle (Barriento et al, 1997; Barazzoni et al, 2000; Pesce et al, 2001), while mitochondrial function declines with aging (Short et al, 2005). AMPK acts as an energy sensor and its activity has been shown to decrease with age, which may contribute to decreased mitochondrial biogenesis and function with aging (Jornayvaz & Shulman, 2010). Indeed AMPK activation protects cells from oxidative stress, and the effect of aging on the tissue appears to be a result of oxidative stress in the tissue (Han et al, 2016). Cultures present with increased mitochondrial mass both during later stages of proliferation and upon challenge with hydrogen peroxide. The increased mitochondrial mass depends on both the synthesis of nuclear DNA encoded proteins and their import into mitochondria which is determined by the mitochondrial membrane potential (Lee et al, 2002).

1.6.4 Calcium and mitochondrial interplay

Calcium and mitochondrial function are highly interrelated. A reduction in mtDNA (mitochondrial DNA) or disruption of mitochondrial membrane potential can influence calcium-dependant retrograde signalling from the mitochondria to the nucleus (Jahnke et al, 2009). Conversely, calcium signalling influences mitochondrial function; it drives mitochondrial biogenesis and at higher concentrations can lead to mitochondrial damage and opening of the mitochondrial permeability transition pore (MPTP; Kim et al, 2007) causing a precipitation of cell death. The schematic below indicates some of the channels and transporters involved in mitochondrial calcium handling.

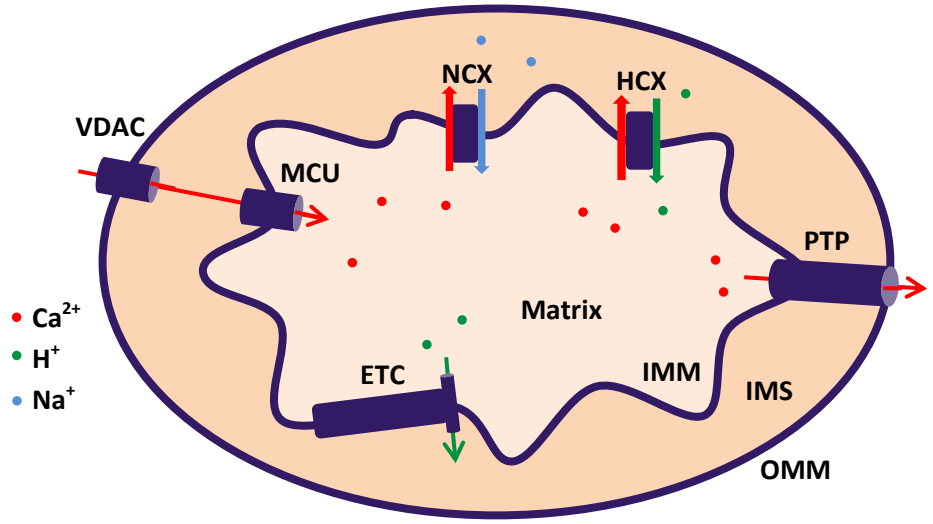

Figure 9: Mitochondrial and associated calcium transporters. *Schematic diagram of a mitochondrion with associated calcium ion (Ca^{2+}) transporters. Voltage dependent anion channels (VDAC) on the outer mitochondrial membrane (OMM) control Ca^{2+} diffusion into the inter membrane space (IMS). The electron transport chain (ETC) removes protons (H^{+}) from the matrix. Ca^{2+}s cross the inner mitochondrial membrane (IMM) and enter the matrix down the resultant electrochemical gradient through the mitochondrial calcium uniporter (MCU). Ca^{2+}s are removed from the matrix by sodium calcium exchangers (NCX) and proton calcium exchanges (HCX). Ca^{2+}s are released through the mitochondrial membrane via the mitochondrial permeability transition pore (PTP). Brief PTP openings facilitate rapid Ca^{2+} release, whereas prolonged openings can trigger apoptosis.*

Mitochondrial calcium levels are maintained under physiological conditions by cycling of calcium ions in and out of the mitochondrial matrix. Calcium enters through voltage dependant anion channels (VDAC) and through the mitochondrial calcium uniporter (MCU)

and it is transported back to the cytosol via NCX and HCX (the proton calcium exchanger). Calcium is released from the SR by activation of IP_3Rs and RyRs. IP_3Rs are enriched at ER-mitochondrial contact sites and are connected to VDACs on the outer mitochondrial membrane (Rizutto et al, 1999; Sabadkai 2006). High calcium micro-domains consequently develop near MCUs, allowing calcium to enter the mitochondrial matrix via the MCU despite its low affinity for calcium uptake (Rizzuto et al, 2012).

Under pathological conditions the association of SR and mitochondria can be tightened leading to mitochondrial calcium overload (Csordas et al, 2006). Mitochondrial calcium overload leads to the production of reactive oxygen species (ROS) and opening of the MPTP. MPTP opening leads to a sudden influx of ions and solutes, mitochondrial swelling, dissipation of the membrane potential and ultimately cell death. Opening of the MPTP leads to the downstream activation of apoptosis via release of cytochrome c into the cytosol. Cytochrome c binds to IP_3Rs on the SR and prevents calcium from having an auto-inhibitory effect on the IP_3Rs. This leads to the initiation of a feedforward mechanism whereby further calcium is released from the SR leading to further release of cytochrome c from mitochondria (Boehning et al, 2003). In addition to contributing to the opening of the MPTP, mitochondrial dysfunction and calcium influx can contribute to cell death by promoting the production of ROS which can then damage proteins, lipids and DNA (Wei et al, 1998).

1.6.5 Oxidative phosphorylation

Mitochondria promote phosphorylation of ADP to ATP in a process called oxidative phosphorylation. Energy for this phosphorylation is produced by the transfer of electrons between a series of complexes. These complexes are referred to together as the electron transport chain (ETC) or the electron transfer system (ETS; see figure 10 below).

During oxidative phosphorylation, oxygen is transformed to water. Consequently oxidative phosphorylation can be monitored by taking measurements of oxygen consumption. The activity of each mitochondrial complex can be investigated by chemically targeting the complex while monitoring oxygen consumption. Inhibiting ATP synthase with oligomycin for example abolishes the flow of protons through the channel and thus inhibits respiration that is coupled to oxidative phosphorylation. The resultant reduction in oxygen consumption thus reflects the level of activity of ATP synthase. FCCP (carbonyl cyanide 4-

(trifluoromethoxy)phenylhydrazon) is an ionophore that uncouples ETS facilitated respiration from oxidative phosphorylation in order to induce maximal ETS capacity. Rotenone inhibits complex I and can thus be used to deduce the contribution that this complex makes to respiration while antimycin inhibits complex IV mediated respiration, providing an estimate of non-mitochondrial respiration.

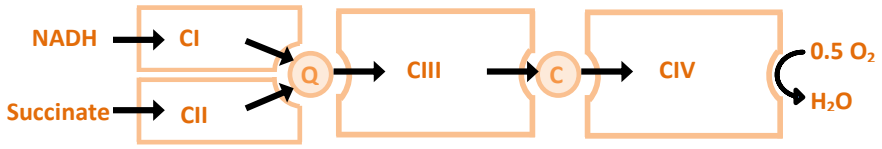

Figure 10: The electron transfer system. *The electron transfer system, adapted from E Gnaiger (E Gnaiger, 2007). NADH linked substrates provide complex I (CI) with electrons and succinate linked substrates provide complex II (CII) with electrons. From here electrons are passed to the Q junction (a ubiquinone linked enzyme; glycerol-3-phosphate dehydrogenase). Complex III (CIII) accepts electrons from the Q junctions and passes them to cytochrome C (C) which then passes them to complex IV (CIV). CIV catalyses the formation of H_2O using oxygen provided by respiration, electrons from electron transfer and protons from the cell matrix.*

The role of the different mitochondrial complexes in the electron transfer system can also be monitored by *in vitro* analysis of tissue homogenates, where enzyme activity can be compared to activity of a control enzyme such as citrate synthase (Hargreaves et al, 1999).

1.7 HYPOTHESIS

I hypothesise that calcium handling and mitochondrial function will be affected. The frequent attacks of paralysis in PP are associated with unusually frequent and extensive calcium fluctuations within skeletal muscle. Such excessive calcium cycling could lead to mitochondrial damage through mitochondrial calcium overload and the associated production of ROS. ROS can lead to protein, lipid and DNA damage and may thus be associated with the generalised skeletal muscle tissue damage observed in PP. Calcium handling and mitochondrial function are measured in order to determine their role in the progression of PP.

2. AIMS

2.1 AIMS

The aim of the work described in this thesis is to improve the current understanding of how PP progresses from intermittent attacks of paralysis to a generalised muscle weakness and in some cases myotonia. This aim is approached by developing both cell and animal models of PP, as detailed below:

I. Fibroblast derived myotubes: fibroblasts are virally converted to myoblasts. These are then differentiated into myotubes. Culture conditions are optimised in order to improve efficiency of this transformation.

II. A mouse model of PP: This model is characterised in vivo and in vitro.
In vivo testing of a mouse model of PP includes tension and fatigue tests and motor neuron counts.
Ex vivo characterisation of the mouse model is carried out by isolating single fibres from the Flexor Digitorum Brevis (FDB)

III. A drug model of PP: The disease phenotype is simulated in neonatal cultures of Sprague Dawley rats by addition of barium chloride

2.2 APPROACHES

Previous approaches have focused primarily on direct electrophysiological effects of the PP mutations in heterologous expression systems and on *in vivo* physiological investigations. Effects downstream of the mutations that lead to the observed physiological effects have not been extensively investigated. The approaches pursued here allow for the roles of calcium handling and mitochondrial function in the development of physiological features of periodic paralysis to be investigated. The *in vivo* approach should allow for gross physiological changes in mutants to be determined, and thus inform the *ex vivo* work – so that *ex vivo* work can be conducted in tissue that is known to be affected. *Ex vivo* investigations should allow for trends in mitochondrial function and in calcium handling to be evaluated within the skeletal muscle fibre structure.

The *ex vivo* investigations focus on the specific effects of an animal mutation in animal tissue. Further analysis of mitochondrial function and calcium handling in patient derived cell culture models are employed to determine whether similar changes are associated with human mutations in human cells. Such investigations could confirm whether or not trends that are observed in the animal model are true effects of PP rather than effects that are specific to the animal mutation.

The patient derived model could be particularly advantageous in this regard as it allows for the downstream effects of a wide range of mutations to be observed, by culturing cells from different patients. The patient model should thus be a useful genetic model of the disease. However features of the condition may not be observed in the cultured cells because culture conditions do not replicate the exact growth conditions in vivo. In particular, the cultured cells do not display attacks of paralysis.

I will therefore compare observations from the mouse and patient derived models of the disease to a model produced by drug treatment of neonatal rat cultures. Treatment with barium and low potassium can be used to simulate attacks of hypokalaemic. The drug model may complement the investigation, as it is focused on whether or not attacks of paralysis associated with low potassium have downstream effects on calcium handling and mitochondrial function.

Whereas pathophysiological outcomes are monitored *in vivo*, calcium handling and mitochondrial function are studied *ex vivo*, and *in vitro* (in isolated single fibres, in the fibroblast derived myotubes and in the drug treated myotubes). The spatiotemporal dynamics of calcium signals (upon stimulation with caffeine or high potassium or upon electrical stimulation) are characterised and the mitochondrial structure and mitochondrial membrane potential are monitored.

The use of several different models of PP is important when testing for a common final pathway leading to myopathy in PP. If the different models lead to the same downstream pathway, this would suggest that the observed outcome was significant in the development of the myopathy. In particular, this could be assumed if the same features are seen both in models of HypoPP and HyperPP, because of the distinct direct effect of their mutations and the common downstream pathological characteristics.

3. MATERIALS AND METHODS

3.1 ETHICS STATEMENT

All animal studies were carried out in accordance with UK Home Office legislation and local ethical guidelines.

3.2 REAGENTS

The following reagents will be referred to in this text.

I. 4-12% polyacrylamide gel (NuPAGE 4-12% Bis-Tris Protein gel, NP0322)
II. Anti-fast skeletal myosin, mouse (SIGMA, M1570)
III. Anti-MyoD, mouse (Millipore, MAB3878)
IV. Anti-CaV1.1, rabbit (Santa-Cruz biotechnology, H-240)
V. Anti-desmin, mouse (Invitrogen, 180016)
VI. Anti-GAPDH, rabbit (SIGMA, G9545)
VII. Anti-IRK2.1 (abcam, ab109750)
VIII. Anti-mouse IgG conjugated to alexa Fluor 555, goat (Invitrogen, A32727)
IX. Anti-SERCA1 ATPase, mouse (ABCAM, ab2819)
X. Anti-TFAM, rabbit (Santa-Cruz biotechnology, H-203)
XI. AraC (cytosine beta-D-arabinofuramoside, SIGMA, C1768)
XII. Barium (Scientific Laboratory Supplies, B0750-100G)
XIII. BCA Protein Assay Kit (Thermo Scientific Pierce, 23225)
XIV. BSA (bovine serum albumin; SIGMA, A9418)
XV. Caffeine (SIGMA ALDRICH, C0750)
XVI. CEE (chick embryo extract; MP Biomedical, 2850145)
XVII. Collagenase I (SIGMA, C0130)
XVIII. Serum replacement 2 (SIGMA, S9388)
XIX. Creatine (SIGMA, C0780)
XX. Dispase (Invitrogen, 17105041)
XXI. DMEM (DMEM+GlutaMAX-1, 4.5 g/L D-glucose, no pyruvate (GIBCO 31960)
XXII. DMSO (Dimethyl Sulfoxide, SIGMA, D8418)

XXIII. EGF (epidermal growth factor; SIGMA, E9644)

XXIV. FBS (fetal bovine serum, GIBCO 10500)

XXV. FLIPR Membrane Potential Assay Kit (Molecular Devices, R8128)

XXVI. Fluo-4, AM, Cell permeant (Molecular Probes, F14201)

XXVII. FluoVolt (Molecular Probes, F10488)

XXVIII. Fluoromount aqueous mounting medium (SIGMA, F4680)

XXIX. Formaldehyde solution (SIGMA, F8775)

XXX. Gentamycin solution (SIGMA, G1272)

XXXI. Gramicidin (SIGMA, G5002)

XXXII. HBS (SIGMA-ALDRICH, 51558)

XXXIII. Hoechst (Invitrogen , 33342)

XXXIV. HS (horse serum, GIBCO, 16050)

XXXV. IMDM (IMDM with Glutamax: Invitrogen, 31980022)

XXXVI. Insulin (Invitrogen, 12585014)

XXXVII. LDS sample buffer (NuPAGE, NP0007)

XXXVIII. Matrigel Reduced factor (BD Biosciences, 354230)

XXXIX. MOPS SDS running buffer (NuPAGE, NP0001)

XL. Nitrocellulose membrane (Thermo Scientific, 88018)

XLI. PBS (phosphate buffered saline, SIGMA, P4417)

XLII. Phalloidin (Alexa Fluor 488 Phalloidin, Molecular Probes, A12379)

XLIII. PI (BD Pharmingen, 556463)

XLIV. PMSF protease inhibitor (phenylmethylsulfonyl fluoride; Thermo Scientific, 36978B)

XLV. Protein ladder (Precision Plus Protein™ Dual Color Standards, Bio-Rad, 1610374)

XLVI. P/S (Penicillin/streptomycin, GIBCO 15070)

XLVII. PVDF (Immobilon-P Membrane, IPVH00010 EMD MILLIPORE)

XLVIII. RIPA lysis and extraction buffer (Thermo Scientific, 89900)

XLIX. TMRM (Tetramethylrhodamine; Invitrogen, I34361)

L. Transfer buffer (NuPAGE, NP0006)

LI. Triton x-100 (SIGMA, T8787)

LII. Trypsin (0.05% Trypsin-EDTA, Gibco 25300)

3.2.1 Viral vectors of MyoD

Two viral vectors were used to promote conversion of fibroblasts to myoblasts by delivering the transcription factor MyoD. These were an adenovirus and a lentivirus. The adenoviral vector was acquired from The Native Antigen Company (Ad5.f50.AdApt.MyoD). The lentiviral vector was prepared as described below and in Kimura et al (2008).

A transfer vector was a kind gift from Jeffrey Chamberlain. Briefly, the transfer vector was produced by inserting a modified oestrogen receptor responsive to tamoxifen and 4-hydroxytamoxifen into the NarI site (amino acid 173) in the middle of full length cDNA for mouse MyoD (Kimura et al, 2008). The Lentiviral vector was produced by inserting the corresponding coding sequences into the polylinker of the pRRL-cPPT-CMV-XPRE-SIN vector as described in Kimura et al (2008). The Lentiviral vector was produced by inserting the corresponding coding sequences into the polylinker of the pRRL-cPPT-CMV-XPRE-SIN vector as described in Kimura et al (2008). Fresh medium was applied to HEK293T cells two hours before addition of a plasmid DNA mixture. The plasmid DNA mixture was prepared by adding REV at 6.25 µg/µL, VSV-G at 7 µg/µL, Δ 8.74 at 16.25 µg/µL and the transfer vector plasmid at 30 µg/µL to purified nuclease free H2O (2:1). REV is a packaging plasmid which binds the Rev response element to facilitate nuclear export and VSV-G (vesicular stomatitis virus G protein) is an envelope plasmid used to pseudotype most lentiviral vectors. Finally 125µL of 2.5M calcium chloride was added and the mixture incubated at room temperature for five minutes. A precipitate was then formed by dropwise addition of a 2x solution of HEPES buffered saline (HBS). After a further 15 minutes of incubation at room temperature the mixture was added to the 293T cells. Cells were incubated at 37 °C for 14 hours. The mixture was then replaced with fresh medium and supernatant was collected after a further 30 hours of incubation at 37 °C. Media was filtered and the lentiviral vector was purified by ultracentrifugation for two hours at 20000 rpm at 20^{o}C.

3.3 CELL CULTURE

Cells were cultured at 37^{o}C with 95% oxygen and 5% carbon dioxide.

3.3.1 Fibroblast cell culture

Skin biopsies were taken from control subjects and from patients. Fibroblasts from these were isolated and were cultured at the biobank of the MRC Centre for Neuromuscular Diseases. Fibroblasts from control subjects (biobank ID: 8203) and from patients (biobank ID: L937/1264F) were transfected and differentiated to produce myotubes. Although investigations with equivalent biopsies from muscle could be more straightforward, ethical approval for this project did not cover the removal of muscle biopsies from patients.

Fibroblasts were grown in a proliferation medium of DMEM with 10% FBS and 1% P/S and were sub-cultured upon reaching 90% confluency. In order to subculture cells, media was aspirated from flasks, cells were washed with PBS to remove serum and were incubated for 10 minutes in 0.05% Trypsin until round and freely moving. The trypsin was then inactivated by addition of further medium. At this point, cells were allowed to proliferate as before, frozen or seeded and differentiated on coverslips for imaging or in dishes for western blotting.

I. **Freezing cells**: Cells were spun at a relative centrifugal force (RCF) for 500 for 4 minutes, and supernatant was aspirated. Cells were aliquoted in cryovials with 1mL freezing medium of FBS with 10% DMSO per approximately one million cells. Cryovials were frozen in a Mr frosty (Nalgene) at -80^{o}C. Cells were then stored at -80^{o}C or in liquid nitrogen.

II. **Seeding cells:** Coverslips were prepared for seeding by coating with 10% matrigel (BD Biosciences) in DMEM and incubating for 20 minutes. Matrigel was then aspirated, and cells were seeded at 100,000 cells per 22mm coverslip (for live imaging) and 50,000 per 13mm coverslip (for fixed imaging). Cells were allowed to settle on coverslips for 10 minutes before addition of proliferation media. Alternatively cells were seeded directly into dishes for western blotting.

III. **AV transduction:** Upon reaching confluency, 1 to 2 days after seeding, cells were incubated with AV for 4 to 5 hours before changing to differentiation medium.

IV. **LV transduction:** Lentivirus was introduced to cell cultures before seeding, and MyoD expression activated after seeding. Lentivirus was introduced by application to confluent cells at a concentration at 8.6*10^8ptu/ml (MOI of 10). Cells were incubated with the lentivirus for 24 hours and then grown in proliferation medium again until confluent. At this stage cells could be sub-cultured and seeded for investigations. Upon reaching confluency 0.1µM 4-OH tamoxifen (sigma) was applied to activate expression of MyoD. Cells were incubated with proliferation medium with tamoxifen for 24 hours and for a further 24 hours with differentiation medium of DMEM with 2% HS and tamoxifen. Fresh differentiation medium without tamoxifen was then applied.

V. **Differentiation:** Differentiation medium was changed every 3 to 4 days, either complete changes of differentiation medium were made, or in some cases half of the medium was changed and half maintained. Cells were differentiated for a duration of 7 to 11 days whereupon cells were imaged or fixed for immunofluorescence assays. Three different differentiation media were tested:

- 2% HS (containing DMEM with 2% HS and 1% P/S)
- 1% HS (containing DMEM with 1% HS and 1% P/S)
- SupM (containing DMEM supplemented with 0.05% BSA, 10 n*g*/mL EGF, 0.15 m*g*/mL Creatine 5 ng/mL Insulin and 1% P/S)

3.3.2 Myoblast cell culture

Control immortalised human myoblasts were received from the MRC biobank (biobank ID: i7403) produced at Institut Pasteur, Paris (Zhu et al, 2007). These cells were used between passage 4 and 12. Cells were grown in a proliferation medium of DMEM with 10% FBS and 1% P/S until confluent and differentiated in DMEM with 2% HS and 1% P/S for 7 to 10 days before imaging or fixing for immunofluorescence assays (see section 3.4.7).

The production of a greater proportion of multinucleated myotubes was supported by addition of 10mM β-D-arabinofuranoside (araC) during differentiation. AraC interferes with DNA production and therefore reduces the proportion of proliferating cells (myoblasts and fibroblasts) without affecting myotubes which have left the cell cycle.

3.3.3 Primary neonatal cell culture

P5 neonatal rats were sacrificed by cervical dislocation. The gastrocnemius and soleus were removed and placed in ice cold PBS. The PBS was then removed, and muscle was cut finely before digesting in an Eppendorf tube with 500uL digestion solution of 0.5mg/mL Collagenase and 3.5mg/mL Dispase and shaken vigorously for 50 minutes at 37^{o}C. Digestion was inactivated by addition IMDM with 10% FBS and 0.1% gentamycin and myoblasts were purified by centrifugation. Undigested material was removed by centrifugation for 5 minutes at 70 RCF and then cells were extracted by centrifugation for 5 minutes at 340 RCF. The pellet was re-suspended in IMDM with 10% FBS and 0.1% gentamycin and strained through a 40µm mesh. The cells were then pre-plated for 45 minutes at 37^{o}C to remove fibroblasts. Thereafter cells were centrifuged a final time for 9 minutes at 420rmp, and re-suspended in IMDM with 20% FBS and 1% CEE. Cells were seeded on 1% Matrigel Reduced Factor. Media was not changed for 2 to 5 days, until cells were approximately 80% confluent, and beginning to fuse. The proliferation medium was then removed and replaced with a differentiation medium of IMDM with 2% HS and 0.1% gentamycin. This medium was changed daily until cells were ready to image (typically after two days).

3.3.4 Cell culture for drug model preparation

The effects of treatment with low potassium and barium were tested in neonatal myotubes and in isolated single fibres, where treatment was applied both before and during imaging. The direct effects of gramicidin were also tested in neonatal myotubes.

For pre-treatment studies cells were incubated for one hour in medium containing 0.5mM, 1mM, 2mM or 5.3mM potassium, either with or without 50µM barium. Cells were then incubated for a further three hours in normal conditions before imaging.

The direct effects of drug treatment were studied by imaging while exposing cells to 0.5mM, 1mM, 2mM or 5.3mM potassium both in the presence and in the absence of 50µm barium and in the presence and absence of 0.1µM gramicidin while imaging.

3.4 MICROSCOPY

3.4.1 Confocal laser scanning fluorescence microscopy

Confocal laser scanning microscopes increase optical resolution. The laser beam scans across a visual field in a series of lines. These microscopes feature a pinhole that is positioned in the confocal plane of the lens. The pinhole aperture can be adjusted to eliminate light from above or below the focal plane, ensuring that only light from the focal plane is detected. Depth can be achieved by scanning and combining information from several different planes. A collimator is introduced to achieve concentricity of the laser light on its path towards the specimen. Rotating mirrors allow for light to be directed between the dichroic mirror and the objective (not shown in figure below). A dichroic mirror is a mirror that can reflect or transmit light according to its wavelength, allowing for excitation light to be reflected toward the objective and emitted fluorescence to be transmitted back through the dichroic mirror toward the detection system. Any residual excitation light that is reflected back by the sample is reflected again by the mirror, preventing it from reaching the detectors.

The detection system includes the pinhole aperture which allows light to pass to the detectors. Fluorescent light can be separated from reflected laser light by emission filters. Light reaching the detection system is amplified by a photomultiplier tube (PMT). PMTs detect photons emitted by the sample, amplify it around a million fold without introducing noise, and transform the light signal into an electrical one.

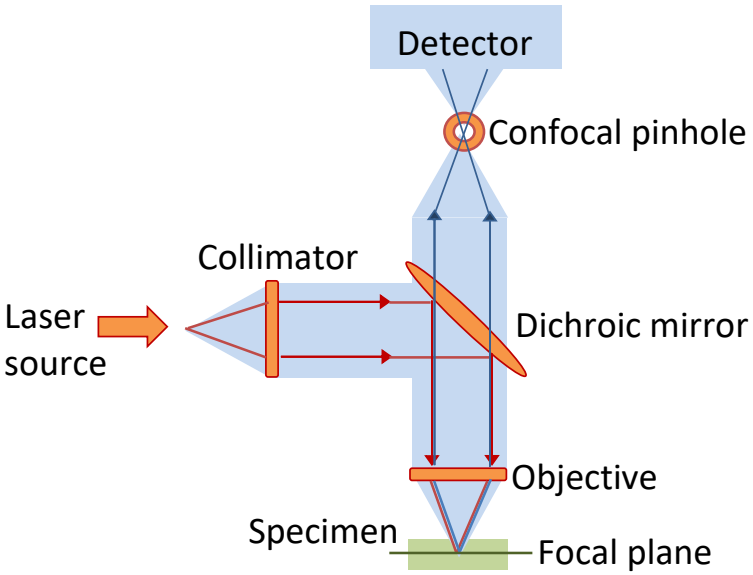

Figure 11: A confocal laser scanning fluorescence microscope. *Light from the laser source is concentralised by a collimator and travels via a dichroic mirror toward the specimen. Fluorescence at the focal plane is directed toward the confocal pinhole where other sources of light can be excluded and the fluorescence is detected.*

Different lasers are used to detect fluorescence signals of different wavelengths. Cells were typically stained with Fluo-4 and TMRM, which emit fluorescence at wavelengths of 488nm and 555nm respectively. A transmitted light detector was also used in some cases to produce bright field images, in particular for confirming the presence of striations in single muscle fibres.

3.4.2 Calcium imaging

Fluo-4 is a labelled calcium indicator used to follow spatial dynamics of calcium signalling. Cells are loaded with the AM ester form of the indicator (Fluo-4, AM). The Fluo-4 molecules increase in fluorescence upon binding to calcium ions.

3.4.3 Measuring mitochondrial membrane potential

TMRM is a cell-permeant dye that accumulates in mitochondria of healthy cells as a result of the difference in electrical potential between the mitochondrial matrix and the cytosol. If mitochondrial membrane potential decreases, TMRM accumulation is reduced and the resulting signal becomes faint or disappears.

3.4.4 Plasma Membrane potential assays

Changes in plasma membrane potential were studied in order to monitor the effects of the treatment with low potassium, barium and gramicidin.

I. FluoVolt

FluoVolt is a fluorescent sensor which acts by modulating photo-induced electron transfer via a synthetic molecular wire to a fluorophore (Miller et al, 2012). FluoVolt has an emission/excitation spectrum of 522/535nm.

Neonatal cultures were grown as described above. Differentiation medium was removed and cells washed twice in recording solution before loading with FluoVolt for 30m minutes. FluoVolt was removed by a further two washes before imaging by confocal microscopy. Changes in membrane potential were followed upon challenge with 40mM extracellular potassium.

II. FLIPR

Changes in membrane potential upon treatment with low potassium and barium, was investigated using a Fluorescent Imaging Plate Reader (FLIPR). This dye, the FLIPR Membrane Potential Assay Kit (Molecular Devices) has a negative charge and thus enters the cell upon depolarisation following an inflow of positive ions which create an inward current. Hyperpolarisation on the other hand results in a decrease in fluorescence as positive ions flow out creating an outward current, followed by an outflow of the dye. A quenching dye is also included in the kit to reduce background fluorescence. There are two versions of the quenching dye, a red quencher and a blue quencher, and thus two versions of the assay kit – the “red” kit and the “blue” kit.

Cells were grown and differentiated in a 96 well plate. Cells were bathed in HBSS with the membrane potential assay kit dye for half an hour before washing with 3 changes of HBSS without the dye. Cells were inserted into the FLIPR and control readings were collected for 10 minutes. Solutions were then switched to a range of conditions and

further readings were taken for a duration of two hours – they were tested with 0.5, 1, 2 and 5mM potassium, both in the presence and in the absence of 50µM barium. Finally solutions were returned to control conditions and recordings were taken for a further 30 minutes. This investigation was repeated with both the "blue" and the "red" versions of the plasma membrane potential assay kit.

3.4.5 Live cell imaging

All fluorescence images were obtained using a Zeiss (Oberkochen, Germany) 700 confocal laser scanning microscope with a 10×, 20x or 40× objective. Fluo-4, AM fluorescence was excited using a 488nm argon laser line, TMRM using 555nm and Hoechst using 405nm. Emitted light was collected at wavelengths of 510-553nm, 559-700nm and 426-700nm respectively. Fluo-4 AM was used for imaging intracellular calcium, TMRM as a mitochondrial membrane potential stain and Hoechst was used to stain the nuclei.

During live cell imaging, cells were kept in buffered physiological saline (recording solution) which consisted of 156mM NaCl, 3mM KCl, 2mM MgSO4, 1.25mM KH2PO4, 2mM CaCl2, 10mM D-Glucose and 10mM HEPES, and this solution was adjusted to pH 7.4 using NaOH or HCl.

Cells were loaded in the buffered physiological saline with TMRM and/or Fluo-4, AM for half an hour before imaging. TMRM was added both to the loading and the recording solutions at 25nM whereas Fluo4-AM was added at 5µM to the loading solution only, and washed off before imaging.

3.4.6 Live cell stimulation

Calcium release in response to several different stimuli was used to monitor calcium handling.

I. **High potassium**: High potassium leads to increased cytosolic calcium by depolarising the cell. Potassium was applied at 40mM.

II. **Caffeine**: Caffeine is an agonist for RyRs on the SR, and potentiates the release of calcium from the SR to the cytosol. Caffeine was applied at 10mM or less.

III. **Electrical stimulation**: A lid with two electrodes was placed on the culture dish and a series of electrical stimuli applied. The stimuli were as follows unless stated otherwise. Stimuli from 20 V up to 60 V were given as five 100ms pulses at a 1 Hz frequency increasing in 10 V increments with a 10 second gap in between each subsequent voltage.

3.4.7 Fixed cell imaging – Immunofluorescence

The presence and localisation of several different proteins was determined by immunofluorescence. The following antibodies were used to test for proteins: anti-fast skeletal myosin, anti-MyoD, anti-CaV1.1, anti-desmin and anti-IRK2.1.

Cells were seeded on glass coverslips and cultured as usual until ready for imaging. They were then fixed by washing twice with PBS and incubating at room temperature with 4% [W/V] formaldehyde for 10 minutes. Formaldehyde was removed by washing three times with PBS. Cells were incubated for 5 minutes and washed three times over 10 minutes with a permeabilising solution of 0.2% [V/V] Triton X-100 in PBS. At this point the antibody was added at the concentration indicated by the manufacturer in an antibody dilution media of PBS with 3% BSA and 0.2% Triton X-100. 50 µL were added per coverslip and incubated for 60 minutes. The antibody solution was removed by four changes of the permeabilising solution over 10 minutes, and labelled secondary antibody was added in the antibody dilution media at the concentration indicated by the manufacturer. A goat anti-mouse IgG conjugated to alexa Fluor 555 was used as a secondary antibody for both myosin and MyoD. As well as the labelled secondary reagent, Phalloidin conjugated to Alexa Fluor 488 was added to some coverslips at this point for imaging actin filaments. 50µL of secondary solution was added per coverslip, and coverslips were incubated for 30 minutes in the dark. The secondary solution was removed by three changes of permeabilising solution over 5 minutes, and Hoechst was added to the last wash at a

concentration of 5µg/mL and incubated for 5 minutes. After one final wash, coverslips were mounted onto coverslip slides using Fluoromount mounting medium and sealed with clear nail varnish.

As with live cell imaging, all immunofluorescence images were obtained using a Zeiss 700 confocal laser scanning microscope with a 10×, 20x or 40× objective.

3.5 WESTERN BLOTTING

Expression of proteins can be tested by Western blotting. Protein from cells is extracted and separated out in bands along a gel according to size. The protein bands are then transferred to a nitrocellulose membrane and incubated with a primary antibody that targets the protein of interest. An enzyme labelled secondary antibody which associates with the primary antibody is applied. A substrate for the enzyme is then added to produce a detectable product. Relative amounts of the protein of interest can then be detected in each band. The protein identity is confirmed by the position it takes along the band, which is related to the protein size.

For Western blotting cells were differentiated as described in section 3.3.1. Following trypsinisation cells were spun down and re-suspended in PBS, and spun again in order to remove supernatant. RIPA lysis and extraction buffer and PMSF protease inhibitor were added to the pellet (at a ratio of 100:1) and triturated and left on ice for 25 minutes. The solution was then spun at top speed for 5 minutes to remove solubilised protein (supernatant retained).

At this stage the protein content of each sample was tested so that equal amounts of protein could be added to each well of the gel. A BCA Protein Assay Kit was used for this test, according to manufacturer's instructions. 20 µg of each sample was mixed with 10µL loading dye (RIPA buffer with 5ul β-Mercaptoethanol and LDS sample buffer) and put in a thermomixer at 800 RPM at 99^{o}C for 5 minutes. The samples were then added to wells of a 4-12% polyacrylamide gel in a solution of MOPS SDS running buffer with a protein ladder in one of the wells. The gel was then run at 100 volts for approximately

two hours, until the dyes moved to the end of the gel. Proteins from the polyacrylamide gel were transferred to a PVDF membrane by placing them between two sets of filter papers and electrodes and applying an electric field of 20 volts for one hour, in a solution of transfer buffer with 20% methanol.

Membrane used in western blotting have a high affinity for proteins. Non-specific sites were therefore blocked by rocking in a solution of PBS with 0.01% TWEEN 20 and 5% milk for one hour. Primary antibodies were then applied at a dilution indicated by the manufacturer in the milk buffer and rocked overnight. Primary antibodies used in this study include an IRK2.1 antibody and a TFAM antibody. The membrane was then washed in PBS with 0.01% TWEEN 20 for 5 minutes, changing solution twice. Before applying secondary antibodies (at a dilution indicated by the manufacturer) in the PBS/TWEEN solution and incubated at room temperature for one to two hours and washed before developing.

The ECL western blot detection kit was used to view bands on the membrane in a ChemiDoc machine. The membrane was then washed again and treated with another primary antibody anti GAPDH as a loading control to determine relative changes in the primary antibody of interest in the different bands.

3.6 COMPLEX ACTIVITIES

Complex activities were analysed as described in Hargreaves et al (1999). Briefly, muscle biopsies were homogenized on ice, using a pre-chilled glass hand-held homogenizer. Briefly, the biopsies were homogenized 1:9 (w/v) in: 320mMol/L, 1mmol/L ethylenediamine tetra acetic acid dipotassium salt, and 10mmol/L Trizma-base, pH 7.4.

Mitochondrial respiratory chain enzyme and citrate synthase (CS) activities were determined in muscle homogenates which had been subjected to three cycles of freeze thawing to lyse the mitochondrial membranes by spectrophotometric enzyme assay as described in the study by Duberley et al (2013).

Complex IV (cytochrome c oxidase; EC 1.9.3. 1) activity was measured by the potassium cyanide sensitive oxidative of reduced cytochrome c at 550nm. CS (EC

2.3.3.1) activity was determined by the formation of 5-thio-2-nitrobenzoic following the incubation of tissue homogenate with acetyl-CoA, oxaloacetate and 5,5¢-Dithiobis-(2-nitrobenzoic acid). 5-Thio-2-nitrobenzoic absorbs at 412nm. Complex IV activity was expressed as a ratio to CS (mitochondrial marker enzyme) activity to account for the mitochondrial enrichment of the sample (Selak et al, 2000).

Complex I (NADH:ubiquinone reductase; EC 1.6.5.3) activity was measured by the rotenone sensitive oxidative of NADH at 340nm. Complex II/III (succinate: cytochrome c reductase; EC 1.3.5.1 + EC 1.10.2.2) activity was measured by antimycin A sensitive succinate dependent reduction of cytochrome c at 550nm.

3.7 FLOW CYTOMETRY

Flow cytometry or Fluorescence Activated Cell Sorting (FACS) can be used to count and analyse thousands of particles at a time, and as such may be a useful tool for assessing cell fusion. Each particle (in this case each cell) that passes through the machine, is exposed to a laser beam and causes the light from this beam to be refracted. Some of the light is refracted a little but still moves in a forward direction and is detected as “forward scattered light”. Some light is refracted more so that it hits detectors that are orthogonal to laser beam and such light is considered as “side scattered light”. Light that is not refracted is blocked by an obscuration bar and thus not detected. The forward scattered light provides an indication of overall cell size while the side scattered light is associated with internal cell complexity. In addition fluorescence staining can be quantified per particle. Flow cytometry is used here to detect PI fluorescence staining per particle. This indicates the relative quantity of nuclear material present in each detected particle, such that particles with more PI staining are assumed to contain a greater number of nuclei.

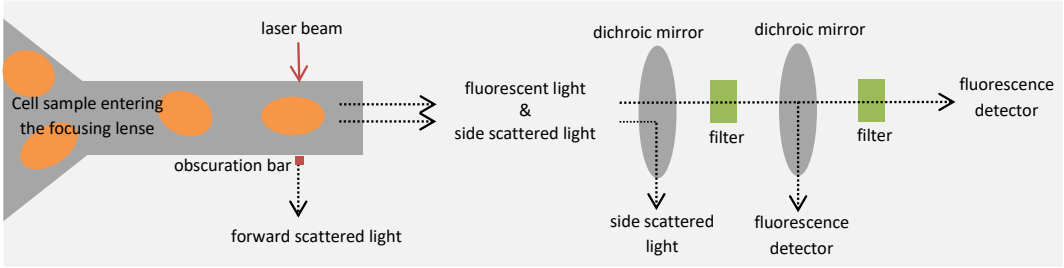

Figure 12: A flow cytometer. *In a flow cytometer, cells are delivered single file into a chamber where they cross the path of a laser beam. Light from the beam is detected according to the manner in which it is scattered, where more sideways scattered light is correlated with internal cell complexity, and forward scattered light with cell size. Light that is not scattered at all is obscured.*

FACS was used to quantify cells with single and those with multiple nuclei. Cells were stained in a solution of 2, 10 or 20 µ g/mL propidium iodide (PI), a marker of nuclear DNA, and passed through the FACS machine (BD Accuri, Michigan). PI is commonly used in cell cycle analysis to quantify cells at different stages of the cell cycle. The DNA mass per particle indicates the number of copies of DNA per cell and can be used to determine whether the cell is in G0/1 phase (where DNA is in use and thus not replicated), G2/M phase (where DNA is doubled) or in S phase (where DNA is partially replicated).

Cell preparation: Cells were first cultured as described above, and then trypsinised as for subculture. They were then centrifuged and the supernatant was discarded and cells re-suspended in PBS (while triturating to avoid clumping of cells). After centrifuging (5 minutes at 300 *g*) again and re-suspending in 0.5mL PBS, cells were added drop wise to 4mL of cold (-20^{o}C) 70% ethanol. This was done while vortexing to ensure that cells did not aggregate during fixation. Cells were stored for a minimum of 2 hours at -20 before centrifuging (5 minutes at 300 *g*) and discarding ethanol. Cells were re-suspended in 5mL PBS and centrifuged one last time (5 minutes at 200 *g*) before being re-suspended in 1mL PI staining solution and incubated at 37^{o}C for 15 minutes.

Cells were detected as they passed through the FACS machine. The distribution of cell size and density was determined by detecting forward and side scatter of light. PI levels were determined using an FL2 laser (Hamamatsu, Japan).

3.8 IN VIVO STUDIES

In vivo investigations were performed in order to test the Draggen model for similarity to the human PP phenotype. This was part of a study performed at Harwell to verify the characterisation of their model. Tension tests indicate muscle strength, motor neuron count indicates condition of the nervous system, and fatigue investigations test whether or not endurance is affected.

3.8.1 Mouse preparation

70 to 80 week old mice were used. Mice were anaesthetised with chloral hydrate, at 1 μ L/0.1*g* mouse, which takes approximately 2 minutes to take effect. The responsiveness of each mouse was assessed by monitoring flinching (when its toe was pinched) or blinking (when its eye was stoked). If a response was seen, chlorohydrate was topped up at a quarter of the original dose. Once anaesthetised, the animal's lower body was shaved, and its hind limbs were skinned. The tibialis anterior (TA) and flexor hallucis longus (FHL) tendons were then loosened, the EHL was cut, and the TA tendon was tied just below the TA muscle. The extensor digitorum longus (EDL) was then exposed and tied in a similar manner. The sciatic nerve was exposed and cut off, and the muscles and nerve were protected with moist cotton wool. The mouse was secured to a board, and the TA and EDL threads were attached to gauges while the sciatic nerve was connected to an electrode

3.8.2 Tension tests

In order to check if muscle strength was affected, the level of tension was compared in Draggen and control mice. The muscle was stimulated via the sciatic nerve, and contraction was quantified via the gauges which were connected to electronic transducers. An initial tetanic stimulation relaxed the muscle, and then the tension was adjusted manually to achieve maximal twitch response. Tension

responses to a single pulse and to tetani at 40, 80 and 100 Hertz were recorded for TA and EDL.

3.8.3 **Motor neuron count**: In order to monitor changes in cell signalling, the number of motor neurons was compared in Draggen and control mice. The number of motor neurons that innervate the EDL was quantified by changing the voltage in small increments, while continually stimulating the muscle. Because the muscle contracted proportionally to the amount of motor neurons stimulating it, the amount of bands that resulted could be taken as an estimate of the number of motor neurons that were stimulated. Therefore, the number of motor neurons could be estimated. Control mice typically have near to 30 bands corresponding to 30 motor neurons connecting the sciatic to the EDL.

3.8.4 **Fatigue tests**: In order to check if the time taken for muscle to fatigue is affected, changes in response to repeated stimuli were monitored in Draggen and control mice. Tetanic responses to repeated stimulations were then recorded and quantified. Stimulations were produced at 40 Hz, each lasting 251ms, at a rate of 1 cycle per second for 180 seconds.

3.9 EX VIVO STUDIES

3.9.1 **Tissue isolation:** P20 mice were euthanised, and hind limbs were sprayed with 70% ethanol. The flexor digitorum brevis (FDB) is a superficial muscle in the sole of the paw arising from the tendon of the plantaris. The FDB was isolated in PBS with 10% P/S (dissecting solution) and transferred to a tube containing 0.2% type I collagenase. The tissue was incubated at 37^{o}C for 90 minutes with gentle agitation. It was then incubated in DMEM with 10% FBS and 1% P/S for 30 minutes. The muscle was then carefully triturated using a polished thin-bore Pasteur pipette in order to separate individual fibres directly into 35mM FluoroDish (World Precision Instruments, FD35) dishes loaded with 10% matrigel reduced factor. Fibres were allowed to settle in a maintenance medium of 20% serum replacement solution in DMEM with 1% P/S.

3.9.2 Single fibre imaging

Single fibres were imaged after 24 hours, by confocal microscopy. Mitochondrial membrane potential was studied by confocal microscopy using TMRM and analysed using Fourier transform techniques (see section 3.9.3). Calcium handling was followed during electrical stimulation (as described in section 3.4.6 III.) of the fibres loaded with Fluo-4.

3.9.3 Fourier transform analysis

A Fourier transform calculates the amplitudes and frequencies of the different components of a signal. In an image, this gives an analysis of frequency distributions in space and intensity, generating a quantitative analysis of repetitive patterns in the image. The Fourier tranform image contains all the information required to make the original image, such that repeating a Fourier transform of the image will reproduce the original image. Therefore certain components of the original signal can be removed from the transformed signal, and the Fourier transform repeated in order to produce the original image with the correlating components missing. In this way the the subsarcolemmal mitochondria can be removed to produce an image of the intermyofibrillar mitochondria, or vice-versa (see below). Fourier transform has been used to analyse TMRM staining in muscle in other work, although using different methodology, and with different aims (Venable et al, 2013).

Mitochondria can be found in muscle fibres in two different subcellular populations, one that runs along the fibre's striations, called the subsarcolemmal mitochondrial population, and another that runs along the length of the fibres, which is referred to as the intermyofibrillar mitochondrial population (Smith et al, 2013). These subcellular populations were distinguished by Flourier transform analysis.

Fourier transform analysis was carried out using Image J. The Fourier transforms had strips at 90^{o} to each other, representing periodic signals in the original figures. Blocking out the strip correlating to intermyofibrillar mitochondria and repeating Fourier transform resulted in a figure showing the subsarcolemmal

mitochondria only, and vice-versa. Figures (A) and (B) show a sample original image of a single fibre with TMRM staining, and the associated Fourier transform. Figures (C) and (D) show the Fourier transform with the area associated with subsarcolemmal mitochondria blocked off, and the resulting image of intermyofibrillar mitochondrial. Conversely, figures (E) and (F) show the Fourier transform with the area associated with intermyofibrillar mitochondria blocked off, and the resulting image of subsarcolemmal mitochondrial.

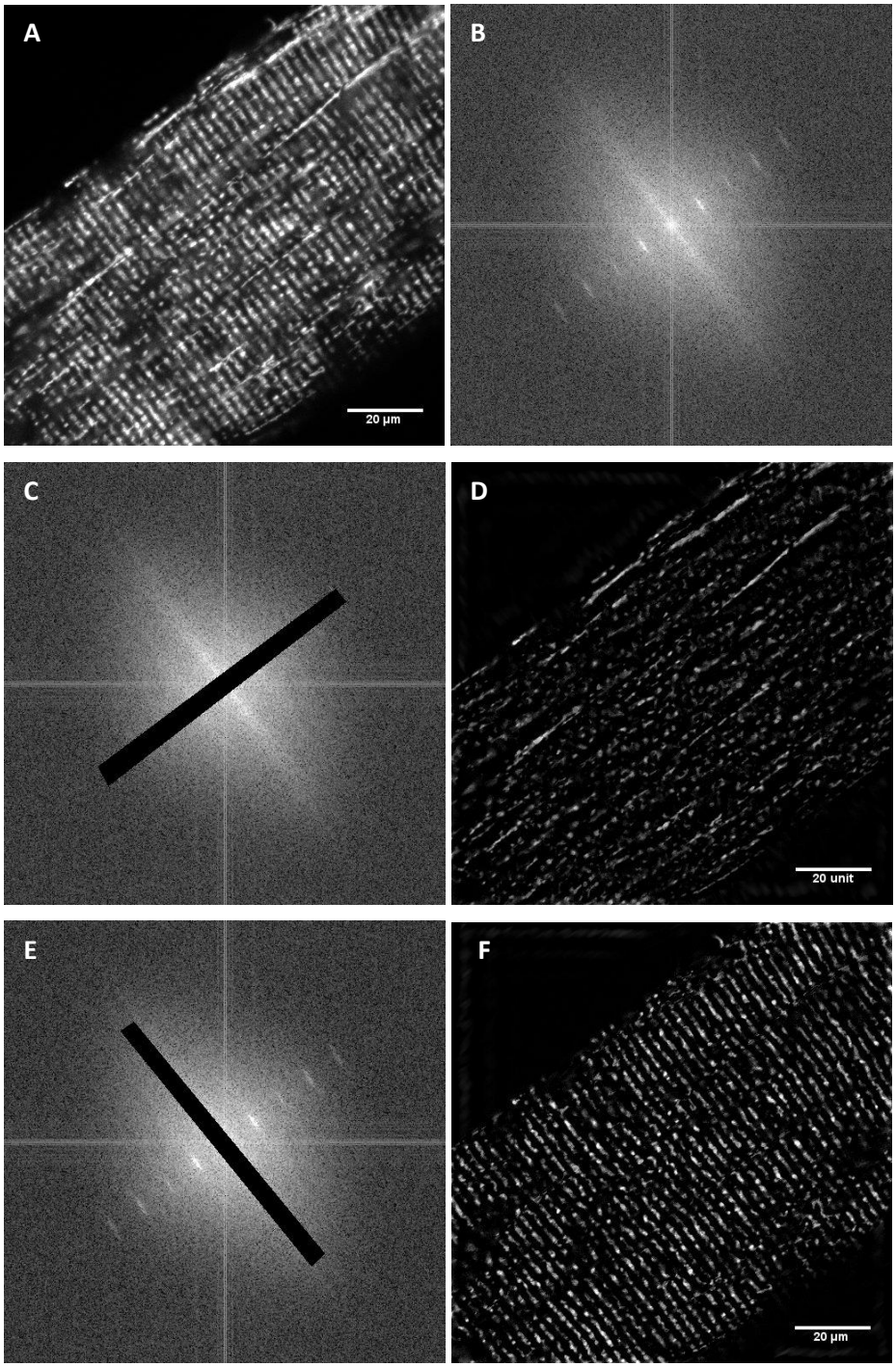

Figure 13: Fourier transform analysis. *Example of Fourier transform analysis of mitochondrial structure. (**A**) Original TMRM staining of a muscle fibre from FDB muscle of a Dgn mouse. (**B**) The transformed image. (**C**) Areas of the transform that correspond to subsarcolemmal mitochondria are obscured. (**D**) Intermyofibrillar mitochondria, produced by reverse-transform of C. (**E**) Areas of the transform that correspond to intermyofibrillar mitochondria are obscured. (**F**) Subsarcolemmal mitochondria, produced by reverse-transform of E.*

3.10 ELECTROPHYSIOLOGY

Fresh patch pipettes were made on the day of recording using borosilicate glass capillaries. Thick walled capillaries were used for whole cell patching (GC150F-7.5, Harvard Apparatus) and thinner ones with a filament for sharp electrode patching (30-0056F, Harvard Apparatus). Capillaries were polished briefly with a Bunsen burner to smooth ends and ensure they did not damage the electrode holder. The patch-pipettes were then fabricated in an electrode puller (Narashige PC10, Tokyo, Japan), producing thin tipped electrodes of 4-7MΩ for whole-cell recordings and 22-30 MΩ for sharp electrode recordings.

Cover slips were positioned in the centre of the chamber. An external solution was applied to the bath by gravity driven perfusion. The external solution contained 125mM NaCl, 5mM/4mM/2mM/1mM KCl, 1.8mM $CaCl_2$, 1mM $MgCl_2$, 25mM glucose and 10 HEPES, (pH 7.4, NaOH). Pipettes were filled with a filtered solution (0.2µm) containing 150mM Na Gluconate, 10mM HEPES, 10mM EGTA, 1mM $CaCl_2$, 1mM $MgCl_2$, 5mM Glutathione and 1mM ATP/ (pH 7.2 with NaOH). Currents were recorded at room temperature.

An isolated yet anchored cell was selected and approached by the electrode while applying positive pressure (to remove dust and cellular debris from the pipette tip). The pipette was moved down till contact was made with the cell, and negative pressure was applied to draw the membrane onto the patch pipette. Once a tight electrical seal had been achieved (cell attached mode), further negative pressure was applied, along with short pulses of suction. This ruptured the membrane allowing direct electrical access to the inside of the cell (whole-cell mode).

The whole-cell capacitance and series resistance were estimated for whole cell investigations via the capacitance transients produced by a 5mV test pulse and the series resistance compensation circuit set to 80% compensation, and a computer controlled voltage-clamp protocol was initiated, where the membrane voltage was ramped (using WinWCP: Strathclyde Electrophysiology Software

V4.4.1.) at a rate of 100mV/s. After observing several control sweeps, control solution was replaced by a solution with low potassium, to test if this produced a change in the I-V relation of the cell. For Sharp electrode investigations recordings were made at a constant membrane potential value (V_m) which was achieved by setting current at zero and recording voltage on the screen. After achieving a seal, the cell was allowed to stabilize for 15 minutes, and thereafter each condition was allowed to equilibrate for at least 5 minutes before taking a reading.

3.11 DATA ANALYSIS

Data analysis was performed using Image J for live cell imaging and using C-Flow Plus for FACS investigations. Fixed, stained cells were counted directly while imaging. Data were then analysed using Microsoft Excel 2010 and GraphPad Prism 7. Statistical significance of the differences between two sets of results was assessed by unpaired Student's t-test. Where more than two sets of results were being compared I used analysis of variance (ANOVA). One-way ANOVA tests were carried out where one factor was being compared and two-way where two factors were compared. Groups which were significantly different according to the ANOVA test were identified by post hoc Tukey's test. Error bars represent the mean +/- standard deviation (SD) or standard error of mean (SEM). Differences were considered to be statistically significant if the Student's t-test or ANOVA test produced a probability value of less than 5% ($P < 0.05$).

4. RESULTS

4.1 MUSCLE DISEASE INVESTIGATION USING FIBROBLAST DERIVED MYOTUBES

At the Institute of Neurology we have access to patients with PP and thus have the opportunity to harvest patient specific skin biopsies. These provide a resource for investigating the effects of a range of mutations responsible for PP and other muscle diseases. However the PP mutations are expressed in skeletal muscle whereas the skin biopsies provide fibroblasts. In this chapter I describe how I optimised the process of generating myotubes from fibroblasts, and, to that end, developed methods of monitoring the efficiency of myotube formation.

4.1.1 Evaluation of transduction with MyoD using lentivirus or adenovirus

Investigations were carried out with both control and patient derived fibroblasts. Patient cells were taken from a 64 year old male with an M1592V mutation who experienced symptoms of HyperPP. Myoblasts were produced by viral application of MyoD-ER in order to transfect the fibroblasts with MyoD. Two viral vectors, an adenovirus and a lentivirus, were used to deliver the transcription factor MyoD. The adenoviral vector was acquired from The Native Antigen Company (Ad5.f50.AdApt.MyoD). The lentiviral vector was prepared as described in methods section 3.2.1 and in Kimura et al (2008).

The efficiency of transfection was measured by immunofluorescence using an anti-MyoD antibody to stain cells which were then assayed using confocal microscopy. Cells were fixed and stained three days after application of the virus when MyoD expression reaches its peak (Fujii et al, 2006). All nuclei were labelled with Hoechst, I then counted the MyoD positive nuclei as a fraction of the total number of nuclei to determine the percentage of successfully transfected cells. An adenovirus (AV) was first tested with poor results, yielding a transfection efficiency of only 6.2% (n=4; MyoD expression was measured in 100 cells per preparation for four separate preparations). The lentiviral (LV) construct was then tested with improved results, with a transfection efficiency of 31.7% (n=4; MyoD expression was measured in 100 cells per preparation; four separate preparations were tested). I applied the lentiviral vector onto fibroblasts once they were all fully adherent, at approximately 90% confluence and 0.1μM tamoxifen at full confluence. Although the proportion of MyoD expressing cells was improved when using the LV compared to the

AV, it was still low. Other methods of improving efficiency could include transfection at different confluency of cells, or with higher concentrations of the virus or the tamoxifen. Indeed 1mM Tamoxifen has been successfully used in similar protocols, producing cultures of predominantly myogenic cells (Tedesco et al, 2012; Gerli et al, 2014; Maffioletti et al, 2015).

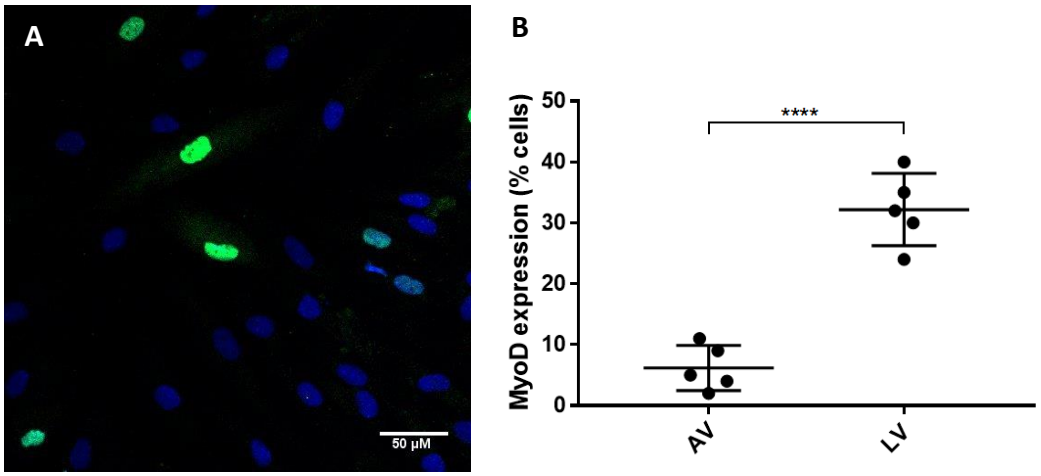

***Figure 14: MyoD expression – with adenovirus (AV) or lentivirus (LV)**. **(A)** Sample micrograph of myocytes stained with a MyoD antibody (green) and with Hoechst (blue). Cells were fixed three days after application of AV. **(B)** Scatter plot showing the mean relative levels of MyoD expressing cells ± SD three days after treatment with AV (6.2 ± 3.7 %) or activation of LV (31.7 ± 5.9 %). Error bars indicate the standard deviation. Cells were imaged using a Zeiss 700 microscope with a 20x objective. N = 5; 100 cells were counted per preparation and five preparations were tested per condition. The difference in MyoD expression is statistically significant. ****P < 0.0001, unpaired t-test.*

4.1.2 Determining the optimal culture conditions for differentiation

In subsequent experiments LV was used as the choice vector for transduction. I then sought cell culture conditions that would encourage higher levels of cell differentiation. Upon removal of the virus several different culture conditions were assessed in order to optimise myoblast to myotube differentiation. Although 2% horse serum (HS) is conventionally used for differentiation of myoblasts to myotubes, it has been argued that serum is not the most effective method for promoting this differentiation (Shoko et al,

1999). HS and serum free media were therefore compared. Cells were cultured either in DMEM with 2% HS or in SupM, a serum free medium supplemented with various growth factors to encourage differentiation. SupM includes insulin (Florini et al, 1989) and creatine (Deldicque et al, 2007) to encourage differentiation. It also contains BSA and EFG for the maintenance of myotube cultures (St Clair et al, 1992) and glutamine which can help to rescue suppressed differentiation (Girven et al, 2016).

In addition, a collaborator observed that retaining half of the medium by only ever replacing half of it at a time, improved differentiation of her neonatal myocyte cultures prepared using CD-1 and C57BL-6 mice (Falcone, personal communication). Such a manipulation may be effective due to retention of growth factors that are important for differentiation within the medium. Therefore, the benefit of changing half rather than all of the medium in each well during differentiation was assessed for the fibroblast-derived myotubes (figure 16 and 20). Growth factors that are known to influence differentiation include fibroblast growth factor (FGF) and transforming growth factor-β (TGF-β) which inhibit differentiation, and insulin or insulin like growth factors (IGFs) which stimulate differentiation (Florini et al, 1989). Retaining part of the medium likely allowed for more IGFs to be retained and thus for differentiation to be promoted. HS does contain an IGF (Prosser and McLaren, 1992), and the SupM was supplemented with insulin, so both media already provided cells with this aid to differentiation. Nevertheless retention of the medium might allow cells to further accumulate IGFs and other factors that aid differentiation.

In order to identify conditions that were optimal for production of myogenic cultures, cells containing three or more nuclei were considered to be myotubes, and indeed such myotubes did form during the treatments detailed above.

As demonstrated in figure 14B, 31.7% of cells transduced with the LV expressed MyoD. Transfected cells were initially grown in proliferation medium, and upon reaching confluency, were transduced with tamoxifen. 24 hours after application of tamoxifen the proliferation medium was replaced with a differentiation medium. I tested whether the level of MyoD expression could be further improved by using SupM as a differentiation medium rather than 2% HS for the first few days of differentiation; however when SupM

was used instead of the HS medium, only 11% of cells expressed MyoD rather than 32% with HS (figure 15). 2% HS medium was therefore the choice differentiation medium during tamoxifen aided activation of MyoD expression. Transfection and differentiation methods using LV and AV are outlined in table 5, page 82.

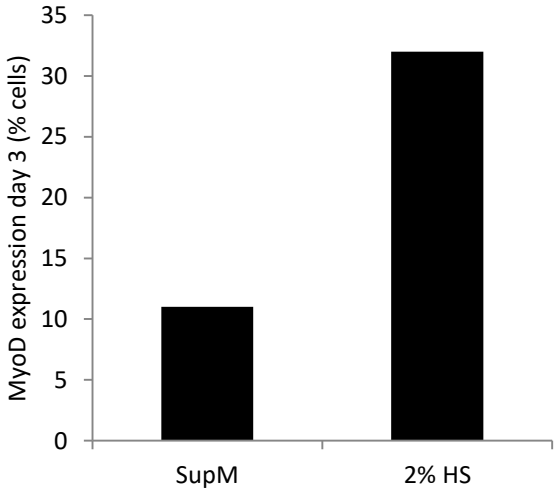

Figure 15: MyoD expression following treatment with supplemented medium (SupM) or horse serum (HS)*. Cells were fixed three days after activation of the lentivirus using tamoxifen. Cells were stained with a MyoD antibody and with Hoechst. This figure shows relative levels of MyoD expressing cells following three days of culture in either SupM (11%) or 2% HS medium (32%). N = 1; 100 cells were counted per preparation with one preparation monitored per condition, where each condition was tested once.*

Taking data from figure 15 into account, cells were treated with 2% HS for the initial 3 days following tamoxifen application in order to encourage higher levels of MyoD expression. Following these three days, cells were cultured for a further seven days before fixation. I tested what culture conditions encourage the highest levels of differentiation during these seven days. I tested four different conditions; complete changes of SupM, complete changes of HS medium, part changes of SupM in order to retain half of the medium and part changes of HS medium. The level of differentiation was assessed by counting the number of cells expressing Myosin. 100 cells were observed per condition. Those treated with complete changes of the SupM had the highest proportion of Myosin expressing cells upon fixation (29%), compared to less than 20% for each of the other conditions (figure 16).

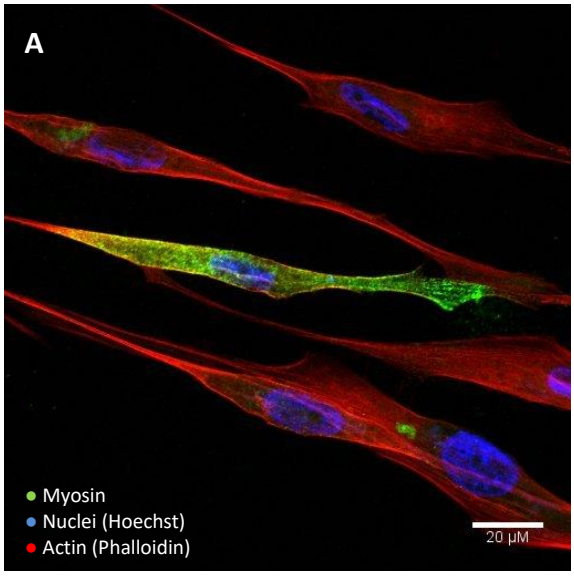

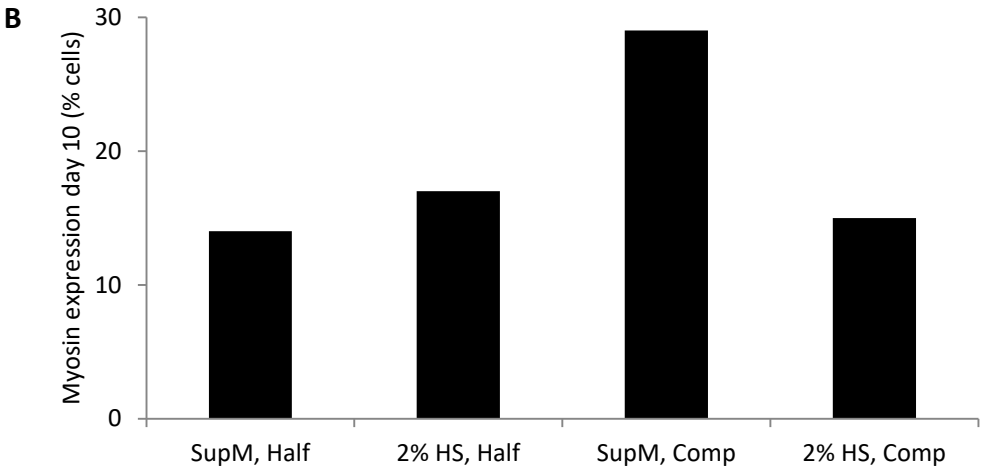

Figure 16: Myosin expression*. Cells were cultured in 2% HS for the initial three days following application of tamoxifen (where tamoxifen was used for activation of the lentivirus-delivered MyoD expression). Cells were then differentiated for seven days with either supplemented medium (SupM) or with 2% horse serum (HS). In addition, during treatment either half medium was replaced at a time (Half) or all of the medium (Comp). (**A**) Sample micrograph of fixed stained cells that were treated according to a "SupM, Half" protocol. Myosin was detected by antibody staining (green), actin by phalloidin staining (red) and nuclei with Hoechst (blue). Myosin was detected using a mouse anti-fast skeletal myosin antibody (SIGMA, M1570) (**B**) Bar graph showing relative levels of myosin expression under the four different conditions. N = 1; 100 cells were counted per preparation with one preparation monitored per condition, where each condition was tested once.*

In cases where SupM was not used, the proportion of myosin expressing cells (figure 16B) is lower than the proportion of MyoD expressing cells (figure 15). This suggests that MyoD negative cells have a proliferative advantage over MyoD positive cells. It has indeed been observed that MyoD has a negative effect on proliferation (Olson et al, 1992). This effect was rescued in cultures that were treated with SupM following the 3 days of HS treatment. It may be that factors in the SupM rescue cultures from the negative effects of MyoD. Together, figures 15 and 16 above suggest that myotube formation was most efficient when HS was used for the first three days (figure 15) followed by complete medium changes of SupM every 2-3 days (figure 16). This treatment protocol is summarised below in table 5, alongside the protocol used when transducing with the adenovirus.

	AV	**LV**
Pre-proliferation step	-	Incubate cells that are 90% confluent in LV for 24 hours, then grow and subculture according to need
Proliferation	Seed cells and grow in 10% FBS until confluent, changing medium every 1-2 days	
Viral transduction	Incubate in 10% FBS with AV for 4-5 hours	Incubate in 10% FBS with 0.1µm 4-OH tamoxifen for 24 hours
Further transduction	-	Incubate in 2% HS with 0.1µm 4-OH tamoxifen for further 24 hours
Differentiation	Change to 2% HS	
Further differentiation	After 3 days change to SupM and change it every 2-3 days	After two days change to SupM and change it every 2-3 days
Test	Test after 7 to 10 days	

***Table 5**: **AV and LV transduction.** The table charts two different protocols for transducing fibroblasts with MyoD and differentiating the transduced cells into myotubes. One approach uses an adenoviral vector (AV) and the other a lentiviral vector (LV).*

Expression of muscle specific proteins was recorded in order to confirm that the fibroblasts were truly converting to a myoblast phenotype. Figure 17 below shows cells stained with SERCA1-ATPase.

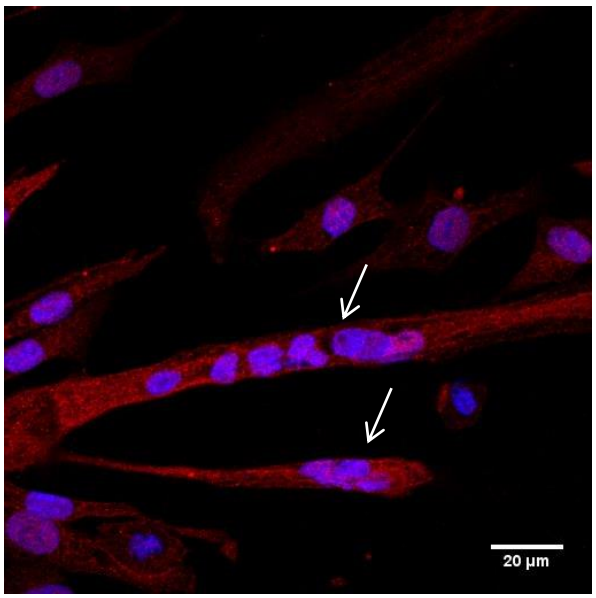

Figure 17: Myotube differentiation. *Micrograph showing nuclei (blue; Hoechst) and SERCA1 ATPase (red; antibody staining). White arrows indicate multinucleated cells. The culture contains a mixed population of fibroblasts and myotubes derived from fibroblasts, following transfection with a LV to deliver MyoD to cells. Cells were cultured in 2% HS for three days followed by SupM for a further seven days before fixation. Cells were imaged using a Zeiss 700 microscope with a 40x objective.*

Staining of the muscle specific protein SERCA1 ATP-ase, along with Hoechst (figure 17) and of myosin (figure 16A) confirm that treated cells were fusing and developing at least some muscle characteristics.

4.1.3 Culture conditions for optimal functional differentiation

Having established the optimal culture conditions with regard to expression of myogenic factors, I investigated how these culture conditions influence functional differentiation. The functional differentiation was assessed by monitoring how calcium handling was influenced. Although myoblasts display minor calcium fluctuations in response to depolarisation, myotubes characteristically display larger and faster calcium fluctuations

than myoblasts (Morabito et al, 2010). I found a good correlation between culture conditions that promoted successful expression of myogenic factors and those that promoted successful functional differentiation.

Cells were loaded with Fluo-4 as the AM ester, and images were acquired by fluorescence microscopy using a confocal microscope. Cells were stimulated with 40mM potassium in order to induce cell membrane depolarization. This develops because resting conductance is predominantly potassium selective, and the potassium equilibrium potential thus largely dictates the resting membrane potential. Initially there is a high concentration of potassium inside relative to outside of the cell and adding potassium to the extracellular solution reduces the outward flow of potassium ions. This shifts the potassium equilibrium potential in a positive direction sufficient to reach the threshold level for activation of voltage gated sodium and potassium channels. In a separate set of experiments cells were stimulated with 10mM caffeine, which acts as an agonist for the RyR and thus triggers calcium release from intracellular stores.

The dynamics of the calcium transients were monitored, in particular the rise time constant, the recovery time constant and the peak fluorescence levels reached. Results presented in this section indicate conditions that promoted the largest fluctuations of cytosolic calcium. These were treatment with 2% HS for three days following viral transduction, followed by culture in the SupM for a further seven days.

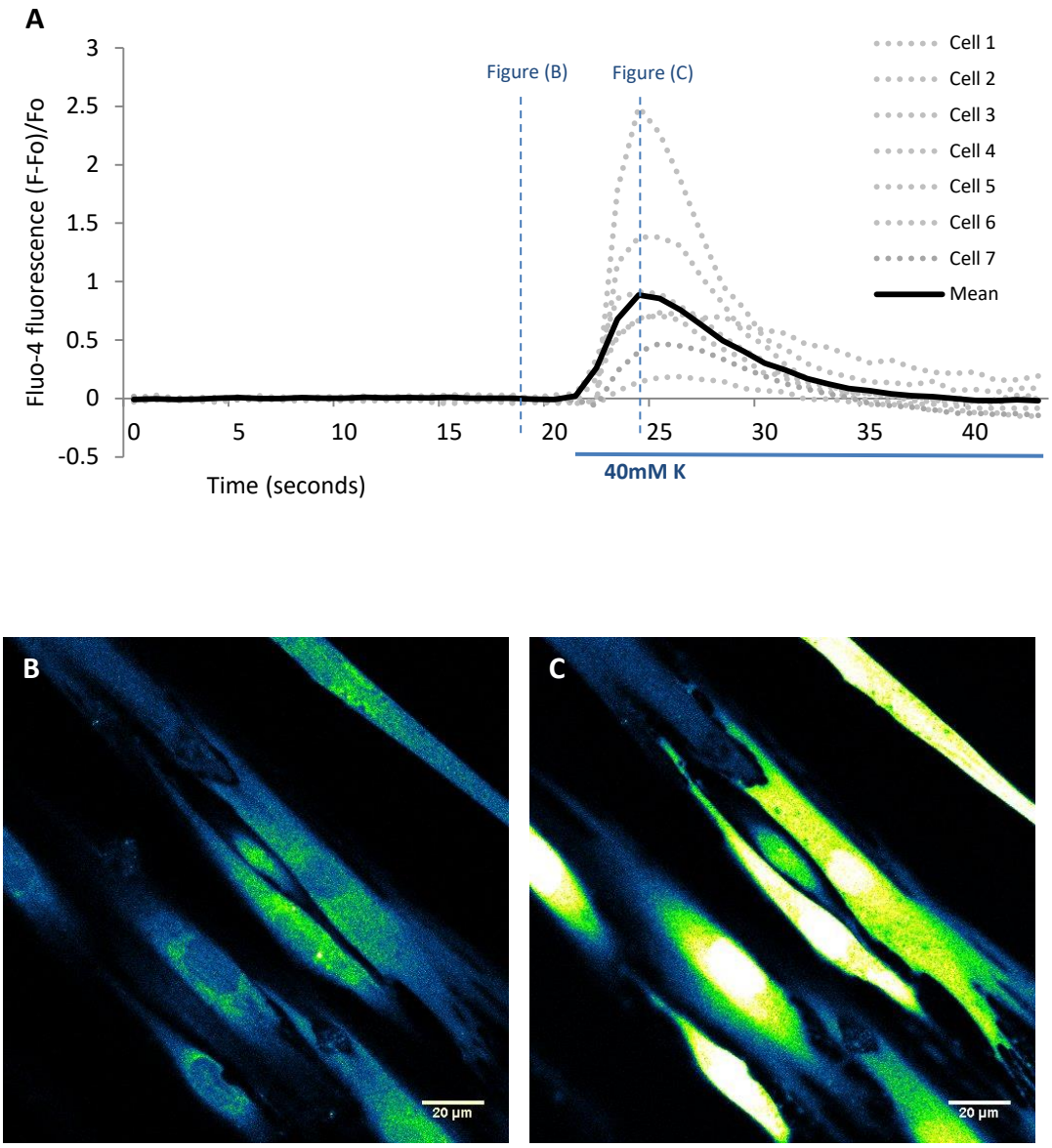

Figure 18: Response to stimulation with 40mM potassium*. An example of a response to application of 40mM potassium in myotubes derived from patient fibroblasts (MRC Biobank ID: L937/1264F). (**A**) Time line of calcium fluctuations in six cells. Cells were initially imaged for 20 seconds without any manipulation in order to identify any spontaneous activity. 40mM potassium was applied at 21 seconds as indicated, resulting in a rise in cytosolic calcium. Calcium concentration was determined by Fluo-4 fluorescence and values were normalised relative to the baseline levels. (**B**) Micrograph of myotube during the baseline period as indicated. (**C**) Micrograph of myotube at the peak of the response. Cells were imaged using a Zeiss 700 microscope with a 40x objective*

There is much variability in the cytosolic calcium levels reached during a calcium transient, as demonstrated in figure 18A. Imaging groups of cells, such as those in figure 18 allows for trends in calcium handling to be measured, however it is also important to minimise such variance in order to detect significant differences between control preparations and those carrying PP mutations. I worked on optimising culture conditions because healthier cultures display more uniform responses.

I tested whether differentiation in different media affect the function of the resultant cultures. In figure 19 I compare the use of SupM and HS medium between days 3 and 10 of differentiation. Results indicate that using SupM rather than HS medium during differentiation does not have a statistically significant effect on peak cytosolic calcium levels reached in response to the application of 40mM potassium, on rise time or on recovery time (figure 19).

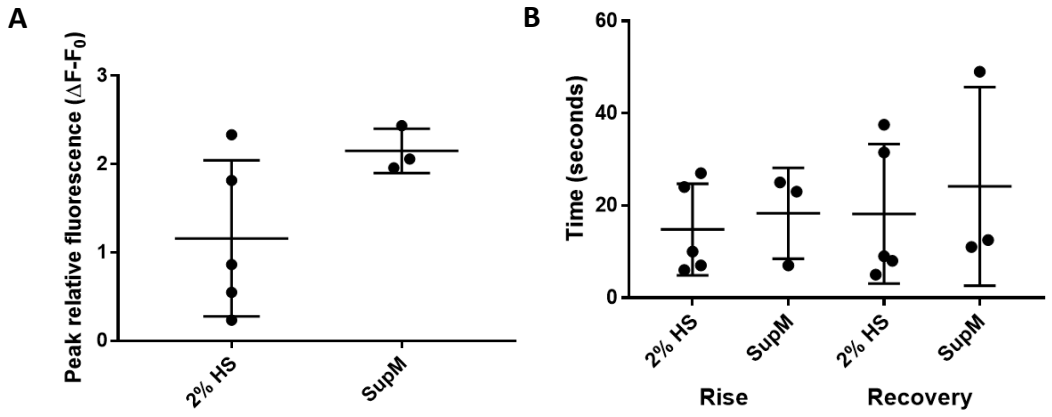

Figure 19: Calcium handling in myotubes treated with horse serum or supplemented medium*. Analysis of calcium handing in myotubes derived from patient fibroblasts (MRC Biobank ID: L937/1264F). Cytosolic calcium was detected by confocal imaging of Fluo-4. (**A**) Scatter plot showing peak cytosolic calcium following application of high potassium (40mM); peak is given relative to a baseline of one. Mean ± SD values are indicated for cultures treated with 2% horse serum (1.159 ± 0.8842) and for cultures treated with the supplemented medium (2.151 ± 0.251) (**B**) Scatter plot showing the rise and recovery time constants for the increase and decrease of cytosolic calcium in the cells. Mean ± SD values are indicated for the rise time (14.8 ± 9.935) and the recovery time (18.2 ± 15.1) of cultures treated with 2% horse serum and for the rise time (18.33 ± 9.866) and the recovery time (24.17 ± 21.52) of cultures treated with the supplemented medium. Differences in peak, rise time and recovery time are not statistically significant. Unpaired Student's t-tests, p = 0.11 for peak, and p > 0.6 for rise and recovery times. N = 3; five cultures were analysed for 2% HS treated cells and three for SupM treated cells. Between three and six cells were analysed per culture.*

Although comparison of differentiation in SupM and HS medium does not highlight any clear differences in calcium handling, I did find that cultures treated with SupM expressed higher levels of myosin (figure 16). I therefore had reason to believe that SupM might improve myogenicity. Myosin expression was only improved in cultures treated with complete changes of medium (figure 16). I went on to investigate whether retaining half of the medium during culture in SupM also improves physical characteristics of differentiation. As indicated in figure 20, peak relative fluorescence, rise time constant and recovery time constant were not significantly affected by retention of medium during culture. It may be that the increased level of growth factors achieved by retaining part of

the medium was not effective, because factors such as those that would be retained in the medium are already present in the SupM.

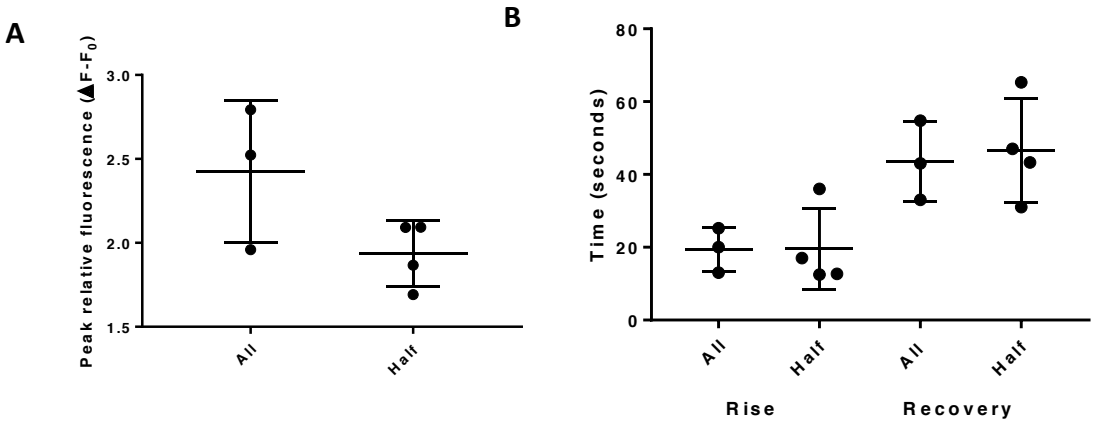

Figure 20: Calcium handling in cultures treated with complete or part medium changes*. Calcium handing analysis of myotubes derived from control fibroblasts (MRC Biobank ID: 8203). Cultures treated with full medium changes are compared to those where half of the medium was retained. Cytosolic calcium was detected by confocal imaging of Fluo-4. (**A**) Scatter plot showing mean peak cytosolic calcium ± SD following application of high potassium (40mM) for cultures that were treated with full changes of medium (2.425 ± 0.245) and for those where half of the medium was retained (1.936 ± 0.195). The peak is given relative to a baseline of zero. (**B**) Scatter plot showing the cytosolic calcium rise and recovery time constants ± SD for cultures treated with full changes of medium (19.42 ± 6.146 and 43.58 ± 10.89, respectively) and rise and recovery times for cultures where half medium was retained (19.54 ± 11.17 and 46.67 ± 14.2, respectively).*
Calcium handling was unaffected by the different treatments. Unpaired Student's t-test, P=0.4 for peak relative fluorescence, P = 0.987 for rise time and P = 0.768 for recovery time. N=3 for cultures where all medium was changed and N=4 for cultures where half medium was retained. Three or four cultures were analysed per condition, and three or four cells were analysed per culture.

4.1.4 Evaluating myogenicity of the fibroblast derived myotubes using myoblast derived myotubes

In order to further evaluate the production of myocyte cultures, I cultured an immortalised human myoblast cell line (MRC biobank ID: i7403) which was produced at Institut Pasteur, Paris (Zhu et al, 2007). This cell line has been shown to produce myotubes that express desmin, as well as embryonic, fast and slow myosin to a level

comparable to that seen in the original cell line (Zhu et al, 2007). I compared the calcium handling in myotubes produced from immortalised myoblasts to that of myotubes produced by transfecting fibroblasts. The close correlation in calcium handling suggests that successful development of muscle characteristics was achieved in the fibroblasts.

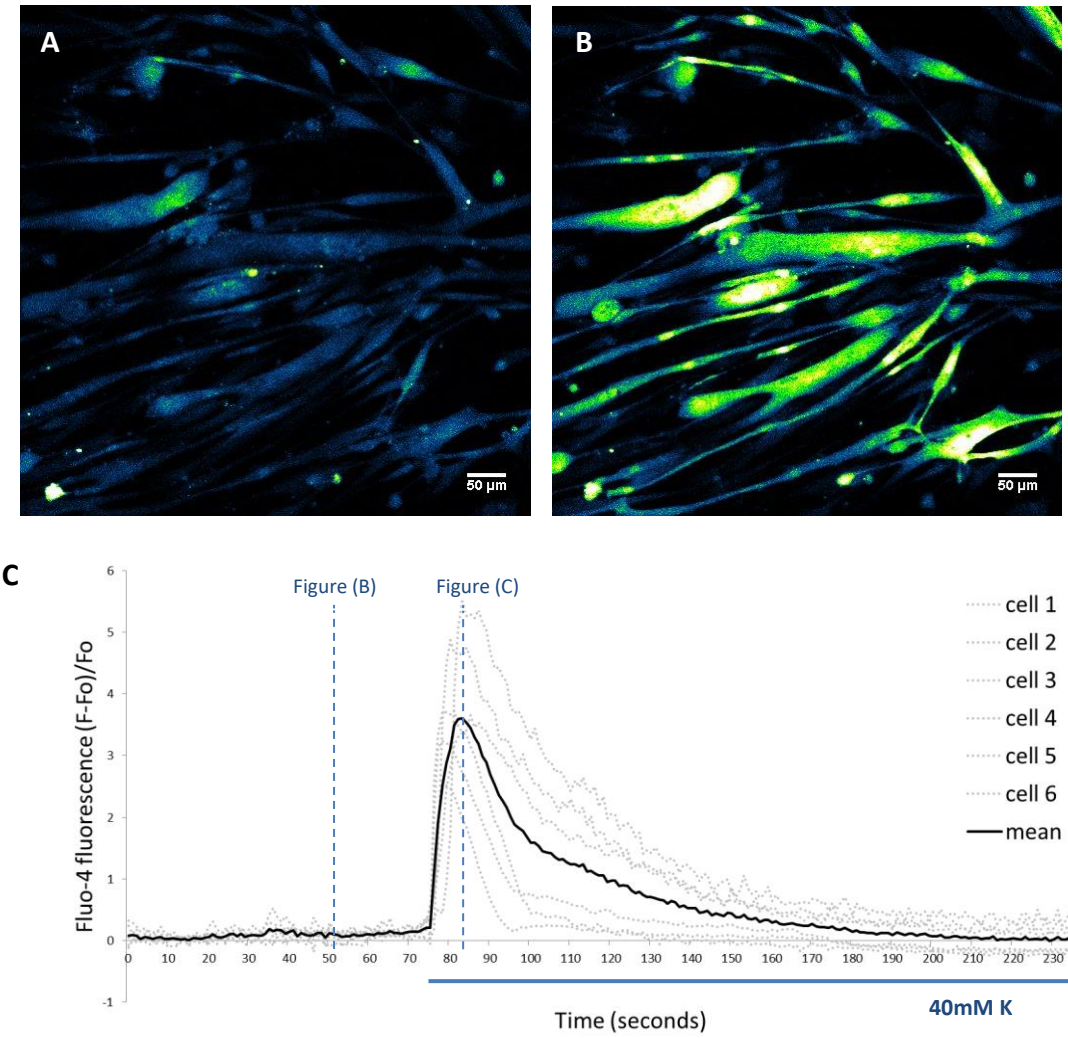

Figure 21: Calcium handling in myoblast-derived myotubes. *Calcium handling analysis of myotubes derived from control immortalised myoblasts (MRC biobank ID: i7403). Cytosolic calcium was detected by confocal imaging of Fluo-4. (**A**) Micrograph showing a representative image of the myotubes before application of high potassium (40mM). (**B**) Micrograph showing a representative image of the myotubes at the peak of the response upon stimulation.* (**C**) Line chart indicating Fluo-4 fluctuations in 6 cells from three separate cultures upon stimulation with 40mM potassium. The solid black line indicates the mean time course of the cell reaction.

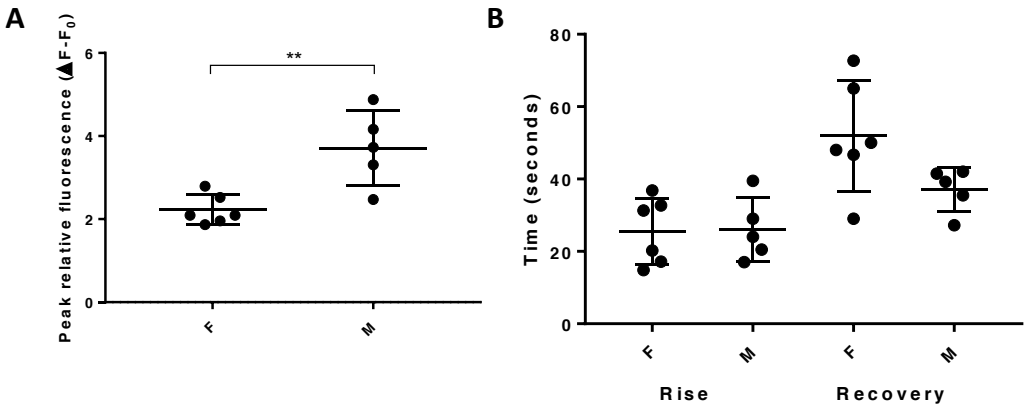

Figure 22: Analysis of calcium handling in myoblast-derived myotubes. *Analysis of calcium handling of myotubes derived from control immortalised myoblasts (MRC biobank ID: i7403) and of those derived from primary fibroblasts (biobank ID 8203). Cytosolic calcium was detected by confocal imaging of Fluo-4. (**A**) Scatter plot showing peak cytosolic calcium following application of high potassium (40mM); mean peak ± SD is given relative to a baseline of zero for fibroblast derived myotubes (F;* 2.22 ± 0.359*) and for myoblast derived myotubes (M; 3.71± 0.903). (**B**) Scatter plot showing the rise and recovery time constants for the increase and decrease of cytosolic calcium in the myotubes. Rise times are 25.52 ± 9.21 for F and 26 ± 3.92 for M. Recovery times are 51.89 ±15.32 for F and 37.1 ± 6.07 for M.*

*Higher relative peak fluorescence was reached in myoblast derived myotubes than in fibroblast derived myotubes. Unpaired Student's t-test, **P =* 0.0020. *Rise time and recovery time were not statistically significantly different for myoblast derived myotubes compared to fibroblast derived myotubes (yielding p values of* 0.9193 and 0.0746, respectively). *Six fibroblast derived cultures and five myoblast derived cultures were analysed, between three and four cells were analysed per culture.*

Cultures of myotubes derived from both the fibroblasts and the myoblasts included some unfused cells. A pure population of myotubes was not achieved. Furthermore some of the mono-nucleated cells did not exhibit calcium fluctuations in response to stimulation with potassium or caffeine. One method of increasing the proportion of multi-nucleated verses mono-nucleated cells could be to apply β-D-arabinofuranoside (araC, sigma: C1768). AraC interferes with DNA production and therefore reduces the proportion of proliferating

cells. This leads to an increase in the proportion of myotubes which have left the cell cycle, while the growth of fibroblasts and myoblasts becomes stunted.

I used 10mM araC, an amount which has been used successfully in myoblast cultures elsewhere to stunt growth of proliferating cells without causing toxicity (Patel et al, 1999; Hinterberger and Barald, 1990). I tried this method on the immortalised myoblast cultures and found that the proportion of multinucleated cells was increased. Approximately 22% of untreated cells were multinucleated, compared to 37% when treated with araC.

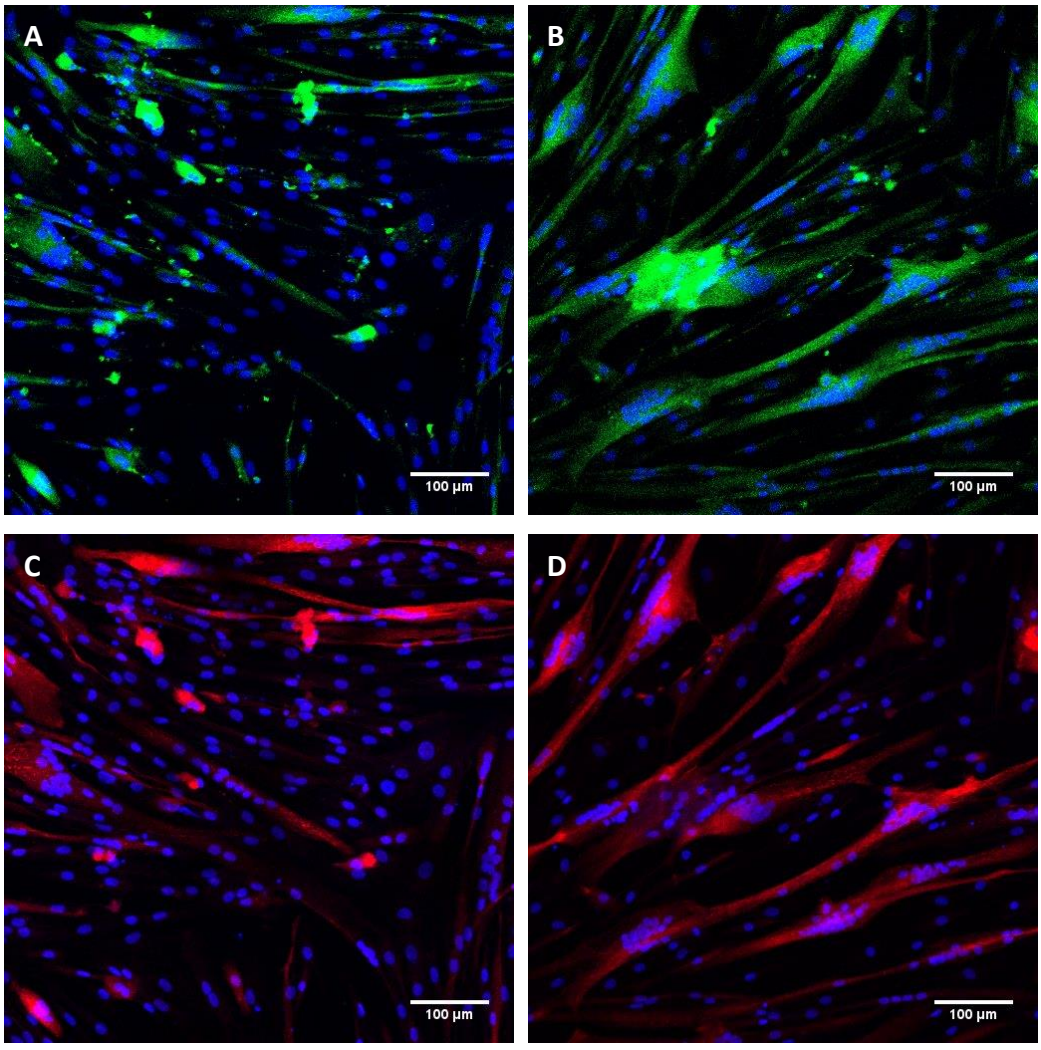

E

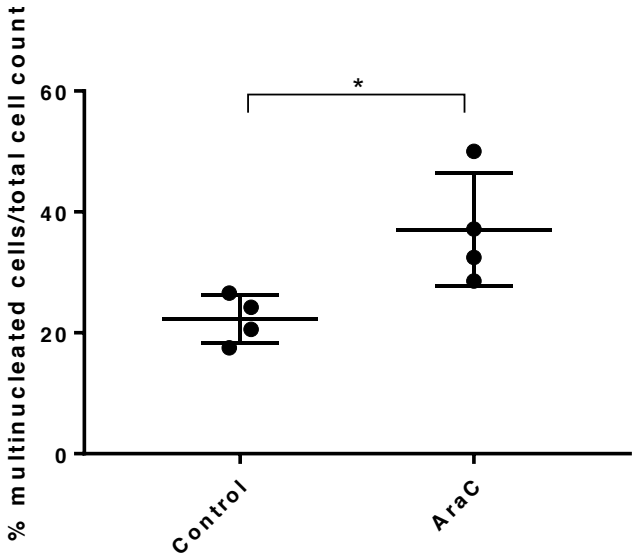

Figure 23: Evaluation of treatment with araC. *Immunofluorescence image of immortalised myoblasts following differentiation. (**A**) Micrograph of a control culture stained with a Desmin antibody (green) and Hoechst (blue). (**B**) Micrograph of a culture treated with araC and stained with a Desmin antibody (green) and Hoechst (blue). (**C**) Micrograph of a control culture stained with a CaV1.1 antibody (red) and Hoechst (blue). (**D**) Micrograph of a culture treated with araC and stained with a CaV1.1 antibody (red) and Hoechst (blue). (**E**) Scatter plot indicating the proportion of myotubes in culture as a percentage of the total cell count. Staining with CaV1.1 and with Desmin allowed for cells to be visualised and thus for nuclei per cell to be determined. Mean percentage of cells ± SD is indicated for control cultures (22.24 ± 3.99) and for araC treated cultures (37.06 ± 9.32). N = 4; four cultures were analysed per condition. A larger proportion of myotubes were detected following treatment with araC. Unpaired Student's t-test,* P = 0.0265.*

This section demonstrates that araC increased the proportion of myotubes relative to mononucleated cells. Although the difference was small with regard to the proportion of nuclei found in myotubes, more homogeneity was observed. More homogeneity would be a useful feature when comparing different treatments. AraC may thus present a valuable addition to the treatment protocol when comparing myotubes cultures from patients and control subjects.

4.1.5 FACS analysis; a method of assessing cell fusion

The methods outlined thus far produced mixed cultures containing both myotubes and mono-nucleated cells (myoblasts and/or fibroblasts). The extent of myotube maturation was determined for some of the cultures by performing immunofluorescence assays in order to confirm expression of mature muscle cell proteins. For example see SERCA1 ATPase staining in figure 17. However immunofluorescence assaying is a lengthy process and was not performed for each culture under investigation.

The presence of multinucleated cells can be determined by staining cells with Hoechst, as in figures 17 and 23, and this is a useful method of determining levels of multi-nucleation either before or after investigations. I was interested in developing a more efficient method of quantifying myotube maturation. To this end I developed a technique using flow cytometry for quantifying cell fusion.

Propidium iodide (PI) is a fluorescent dye that can be used to stain DNA in fixed, permeabilised cells and can be detected by flow cytometry. It is used to quantify DNA copy number per particle, allowing for the cell cycle to be analysed (Pollack, 1990). The cell cycle can be described in phases denoted G0, G1, S, G2 and M. In G0 and G1 cells each have one copy of DNA in one nucleus, in M and G2 nuclear material is doubled. S phase refers to the time when DNA is being transcribed such that there are between one and two copies of DNA in the cell.

This PI protocol also allows for the proportion of cells with more than two nuclei to be estimated in cultures containing myotubes by quantifying nuclear material per particle. This method could thus be used to estimate efficiency of myoblast fusion. Cells with two sets of nuclear material could be either cells in M or G2 phase that have not yet exited the cell cycle, or myotubes formed of two fused myoblasts.

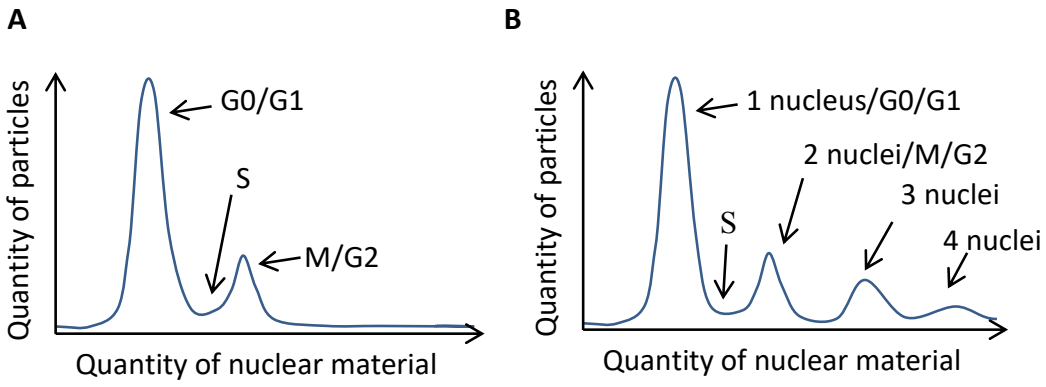

Figure 24: PI testing of multi-nucleation. *Representative diagrams of PI test results indicating what the different peaks represent. (**A**) Diagrammatic representation of PI cell cycle analysis for proliferating cells, with a large peak representing cells containing one set of nuclear material (G0/G1), a small proportion undergoing DNA transcription (S) and a final peak corresponding to cells that have two sets of DNA because they are undergoing mitosis but have not yet become separate particles (M/G2). (**B**) Diagrammatic representation of what one would expect when running the same PI protocol during differentiation of myoblasts to myotubes. This diagram indicates that each consecutive peak has an extra set of DNA material due to cell fusion and also includes the possibility that some cells would not yet have left the cell cycle and could be in G0/G1/S/M/G2.*

The basic PI cell cycle analysis protocol was tested using control undifferentiated fibroblasts. Results from this investigation are presented in figure 25. Figure 25A shows that the general distribution of cell size and internal cell granularity were largely uniform, and that larger cells typically had greater internal granularity. Figure 25B indicates the cell count for particles containing different levels of PI, and it is apparent from this figure that the majority of the cells (approximately 83%) were in G0 or G1 phase with a single copy of DNA. Approximately 13% of cells were in M or G2 phase of the cell cycle with double the level of PI staining and thus two copies of DNA. A small proportion of cells (approximately 2.3%) were in between the two peaks and thus in S phase with one full set of DNA and one set only partially transcribed.

A remaining 0.9% of particles contained more than two copies of DNA. This is likely to be a result of particle aggregation rather than cell fusion given that the fibroblast cultures were not contaminated with myoblasts. It follows that when using the protocol to

quantify cells with more than two sets of nuclear DNA, a small proportion of the particles detected with multiple sets of DNA may correspond to aggregated cells rather than to myotubes. This method thus allows for the extent of cell fusion upon differentiation to be estimated.

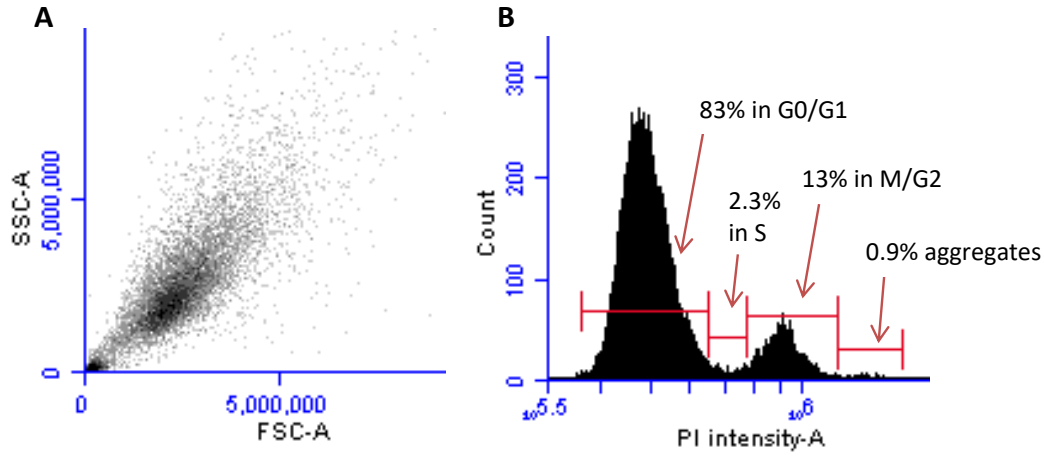

Figure 25: Cell cycle analysis for control fibroblasts. *(**A**) Plot of side scattered light (SSC-A) on forward scattered light (FSC-A). (**B**) Quantification of cells at a range of PI intensities. 83% of detected particles contained one set of nuclear material and are considered to have been in G0 or G1 phase. 2.3% of cells were in the region associated with the S phase of the cell cycle. A further 13% of cells contained two sets of nuclear material and are thus considered to have been in M or G2 phase. A remaining 0.9% of particles contained more than two sets of nuclear material, possibly due to aggregation of cells. Data were gathered on a BD Accuri flow cytometer and analysed using BD Accuri C Flow software.*

PI was then used in the same way with cultures containing multinucleated cells. In figure 26a below, the overall distribution of cell size and internal granularity is plotted. Points outside of region 1 near to zero on the axis were not considered, they result from cell particles or contaminants. Points in region 2 result from detection of cells that were larger than the majority of mono-nucleated cells. Figure 26B indicates the number of particles detected for a range of levels of PI staining; all particles in region 1 of figure 26A were considered. The peak corresponding to cells with two sets of nuclear material is obscured by the large peak produced by mono-nucleated cells. In figure 26c this peak could be observed by only analysing cells that were larger than the mono-nucleated cells (region 2 of figure 26A).

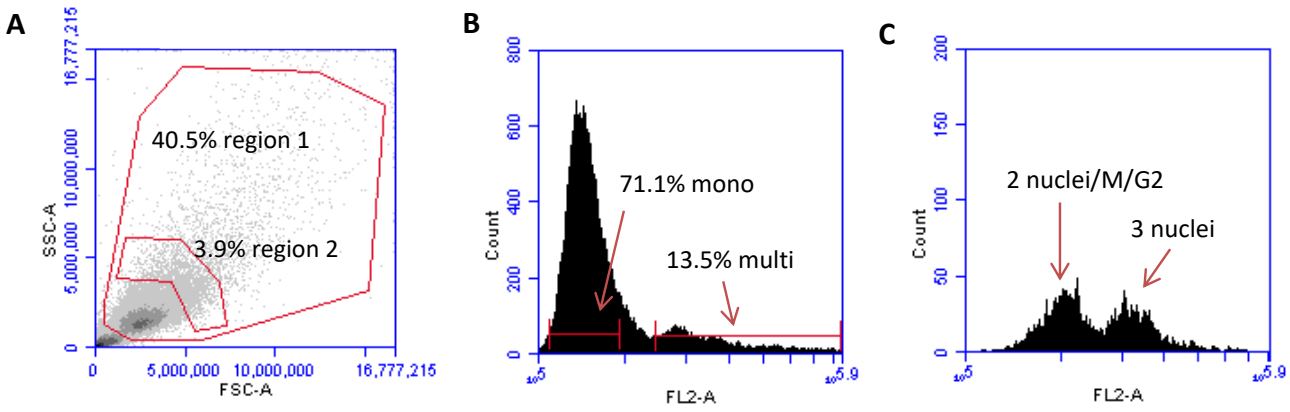

Figure 26: ***Flow cytometry analysis of fibroblast derived myotubes.*** *Cells were fixed and stained according to the PI analysis protocol. (**A**) Plot of side scattered light (SSC-A) on forward scattered light (FSC-A). (**B**) Chart of all particles/cells in region 1 quantified at a range of PI intensities. Approximately 13.5% of cells/particles were shown to contain three or more nuclei. (**C**) Chart of all particles/cells in region 2 (see figure A) quantified at a range of PI intensities. In (C) a peak corresponding to cells with two sets of nuclear material can be seen whereas in (B) this peak is obscured by the larger peak corresponding to mono-nucleated cells. Data were gathered on a BD Accuri flow cytometer and analysed using BD Accuri C Flow software.*

Results presented in figure 26 above indicate that approximately 13.5% of particles that were detected by the flow cytometer contained more than two sets of nuclear material. It is likely that at least 0.9 % of these resulted from aggregation of mono-nucleated cells, as was observed for the undifferentiated fibroblast investigation. Under this assumption it can be estimated that the remaining particles, approximately 12.5%, were fused myoblasts containing more than two nuclei.

However there are a number of issues that are likely to reduce accuracy of this technique. Myotubes are both large and long, whereas flow cytometry is designed for smaller cells that are not elongated. Indeed the nozzle of a flow cytometer is typically around 100µm whereas cultured myotubes are frequently around 300µm or more in length (McMahon et al, 1994). Due it its length, the fixation process and preparation for analysis may lead to fragmentation of myotubes, in particular of more mature myotubes that contain more nuclei. As a result, detection of particles with more than two sets of nuclei may include

fragments of multinucleated myotubes. This would make any quantification of multi-nucleation an even more problematic method of monitoring myogenesis. Furthermore, such large, elongated particles could aggregate and form clumps in the flow cytometer. While I did not experience jamming of the machine during investigations, the possibility of myotube aggregation and fragmentation make this method less suitable for the purpose outlined above.

4.1.6 Mitochondrial structure is affected by differentiation

Mitochondria of different cell populations form structures that are characteristic of those cell populations (Banerjee et al, 2014). In mature muscle fibres, for example, mitochondria align in between sarcolemmal striations. This allows for the mitochondria to form important interactions with surrounding proteins such as desmin and with triadic structures during myotube formation (Smolina et al 2014). Nutrient depletion likewise induces changes in mitochondrial structure. During starvation, it has been observed that mitochondria elongate, and that this elongation can protect the mitochondria from autophagic degradation (Gomes & Scorrano, 2011).

In my investigations, many of the myotube cultures that were developed, contained myotubes that looked well formed, but were unaffected by external stimulation (calcium was not released from the cytosol in response to stimulation with 40mM potassium or 10mM caffeine). I also observed some variation in mitochondrial structure and decided to determine whether or not this can be correlated with successful differentiation of myotubes. During differentiation, the reduced serum levels had a similar effect to that observed by Gomes and Scorrano (2011) during starvation, namely, in more elongated mitochondria. Since such elongation of mitochondria can protect against autophagic degradation, mitochondrial elongation during differentiation could serve as an indicator of myotube integrity, where myotubes boasting more elongated mitochondria are more likely to be responsive to external stimulation. In this section I show how I tested whether or not the mitochondrial elongation that I observed in many of the myotubes could indeed be correlated with an ability to release cytosolic calcium in response to chemical stimulation.

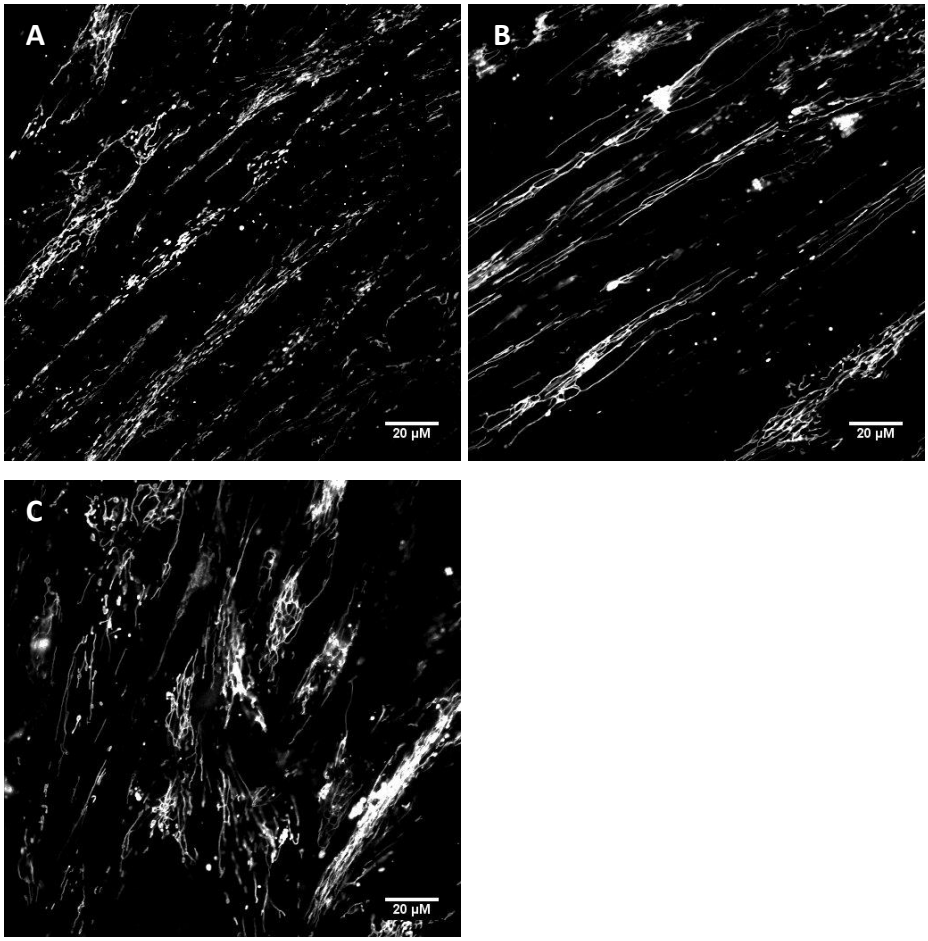
A
20 µM
B
20 µM
C
20 µM

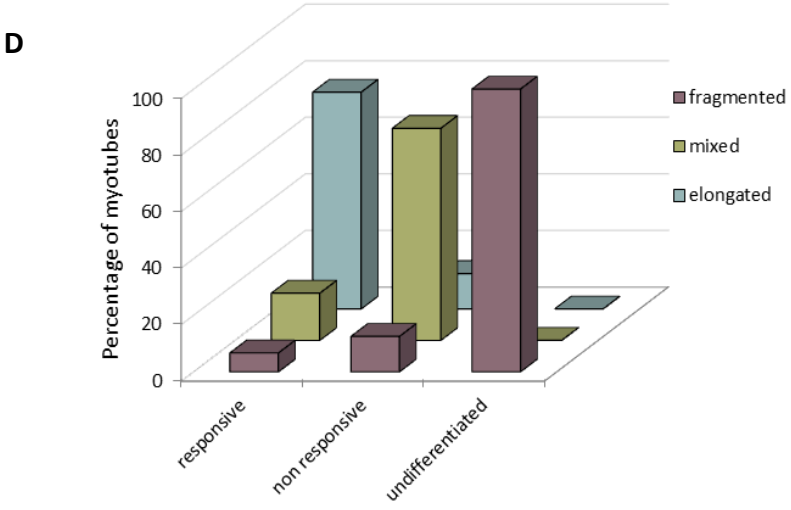
D
Percentage of myotubes
100
80
60
40
20
0
fragmented
mixed
elongated
responsive
non responsive
undifferentiated

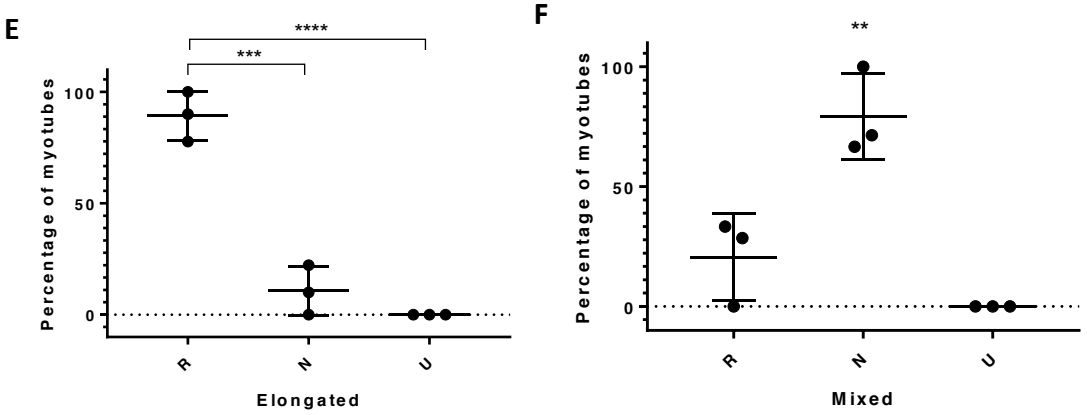
E
****
***
Percentage of myotubes
100
50
0
R
N
U
Elongated
F
**
Percentage of myotubes
100
50
0
R
N
U
Mixed

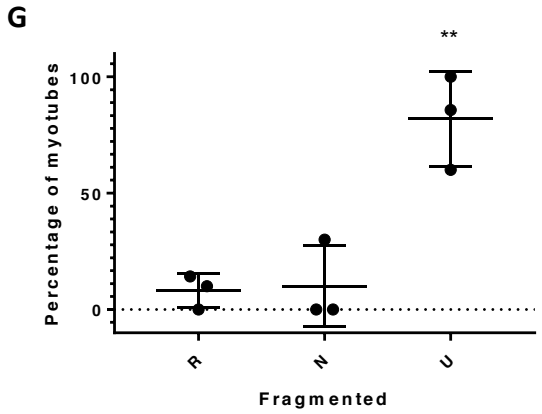

Figure 27: Mitochondrial membrane potential of fibroblasts following MyoD treatment. *Cells were stained with TMRM in order to visualise mitochondrial shape and distribution. (**A**) Mitochondrial membrane potential of fibroblasts following viral treatment with MyoD before differentiation. (**B**) Mitochondrial membrane potential in myotubes responsive to stimulation with 40mM potassium. The myotubes were produced by viral treatment of fibroblasts with MyoD followed by differentiation. (**C**) Mitochondrial membrane potential in cells that were not responsive to stimulation with 40mM potassium. The cells were produced by viral treatment of fibroblasts with MyoD followed by differentiation. (**D**) Bar graph showing the correlation between cells that are responsive, non-responsive and undifferentiated to those with mitochondria that is mostly fragmented, mostly elongated or a mixed population. N=3, data were collected by double blinded visual testing – three subjects were given 30 figures each, depicting cultures of responsive myotubes (R), non-responsive myotubes (N) and undifferentiated fibroblasts (U) and were asked to allocate them visually as mostly fragmented (F),mostly elongated (E) or a mixed (M) population. The correlation between cell type and observed mitochondrial structure was assessed.(**E**) Mitochondria of myotubes that were responsive (89.26 ± 11.13 %) were significantly more likely to be identified as elongated than mitochondria of myotubes which were non-responsive (10.74 ± 11.13) or than mitochondria of undifferentiated fibroblasts (0 ± 0). One-way ANOVA followed by Tukey's post hoc test, ***P=0.0001 and ****P<0.0001 respectively. (**F**) Myotubes that were non-responsive (79.37 ± 18.03 %) were significantly more likely to be identified as having a mixed population of mitochondria than myotubes which were responsive (20.63 ± 18.02) or than undifferentiated fibroblasts (0 ± 0 %). One-way ANOVA followed by Tukey's post hoc test, **P=0.0066 and 0.0014, respectively. (**G**) Mitochondria of undifferentiated fibroblasts (81.0 ± 20.27) were significantly more likely to be identified as fragmented than mitochondria of either responsive (8.10 ± 7.33) or non-responsive (10 ± 17.32) myotubes. One-way ANOVA followed by Tukey's post hoc test, **P=0.0032 and 0.0036, respectively.*

Mitochondria were imaged in 10 cultures of undifferentiated cells (“U”; figure 27A) and seven cultures of responsive myotubes (“R”; figure 27B). In each case the mitochondria were classified as either “mostly elongated”, “mostly fragmented” or “mixed”. Fibroblast cultures were typically classified as “mostly fragmented” and those of myotubes were typically classified as “mostly elongated”. Five cultures of unresponsive myotubes (“U”, where cytosolic calcium was not released upon exposure to 40mM potassium) were also labelled with TMRM (figure 27C). The mitochondria in these myotubes were typically classified as “mixed” (figure 27B). Overall I observed that among the myotubes, those that contained “mostly elongated” mitochondria were more likely to display calcium fluctuations in response to chemical stimulation than myotubes containing a “mostly fragmented” or a “mixed” population of mitochondria.

These observations were made visually and there was consistency when doing so in a blinded set up (figure 27). The blinded set up was achieved by showing pictures of mitochondria from the different cultures to individuals and asking them to assign each to one of the three categories (“mostly fragmented”, “mostly elongated” or “mixed”). 10 pictures of each culture type were used.

I show that mitochondrial structures can help to distinguish between myotubes that release calcium in response to external stimuli and those that do not. Mitochondrial structure could thus be a useful indicator of successful myotube differentiation allowing for a more appropriate selection of cultures to be made on a visual basis.

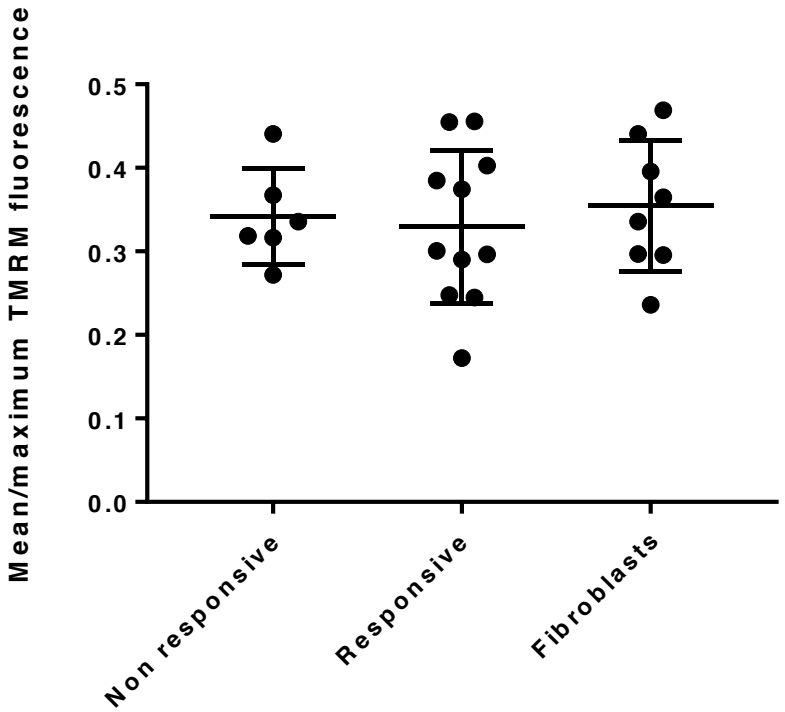

Figure 28: Mitochondrial membrane potential and differentiation. *Mean relative to maximum mitochondrial membrane potential ±SD as measured by TMRM fluorescence in myotubes that were responsive to chemical stimulation (0.330 ± 0.09), those that were not responsive (0.342 ± 0.057), and fibroblasts (0.354 ± 0.079). This scatter plot indicates that mitochondrial membrane potential of fibroblasts was not affected by transfection and differentiation. This was true whether or not the subsequent myotubes were responsive to stimulation using high (40mM) potassium. One-way ANOVA, P =* 0.8045*. N=6, between six and eleven preparations were analysed per category, approximately 4 cells per preparation.*

Mitochondrial membrane potential, as measured by the TMRM, was not affected by the differentiation process. It was also not possible to distinguish between the mitochondrial membrane potential in myotubes that responded to chemical stimulation and those that did not (figure 28).

4.1.7 Concluding remarks for part 1

I show that mitochondria become elongated during differentiation, suggesting that elongation may contribute to the successful formation of myotubes. I also show that lentiviral transduction with MyoD promotes the formation of myotubes more efficiently than adenoviral transduction.

Unfortunately, due to an interruption of studies this work was not further pursued. Upon return to work the field of fibroblast transformation had advanced such that further optimisation of this technique would not have been constructive. A technique for transforming fibroblasts to IPS cells and thereafter to myoblasts has been developed and promises to be more efficient than the procedure used here (Iovino et al, 2016). Nevertheless, it is possible that the differentiation process will be similar and that the optimisation of differentiation presented here will be relevant to the IPS cell culture too.

I also explored the possible use of flow cytometry for assessing cell fusion. I found that this was not a reliable tool for assessing cell fusion in myotubes, primarily because successfully differentiated myotubes are large and long. Such myotubes become easily damaged during analysis by flow cytometry.

4.2 MOUSE MODEL OF PERIODIC PARALYSIS

In this chapter I describe investigations carried out on a mouse model of PP, both *in vivo* and *ex vivo*. Along with investigators at Harwell, I ran *in vivo* tests on a mouse model of PP with an I584V mutation in order to confirm that it exhibits characteristics of PP. This mutation is equivalent to a novel patient mutation (I588V) which results in myotonia and PP. The model is referred to as the Draggen (Dgn) model. The results presented here demonstrate that the model does reflect some characteristics of the disease. These results include published data which was generated with colleagues at Harwell (Corrochano et al, 2014; see introduction section 1.16.3).

Following *in vivo* Dgn characterisation (see below) I isolated single fibres from the mice for *in vitro* investigation of disease progression. Investigations were carried out on hind limb muscle due to observations that the hind limb muscles were particularly affected in Dgn positive mice. Indeed during attacks, the mice were observed to drag their hind limbs which became paralysed. TA and EDL muscles were analysed *in vivo* while single fibres were extracted from FDB muscle for *ex vivo* investigations. Mitochondrial substrates were also quantified in tissue from TA and EDL muscles.

Findings presented here include an indication that hind limb muscles of the affected mice were more resistant to fatigue, and that the mitochondrial membrane potential was less positive. In addition it appears that affected mice had fewer intermyofibrillar mitochondria.

4.2.1 *In vivo* characterization of the Dgn model of periodic paralysis

Female Dgn mice display a less severe phenotype than males, however due to low survival rates, male Dgn mice were not available at the time of the *in vivo* investigation. *In vivo* investigations were therefore performed on female mice. Tests were only carried out on females which had displayed at least one episode of muscle weakness. My *in vivo* investigations on the female mice contribute to a study published on the Dgn phenotype which I cite below (Corrochano et al, 2014).

Female Dgn mice have a later average age of onset (25 weeks for females compared to 16 weeks of age for males). Indeed all males displayed at least one episode of hind limb immobility by 60 weeks compared to only 38% of females (Corrochano et al, 2014). A

similar trend has been observed in patients of HypoPP, where males experienced 100% penetrance with 50 to 150 attacks per year compared to females who experienced less than 30% penetrance with 30 to 50 attacks per year (Ke et al, 2013). Age of onset is also earlier in male patients, although this effect is less pronounced than in the Dgn model. One study suggests onset at 8 years of age in males compared to 11.5 in females with HypoPP (Ke et al 2013).

There was much variation in the age at which Dgn mice started showing symptoms, with first attacks occurring anywhere between 3 and 60 weeks of age (Corrochano et al, 2014). Initially I planned to carry out experiments at three time points in order to characterize progression of the disease. These were early (15 weeks), intermediate (45 weeks) and late (70 weeks), starting with the latest time point in order to gauge maximum effects of the mutation on females. However the early and intermediate time points were latterly not pursued because the effects observed in the aged group were small, and in some cases no effects were observed (see for example TA twitch force in figure 30). The late time point experiment was repeated by Dr Pete Joyce (working at the Institute of Neurology for Harwell) on male mice (figure 29; Corrochano et al, 2014).

The tension generated by electrically stimulating a twitch in TA and EDL fibres (as described in methods section 3.8.2) was compared for fibres from mutant and those from WT control mice. A reduction in both twitch force and the rate of the twitch were anticipated for aged Dgn mice. This would be consistent with the human disease where muscle weakness develops in later stages of disease progression. However neither TA nor EDL twitch characteristics were clearly affected in Dgn compared to WT control muscle. Results presented in figures 30 and 31 indicate that the time taken to reach peak force (rise time) was not affected in either TA or EDL when comparing female Dgn to WT mice. Maximum twitch force was also not affected in the TA muscles of these mice. Maximum twitch force appeared to be greater for Dgn EDL than for WT EDL, however there were large variations in these measurements and WT EDL twitch force was not significantly different to that of controls. Furthermore this trend was inconsistent with the trend seen in data collected by my colleague Dr Pete Joyce from male mice (Corrochano et al, 2014). In the data collected from males, the maximum single twitch force was significantly greater for the WT controls. It may be that the weakness seen in males reflects the progressive weakness observed in later stages of PP in humans and that the females had

not reached the stage where such weakness was evident. Data collected from males by Dr Joyce is copied below (figure 29), as presented in Corrochano's study (Corrochano et al, 2014). While I contributed to the investigations presented in Corrochano's study, the data that I collected show a weaker phenotype with more variable results because the females that I studied were less affected by the mutation than the males studied by Pete Joyce. I include results from investigations on both male (figure 29) and female (figures 30-32) mice below.

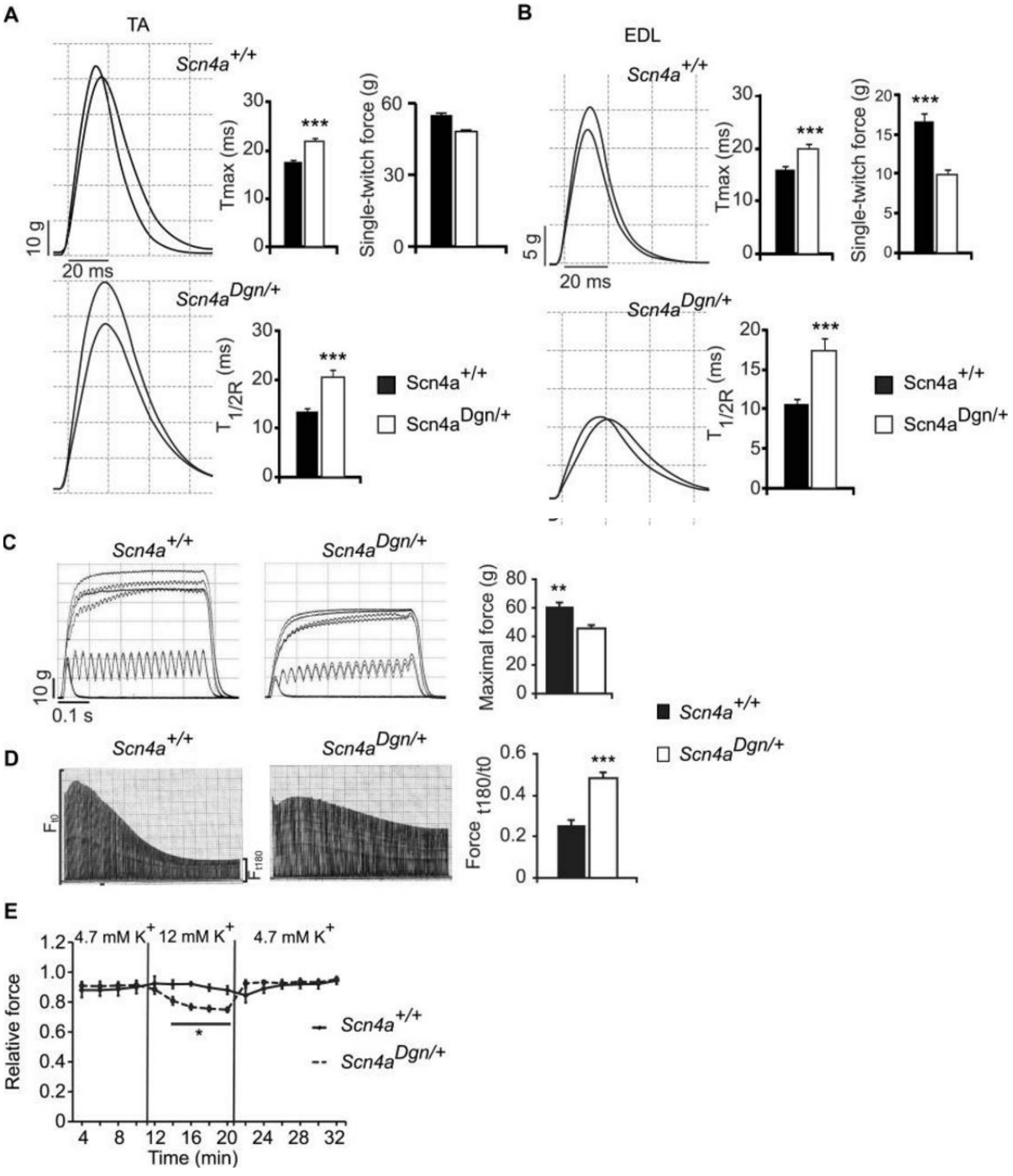

Figure 29: Draggen mice have muscle weakness, (Corrochano et al, 2014). *Data and figure legend as presented in Corrochano's paper (Corrochano et al, 2014). Draggen mice have muscle weakness.* In vivo *physiological assessment of hind-limb muscles of 60-week-old male mice.* $Scn4a^{+/+}$ *(*n = *12);* $Scn4a^{Dgn/+}$ *(*n = *14). (**A**) Tibialis anterior (TA) muscle force showed that the time to peak force (T_{max}) and half-time relaxation time ($T_{1/2R}$) were significantly longer in draggen mice than wild-type controls. For T_{max} (*$Scn4a^{+/+}$ *= 17.5 ms;* $Scn4a^{+/+}$*;* $Scn4a^{Dgn/+}$ *= 21.9 ms;* P < *0.001). For $T_{1/2R}$ (*$Scn4a^{+/+}$ *= 13.3 ms;* $Scn4a^{Dgn/+}$ *= 20.6 ms;* P < *0.001). Single twitch force for tibialis anterior muscles was not significantly different between wild-type and draggen muscles (*$Scn4a^{+/+}$ *= 54.1 g;* $Scn4a^{Dgn/+}$ *= 45.7 g;* P = *0.19). The two traces shown per image represent the right and left hind-limb from the same animal. (**B**) Extensor digitorum longus (EDL) muscles in draggen mice also took longer to reach both T_{max} and $T_{1/2R}$ than wild-type (T_{max}:* $Scn4a^{+/+}$ *= 15.9 ms;* $Scn4a^{Dgn/+}$ *= 20.0 ms;* P < *0.001. $T_{1/2R}$:* $Scn4a^{+/+}$ *= 10.7 ms;* $Scn4a^{Dgn/+}$ *= 17.3 ms;* P < *0.001). Single twitch force was also determined for extensor digitorum longus muscles, with wild-type muscles exerting more force than draggen muscles (*$Scn4a^{+/+}$ *= 16.7 g;* $Scn4a^{Dgn/+}$ *= 9.8 g;* P < *0.001). (**C**) Extensor digitorum longus tetanic force generated by draggen mice (45.8) is reduced compared to wild-type littermates (60.5) (*P = *0.003). (**D**) Representative traces of tetanic tension from wild-type and draggen extensor digitorum longus muscles. The fatigue index (FI) is increased for draggen muscle (0.48) when compared to wild-type (0.25) (*P < *0.001). (**E**) High potassium levels diminish force generated by extensor digitorum longus muscles of draggen mice* ex vivo*.* $Scn4a^{+/+}$ *(*n = *7);* $Scn4a^{Dgn/+}$ *(*n = *9) (*P-*values: 14 min:* P = *0.017; 16–20 min:* P < *0.003). The force generated by extensor digitorum longus was measured every 2 min with muscles submerged in a bath with normal (4.75 mM) and high (12 mM) potassium concentrations for 10 min in each condition. Data are expressed as mean ± SEM. *P < 0.05; **P < 0.01; ***P < 0.001.*

Data presented in figure 29 above suggest that twitch force is greater in EDL and TA muscle of the Dgn mice, but that tetanic force is greater in the wildtype. My studies on females do not identify a difference in force produced in TA (figure 30), but indicate that twitch force is greater in EDL of control mice than EDL of Dgn mice (figure 31). Fatigue was delayed in males (figure 29), but no difference was identified in females (figure 32).

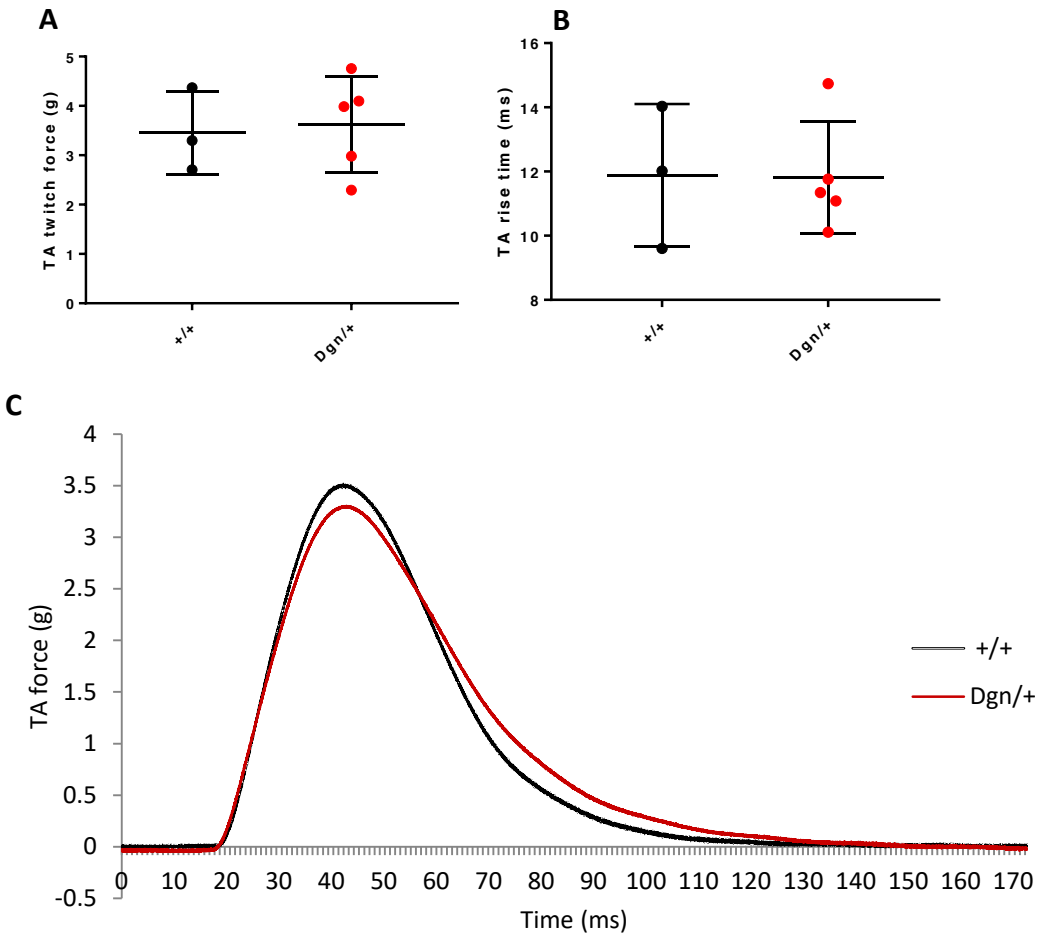

Figure 30: Mouse model – tibialis anterior single twitch force. (A) *In vivo assessment of tibialis anterior (TA) single twitch force ±SD in Dgn mice compared to WT controls (3.62 ± 0.98 for Dgn and 3.46 ± 0.84 for WT). (**B**) In vivo assessment of tibialis anterior (TA) twitch rise time ±SD in Dgn mice compared to WT controls (11.81 ± 1.75 for Dgn and 11.89 ± 2.22 for WT). (**C**) Trace of TA twitch force in WT and Dgn mice. N= 3, the data are collected from three WT mice (+/+) and five Dgn mice (Dgn/+). Neither the peak TA twitch force nor the time taken to reach peak force, were affected in 70 week old females. Unpaired Student's t-test, P=0.816 for TA twitch and p=0.958 for TA rise time.*

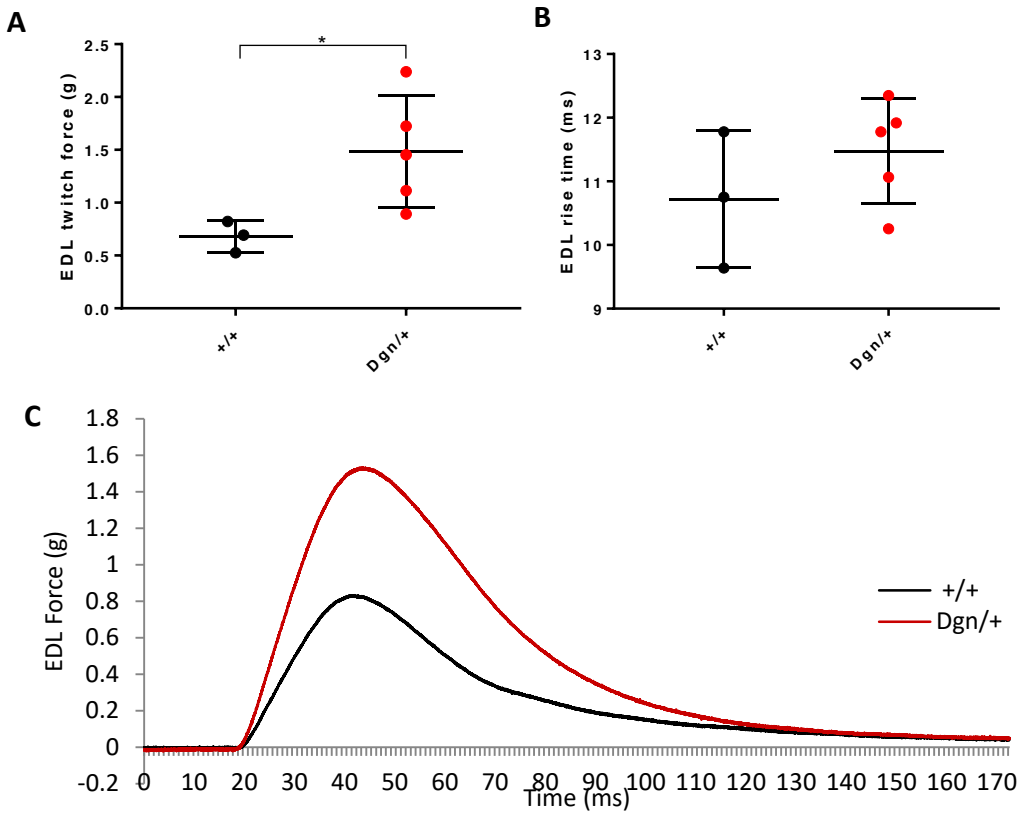

Figure 31: Mouse model – extensor digitorum longus single twitch force. *(**A**) In vivo assessment of extensor digitorum longus (EDL) single twitch force ±SD in Dgn mice compared to WT controls (0.680 ± 0.148 for Dgn and 1.484 ± 0.528 for WT). (**B**) In vivo assessment of EDL twitch rise time ±SD in Dgn mice compared to WT controls (11.47 ± 0.824 for Dgn and 10.72 ± 1.071 for WT). (**C**) Trace of EDL twitch force in WT and Dgn mice. N= 3 for WT and N=5 for Dgn, the data are collected from three WT mice (+/+) and five Dgn mice (Dgn/+), where both hind limbs from each mouse were analysed.*
*EDL single twitch force was increased in Dgn compared to WT controls in 70 week old females. Unpaired Student's t-test, *P= 0.046. The time taken to reach peak force was not affected in Dgn mice compared to WT controls. Unpaired Student's t-test, *P= 0.303.*

Muscle fatigue was measured in EDL muscle of Dgn and WT control mice in order to test for fatigue resistance. Muscle force typically reduces upon repeated stimulation, due to sodium channel inactivation. However in fatigue resistant tissue, the level of force produced upon repeated stimulation is better maintained. In males, EDL muscle from Dgn mice was more fatigue resistant than the EDL of WT mice upon repeated stimulation (figure 29D). Such a trend was also observed in females, however not at a statistically significant level (figure 32).

Control muscles fatigue quickly and thus do not become stimulated for prolonged periods of time. The delayed fatigue in HyperPP muscle likely leads to excessive force generation in antagonistic muscles, resulting in increased metabolic demands and in deterioration of muscle (Khogali et al, 2015). Data collected from male mice by Dr Pete Joyce provided further evidence that Dgn mice present with resistance to fatigue, because the males displayed a more exaggerated phenotype. In the males, the EDL force fatigue was increased for Dgn muscle (0.48) when compared to wild-type (0.25) ($P < 0.001$) (figure 29 above).

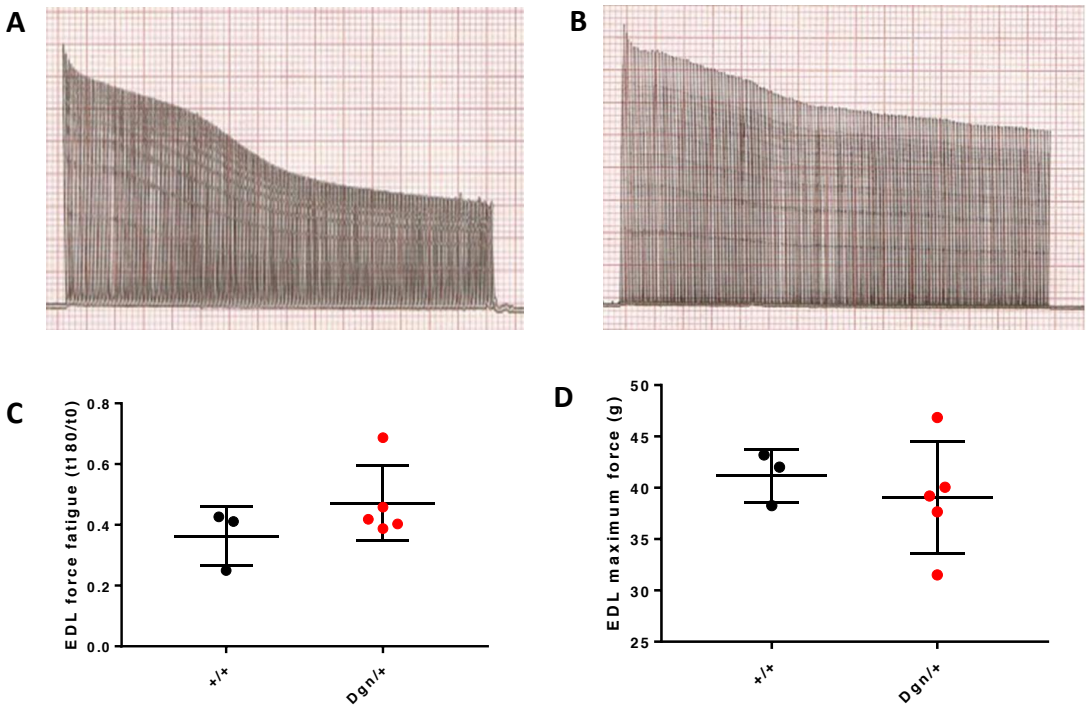

Figure 32: Mouse model – extensor digitorum longus force fatigue and maximum force. *(**A**) Trace of tension fluctuations upon repeated stimulation of EDL in a WT mouse in vivo. (**B**) Trace of tension fluctuations upon repeated stimulation of EDL in a Dgn mouse in vivo. (**C**) Scatter plot of initial tetanic tension divided by the final tetanic tension (t180/t0) ± SD for Dgn and WT (0.362 ± 0.098 for WT and 0.471 ± 0.124 for Dgn). (**D**) Scatter plot of the maximum tension ±SD achieved in EDL of Dgn and WT in vivo during repeated stimulations (41.15 ± 2.582 for WT and 39.05 ± 5.496 for Dgn). These differences were not significant. Unpaired Student's t-test, P=0.1 for fatigue and P=0.5654 for maximum force. N= 3 for WT and N=5 for Dgn, the data are collected from three WT mice (+/+) and five Dgn mice (Dgn/+), where both hind limbs from each mouse were analysed.*

Electromyography of hind limb muscle of these mice indicated that all mice with the mutation presented with myotonia, whether or not they presented with attacks of paralysis (Corrochano et al, 2014). If resistance to fatigue is indeed a feature of the Dgn muscle, this could lead to increased metabolic demand, which would be further pronounced as a result of the myotonia observed in the Dgn mice.

The resistance may also indicate a change in the fibre type of affected muscles from fast twitch (type II) fibres to slow twitch (type I) fibres, as fatigue resistance is a hallmark of type I fibres. Type I fibres are typically more oxidative, which may point toward mitochondrial involvement in disease progression. This was tested in single fibres from FDB muscle. Fibres were isolated and mitochondrial membrane potential as well as calcium handling were assessed (see below; section 2.3).

At the conclusion of each *in vivo* experiment the effect of the mutation on higher centres was assessed by determining the number of motor neurons innervating the EDL muscle. Because the mutation is muscle specific, there is no reason to believe that higher centres should be affected and that the motor neuron count should be reduced. Nevertheless, it may be that at later stages of disease progression motor neuron count would reduce due to a general deterioration of mouse health. Such a phenomenon was not observed: mutant and control mice had an average of 35 and 36 motor neurons innervating the EDL respectively, and so will be considered identical for the purpose of this investigation. This test was not repeated with male Dgn mice.

4.2.2 *In vitro* characterization of the Dgn model of periodic paralysis

As established by the investigations using the males, the Dgn mutation can lead to presentation of some characteristics of PP. A method of investigating disease progression *ex vivo* using tissue from male mice was then sought. To this end, single fibres from FDB were isolated and observed by fluorescence microscopy. Both calcium handling and mitochondrial membrane potential were investigated by fluorescence microscopy. Calcium handling was investigated because it may be affected by the unusual muscle stimulation patterns observed in PP and mitochondria were investigated because of the indications that there may be an oxidative aspect to disease progression. Having shown that only the males display statistically significant features of disease progression, further investigations were performed using male mice.

Cells were imaged during contractions and in some cases during addition of solutions. I therefore sought a protocol that would encourage secure adherence of myotubes to the imaging dish. Good adherence was achieved by coating a plastic dish for three hours with a dilute (1%) matrigel solution. Fibres were cultured in 20% controlled serum replacement medium (SRM, sigma), which resulted in the fibres remaining viable for up to 48 hours compared to approximately 12 hours when treated with 10% FBS. The SRM contains purified serum albumin, transferrin and insulin, but does not contain growth factors, steroid hormones and glucocorticoids. It thus allows for the fibres to be maintained without promoting their growth which could affect structure and function.

Fibres from control mice were first used to optimise culturing conditions and to determine a suitable stimulation protocol. Fibres were imaged with transmitted light (figure 33A) and cells were loaded with Fluo4-AM in order to view cytosolic calcium (figure 33B). Cells were also loaded with TMRM in order to measure the mitochondrial membrane potential (figure 33C).

4.2.3 Characterisation of mitochondria *in vitro*

Measurements of TMRM fluorescence intensity were used both to analyse the mitochondrial membrane potential and to provide an indication of mitochondrial structure and distribution. The mitochondria formed networks along the striations (subsarcolemmal mitochondria), and in some areas intermyofibrillar mitochondria were visible along the cell length. This is consistent with an observation that mitochondria form reticular networks around sarcomeres (Picard et al., 2011).

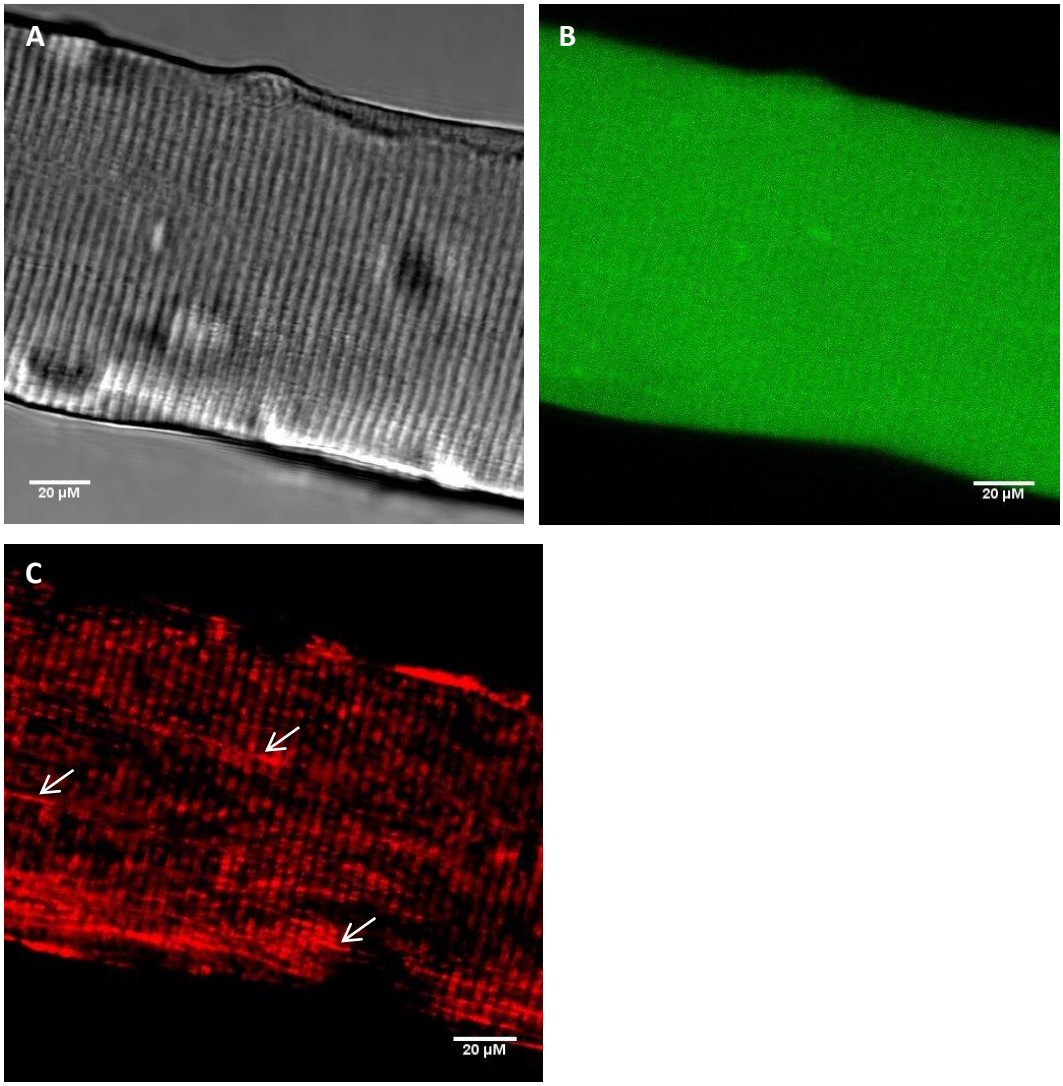

Figure 33: Mouse model – a flexor digitorum brevis fibre. *(**A**) Image of control FDB fibre taken with transmitted light to show striations. (**B**) Image of control FDB fibre taken by fluorescence microscopy with Fluo-4 to show cytosolic calcium. (**C**) Image of control FDB fibre taken by fluorescence microscopy with TMRM to show mitochondrial membrane potential. These images demonstrate that mitochondria were aligned along striations, with some intermyofibrillar mitochondria perpendicular to striations (see arrows in figure C). Cells were imaged using a Zeiss 700 microscope with a 40x objective.*

TMRM fluorescence microscopy of the fibres led the observation that single fibres derived from Dgn mice typically had fewer subsarcolemmal mitochondria than those from controls. This was observed visually and confirmed by Fourier transform of images of TMRM fluorescence (figure 34). I analysed the proportion of intermyofibrillar mitochondria relative to combined intermyofibrillar and subsarcolemmal mitochondria by

performing a spatial Fourier transform on images of TMRM staining, as described in methods section 3.9.3, page 72.

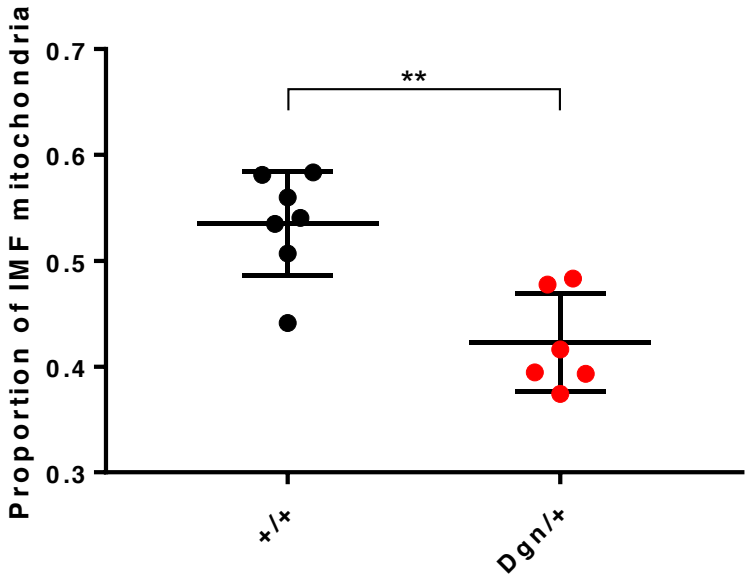

Figure 34: Mouse model – intermyofibrillar mitochondria. *Scatter plot indicating the mean proportions of intermyofibrillar (IMF) mitochondria ±SD in wild type (0.5354± 0.0495) and Dgn fibres (0.423 ± 0.0463). Values were determined by Fourier transform analysis (method described in section 3.9.3, figure 13). N=7 for WT and N=6 for Dgn, with approximately 8 fibres analysed for each animal. The proportion of IMF mitochondria is significantly greater in fibres isolated from the seven WT mice than from the six Dgn mice. Unpaired Student's t-test, **P = 0.0015.*

Intermyofibrillar mitochondria were more prevalent in fibres isolated from wild-type FDB muscle than in those from the Dgn FDB (p=<0.0001). Fourier transform of wild type muscle returned intermyofibrillar mitochondria at 31-56% of the total amount, while Fourier transform analysis of fibres from Dgn mice suggested that 41-75% of mitochondria are intermyofibrillar. Although these are large ranges, the trend is statistically significant. Subsarcolemmal mitochondria in other studies are shown to typically make up 10-15% of the total mitochondrial content in control skeletal muscle (Damirchi et al, 2012). This Fourier transform analysis is a useful tool for identifying trends in mitochondrial populations, but has not been adjusted to produce exact values of the proportions of mitochondrial populations.

Mitochondrial membrane potential was also compared in fibres from control mice to that in fibres from Dgn mice. TMRM staining was typically stronger in fibres from WT mice (figure 35) suggesting that a more positive mitochondrial membrane potential was generated in WT than in Dgn fibres.

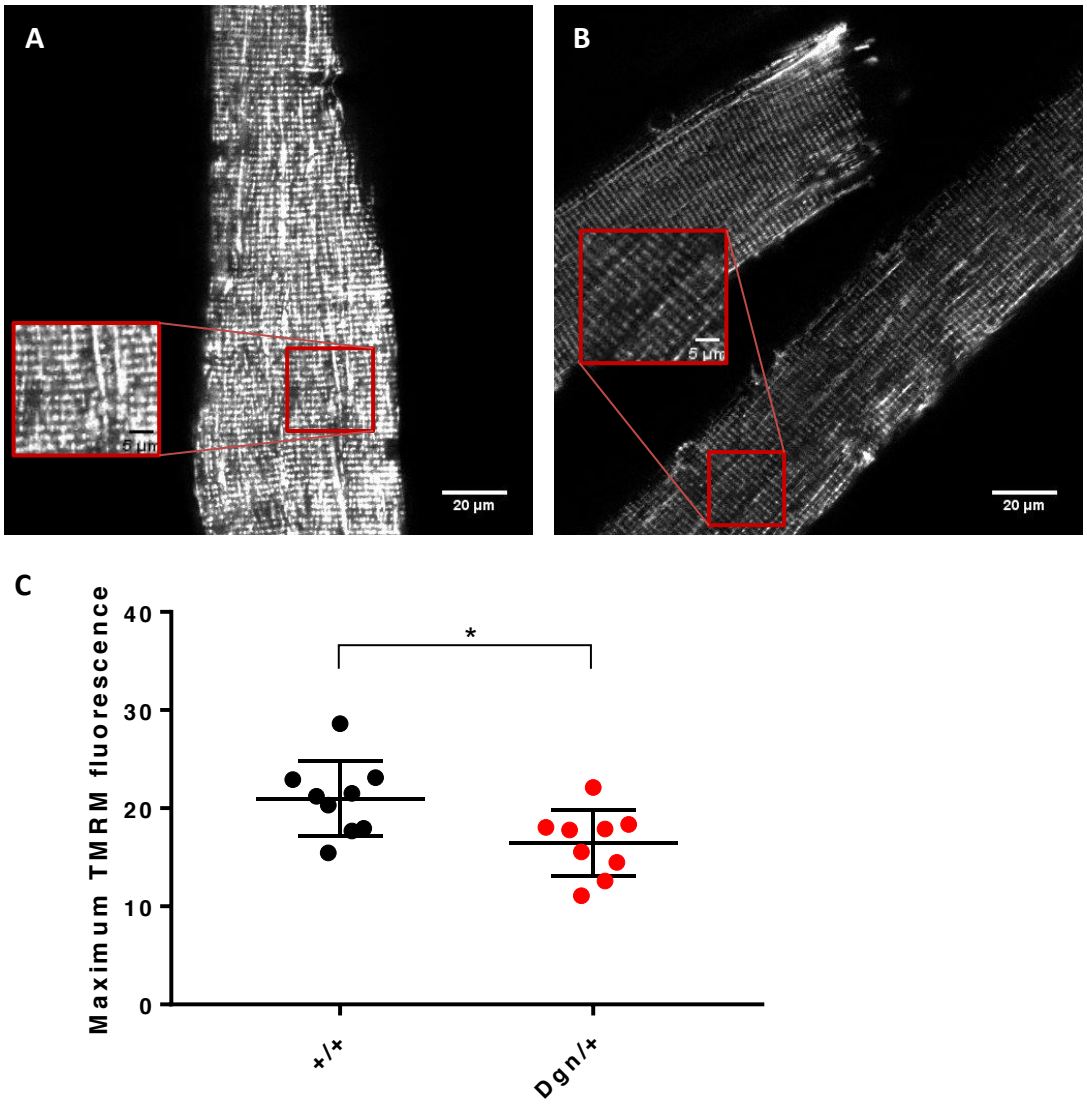

Figure 35: Mouse model – maximum TMRM fluorescence. *(**A**) Micrograph showing intensity of TMRM fluorescence in single fibres of the wildtype control (WT) FDB muscle. (**B**) Micrograph showing intensity of TMRM fluorescence in single fibres of the Dgn FDB muscle. (**C**) The scatter plot shows average maximum TMRM fluorescence for WT and Dgn fibres ± SD (20.97 ± 3.84 and 16.43 ± 3.37, respectively). WT fibres typically have greater mitochondrial membrane potential and this difference is statistically significant (yielding a two-tailed unpaired Student's t-test p-value of 0.0167). N=9, where fibres from nine male Dgn mice were compared to fibres from nine male controls. Cells were imaged using a Zeiss 700 microscope with a 40x objective.*

4.2.4 Characterisation of oxygen consumption and complexes involved in oxidative phosphorylation

I investigated the effects of the Dgn mutation on mitochondria further by analysing oxygen consumption. Oxygen consumption can be measured in freshly isolated and permeabilised fibre bundles using an Oroboros oxygen electrode. The activity of the different complexes in the electron transport chain (ETC) of Dgn and control fibres was determined by application of drugs; rotenone, for example, inhibits complex I and antimycin-A inhibits complex IV. Bundles of fibres from two WT and two Dgn mice were compared. However no differences were seen suggesting that the Dgn mutation did not affect the function of any of these mitochondrial complexes. Alternatively it may be that the tissue preparation, in particular the permeabilisation process required to measure oxygen consumption in freshly isolated fibres, also damaged them to some extent making it more difficult to distinguish between them.

Another method of analysing activity of the mitochondrial complexes was employed in order to better understand if these were affected in Dgn mice. A colleague, Dr Iain Hargreaves (working at the Institute of Neurology, UCL, London) measured mitochondrial complex activity in tissue that I isolated from Dgn and WT male mice (figures 36-38). These investigations also suggested that mitochondrial complex activity was not affected in mice with the condition.

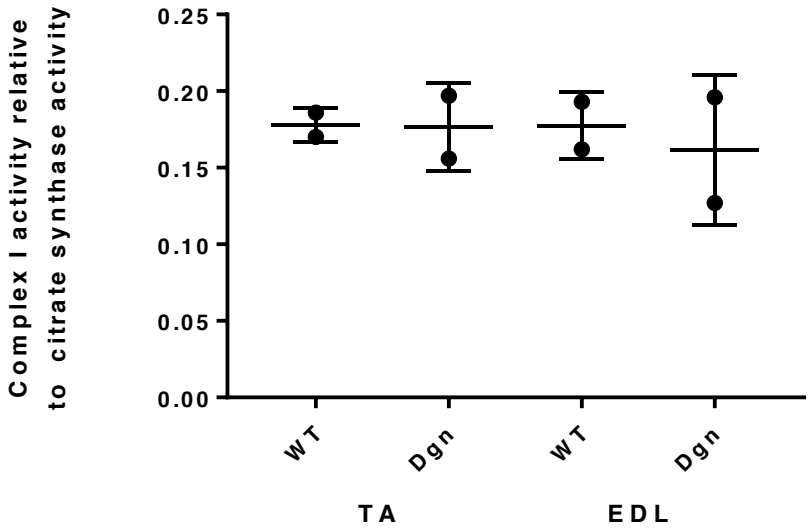

Figure 36: Mouse model – complex I activity. *Complex I activity in hind limb TA and EDL of Draggen (Dgn) and control (WT) male mice. Activity is expressed as a ratio to citrate synthase activity. N=2; tissue from two Dgn and two WT mice aged 20+/-2 was analysed using data provided by Dr Iain Hargreaves (UCL, London). Mean activity of complex IV from TA of WT and Dgn mice ± SD is indicated (0.178 ± 0.008 and 0.1765 ± 0.0205, respectively). Mean activity of complex IV from EDL of WT and Dgn mice ± SD is indicated (0.1775 ± 0.0155 and 0.1615 ± 0.0345 respectively). Differences between activity levels of complex IV in WT and Dgn are not statistically significant yielding two-tailed unpaired Student's t-test p-values of 0.9519 for TA and 0.7134 for EDL.*

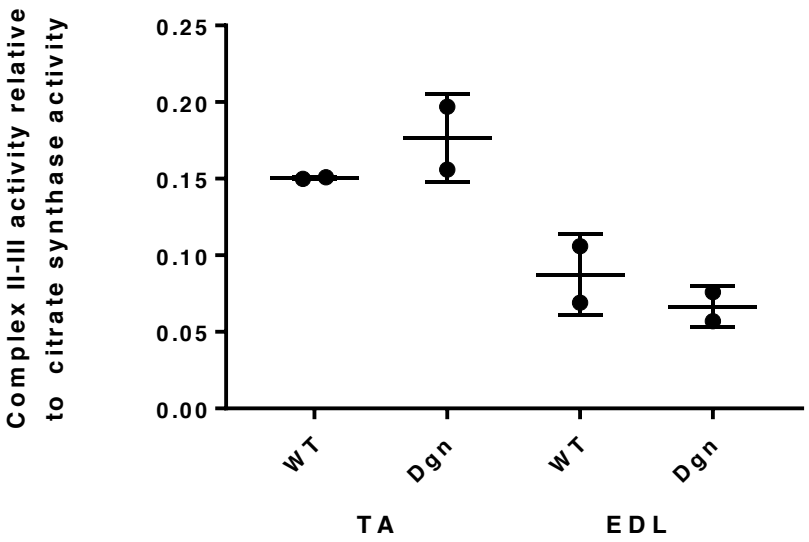

Figure 37: Mouse model – complex II-III activity. *Complex II-III activity in hind limb TA and EDL of Draggen (Dgn) and control (WT) male mice. Activity is expressed as a ratio to citrate synthase activity. N=2; tissue from two Dgn and two WT mice aged 20+/-2 was analysed using data provided by Dr Iain Hargreaves (UCL, London). Mean activity of complex IV from TA of WT and Dgn mice ± SD is indicated (*0.1505 ± 0.0005 *and* 0.1765 ± 0.0205*, respectively). Mean activity of complex IV from EDL of WT and Dgn mice ± SD is indicated (*0.0875 ± 0.0185 *and* 0.0665 ± 0.0095 *respectively). Differences between activity levels of complex IV in WT and Dgn are not statistically significant yielding two-tailed unpaired Student's t-test p-values of 0.3325 for TA and 0.4189 for EDL.*

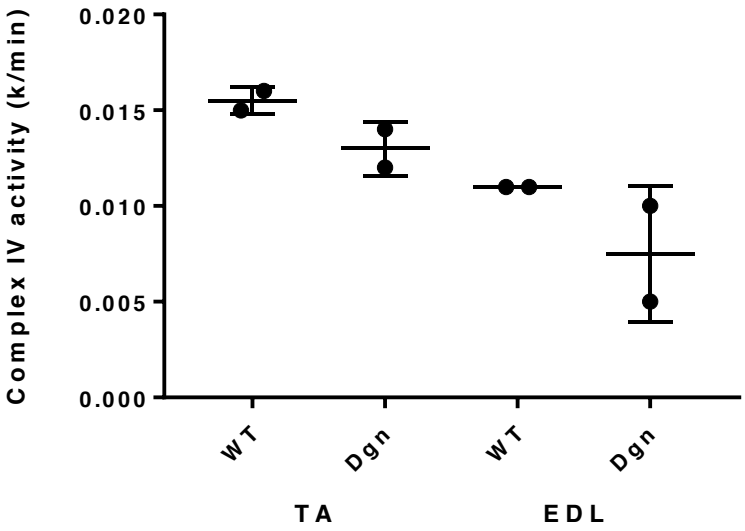

Figure 38: Mouse model – complex IV activity. *Complex IV activity in hind limb TA and EDL of Draggen (Dgn) and control (WT) male mice. N=2; tissue from two Dgn and two WT mice aged 20+/-2 was analysed using data provided by Iain Hargreaves (UCL, London). Mean activity of complex IV from TA of WT and Dgn mice ± SD is indicated (0.0155 ± 0.0005 and 0.013 ± 0.001, respectively). Mean activity of complex IV from EDL of WT and Dgn mice ± SD is indicated (0.011 ± 0 and 0.0075 ± 0.0025 respectively). Differences between activity levels of complex IV in WT and Dgn are not statistically significant yielding two-tailed unpaired Student's t-test p-values of 0.1548 for TA and 0.2965 for EDL.*

4.2.5 Characterisation of calcium handling *in vitro*

Peak cytosolic calcium levels as well as rise and recovery times in response to chemical stimulation were recorded in order to evaluate effects of the mutation on calcium handling. Initially calcium handling in freshly isolated FDB fibres of control mice was assessed by loading with Fluo-4, AM. Relatively high levels of potassium stimulation (60mM) were required to produce a relatively slow (approximately 10 second) rise in cytosolic calcium (figure 39), making it a less suitable method of stimulation. In addition the potassium equilibrium potential plays an important role in PP (see introduction section 1.2) and it would thus not be appropriate for comparing calcium handling characteristics in fibres of WT and Dgn mice. Caffeine on the other hand produced a fast response (in the region of one millisecond). However caffeine acts by opening RyRs to release Ca from intracellular stores, a process that is less relevant to PP. Caffeine also resulted in super-contraction (a term borrowed from Cifelli et al., 2007; see example in

figure 40) of the fibres when applied at 10mM, but did not have an effect on the fibres at lower concentrations. Following super-contraction fibres did not relax and the cytosolic calcium concentration did not return to basal levels, indicating that reuptake was disrupted by the strong contraction (figure 40). Both potassium and caffeine were avoided for the investigation of calcium handling in PP.

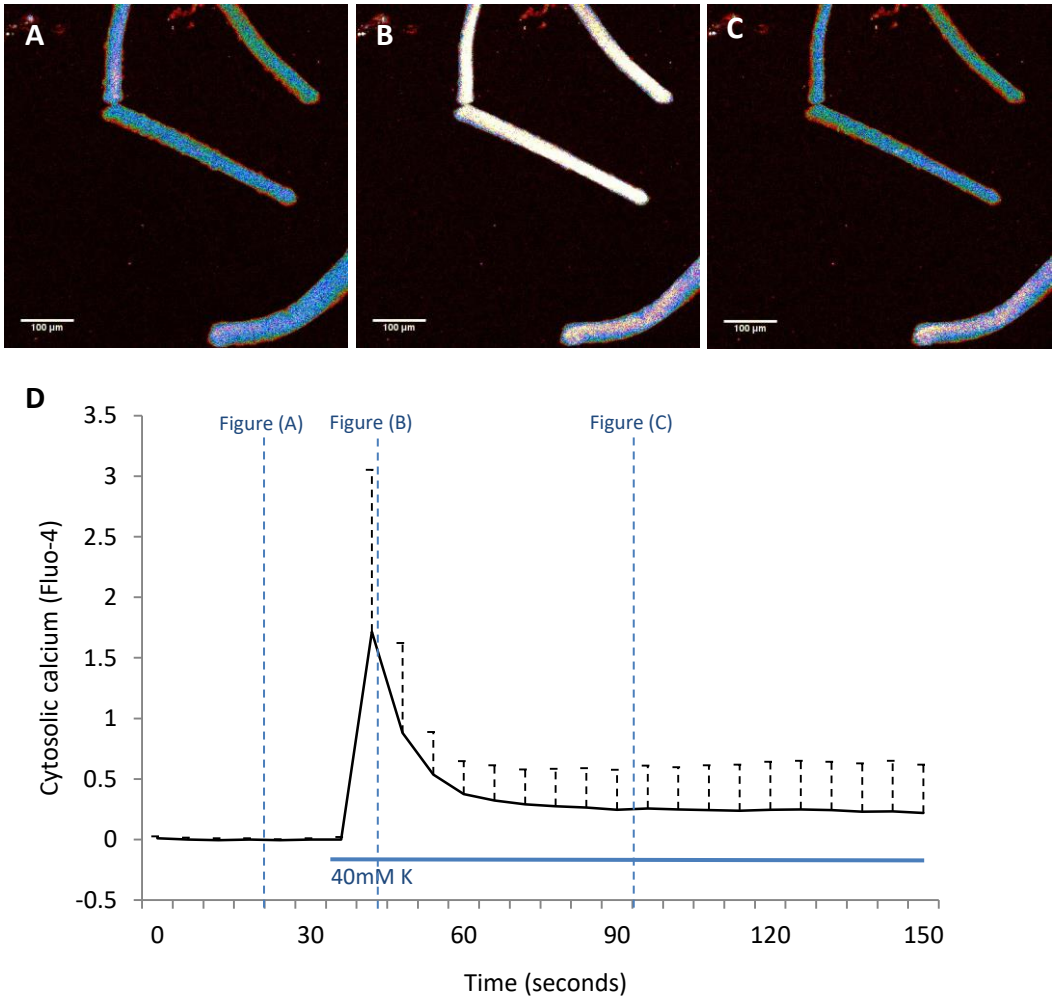

Figure 39: Single fibres – cytosolic calcium upon application of high potassium. *Calcium release in response to application of 40mM potassium after 30 seconds. (**A**) Micrograph of single fibres from the FDB of control mice before application of 40mM potassium. Fibres are stained with Fluo-4 in order to visualise cytosolic calcium. (**B**) Micrograph of the single fibres during application of 40mM potassium. (**C**) Micrograph of the single fibres after application of 40mM potassium. Basal calcium levels were almost recovered within a minute of stimulation with potassium. Fibres were imaged using a Zeiss 700 microscope with a 10x objective. (**D**) Mean values of Fluo-4 fluorescence in six fibres ±SD.*

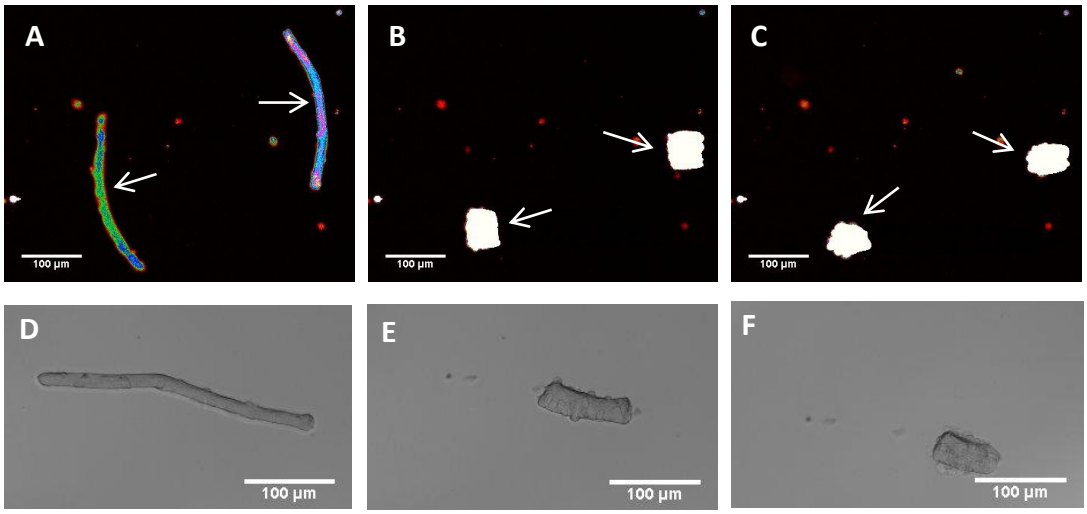

Figure 40: Single fibres – cytosolic calcium upon application of caffeine. *Fibre supercontraction and calcium release in response to application of 10mM caffeine. In figures A-C fibres are indicated by white arrows. (**A**) Cytosolic calcium, stained using Fluo-4, in fibres at rest. (**B**) Cytosolic calcium, stained using Fluo-4, in fibres that have become supercontracted. (**C**) Cytosolic calcium, stained using Fluo-4, in fibres 5 minutes after becoming supercontracted – fibres remained supercontracted and basal calcium levels were not recovered. (**D**) Transmitted light image of a fibre at rest. (**E**) Transmitted light image of a fibre that has become supercontracted. (**F**) Transmitted light image of a fibre 2 minutes after becoming supercontracted. Fibres were imaged using a Zeiss 700 microscope with a 10x objective.*

Due to the difficulties involved in stimulating calcium release using caffeine or high potassium, I developed a protocol for stimulating release of cytosolic calcium electrically. Electrical stimulation resembles physiological initiation of excitation contraction coupling more closely. Both result in the depolarisation of the cell membrane, leading to opening of voltage gated sodium channels.

Changes in cytosolic calcium levels were faster upon electrical stimulation compared to high potassium. As a result imaging settings had to be adjusted in order to record rise and recovery time of cytosolic calcium levels at a sufficient speed for the investigation of electrical stimulation. Highly detailed kinetics could be observed by selecting a section of a cell (10 scans/second; Figure 41A), however this was not practical because cells frequently move a little upon stimulation, resulting in readings being taken from different

parts of the cell rather than from the same area over a period of time. Blebbistatin is a muscle relaxant which acts by binding the myosin/ADP/phosphate complex and interfering with phosphate release. It thus blocks myosin when in an actin-detached state and prevents cross-linking of actin and myosin (Kova´cs et al, 2004). Blebbistatin could have been used to prevent contractions of single fibres during stimulation in order to achieve more stable imaging. Nevertheless the use of blebbistatin was avoided in order to limit disturbance of the fibres before imaging, as solution changes frequently dislodged fibres. The same speed of imaging (10 scans/second) was achieved for imaging whole cells by widening the pinhole of the confocal microscope (230µm instead of 70µm). These same settings could also be used with a lower objective (10x rather than 40x) to capture several cells without increasing the imaging speed. Although the latter settings resulted in less accurate monitoring of the fluctuation pattern, a good level of temporal change in cytosolic calcium could be tracked. These settings were thus used in some instances in order to gain data from a larger number of cells, even though such settings provide less detailed fluctuation patterns.

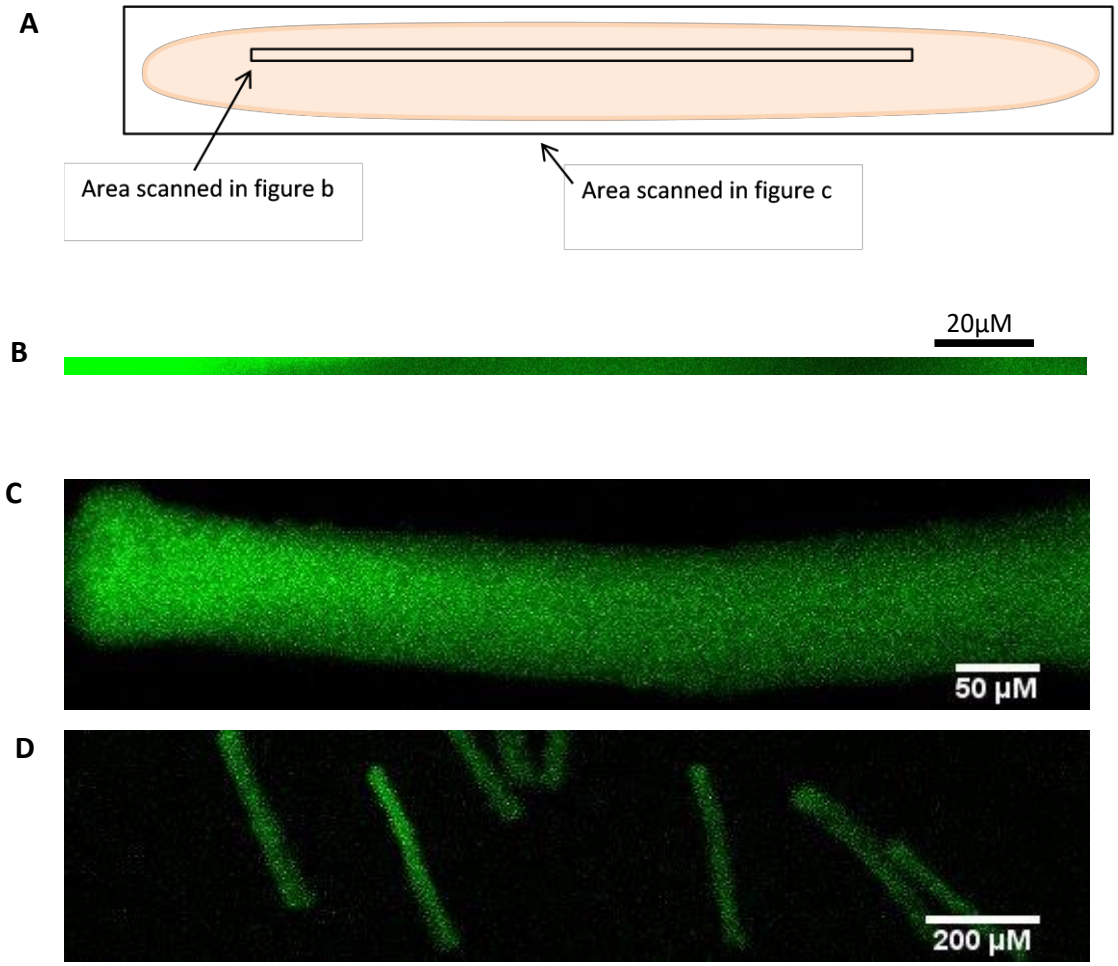

Figure 41: Single fibres – selecting an appropriate imaging method. *(**A**) Diagram indicating the area of cells scanned in figures B and C. (**B**) Fluo-4 fluorescence detected in a thin, longitudinal section of a fibre. Recorded using a Zeiss 700 microscope with a 40x objective. (**C**) Fluo-4 fluorescence detected in the whole fibre. Recorded using a Zeiss 700 microscope with a 40x objective (**D**) Fluo-4 fluorescence detected in several fibres. Recorded using a Zeiss 700 microscope with a 10x objective.*

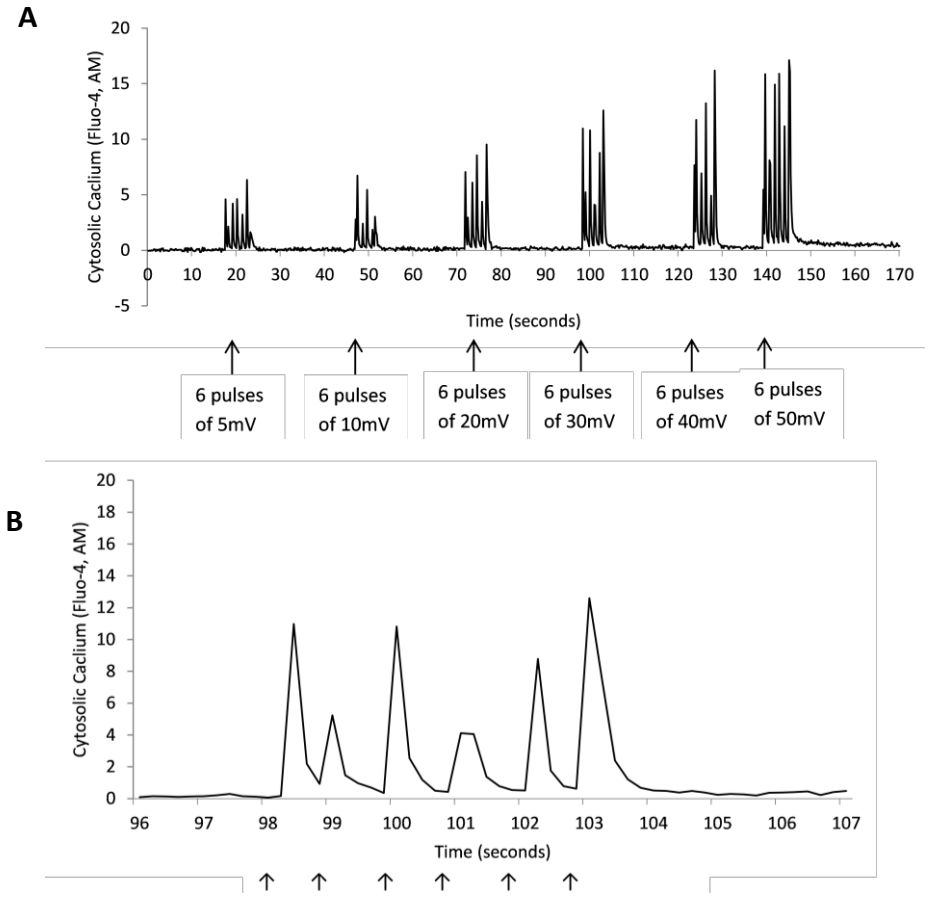

Figure 42: Single fibres – c*ytosolic calcium during electrical stimulation.* ***(A)*** Typical response of a single FDB fibre to electrical stimulation at 20, 30, 40 and 50 mV. Five or six pulses of each voltage were applied at 100ms intervals with 8-10 seconds' interval between each set of stimulations. (**B**) More detailed view of calcium fluctuations in response to the six pulses at 30mV, with some evidence of inadequate sampling frequency. Fluorescence is given relative to background fluorescence.

These imaging settings allowed for some level of comparison to be made between FDB fibres from Dgn and WT mice regarding the rate of cytosolic calcium release and recovery. However in some instances the peak could not be defined due to inadequate sampling frequency – the imaging speed is limited by the acquisition rate of the microscope system. The image acquisition was slower than the response rate and data points at the peak were missed (figure 42B). Figure 42A shows a typical response to electrical stimulation - calcium levels increase upon electrical stimulation, with larger fluctuations occurring in response to more intense stimulation. Some differences were observed in the intensity and rates of calcium release from WT and Dgn mice. Due to the small number of animals used, statistical analysis of these differences would not have been valuable, nevertheless the differences are worth highlighting. Calcium levels in fibres

isolated from WT mice reached a maximal level of stimulation at lower voltages (34mV compared to 57mV in the fibres isolated from Dgn mice - taken as an average from electrical stimulation of 7 fibres). There was no trend in the rate of calcium re-uptake, but calcium release was typically slower in the WT fibres (a p-value of 0.025; figure 43A).

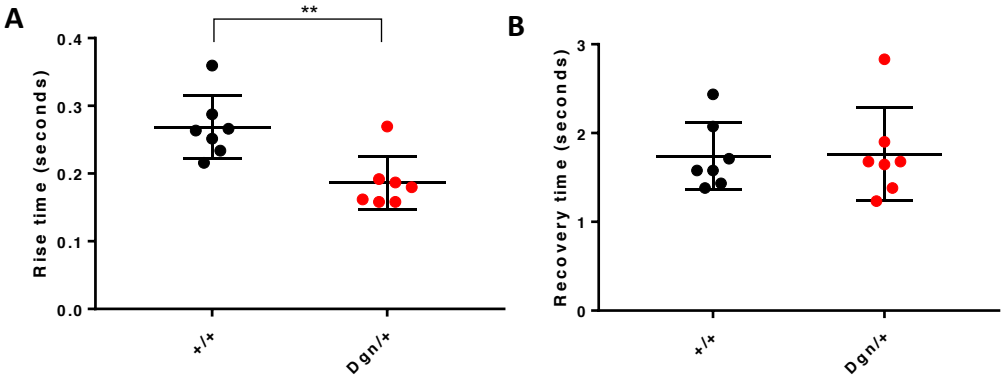

Figure 43: Single fibres – cytosolic calcium rise and recovery times upon electrical stimulation. *(**A**) The mean time ±SD taken for cytosolic calcium to reach maximal levels following electrical stimulation in single fibres from WT (0.268 ± 0.046) and Dgn (0.187 ± 0.039) mice. (**B**) The mean time ±SD taken until basal levels were reached once more following electrical stimulation in single fibres from WT (1.742±0.381) and Dgn (1.764±0.519) mice. Rise time is typically slower for WT fibres. Unpaired Student's t-test, **P=0.025. Recovery does not differ between Dgn and WT fibres (Unpaired Student's t-test, P=* 0.9298*). N=7, fibres from seven Dgn and seven WT mice were analysed, two to four fibres were analysed per mouse.*

4.2.6 Concluding remarks for part 2

Ex vivo investigations on male mice indicate that mitochondrial membrane potential was reduced in Dgn mice, and that the proportion of intermyofibrillar mitochondria is greater in controls. This differences were not correlated with any changes in the activity levels of mitochondrial complexes I, II, III and IV. The *ex vivo* investigations also indicate that calcium release into the cytosol was faster in Dgn fibres from males than in control fibres from males. Overall the *ex vivo* investigations indicate that calcium handling and mitochondrial membrane potential were affected in single muscle fibres. The *in vivo* investigations on the Dgn model of PP indicate that hind limbs of female Dgn mice do not display a statistically significant degree of resistance to fatigue. Investigations on males with the Dgn mutation indicate that males do display resistance to fatigue, as presented in Corrochano et al, (2014).

4.3 DEVELOPING A DRUG MODEL OF HYPOKALAEMIC PERIODIC PARALYSIS

In this chapter I explored the potential of creating a drug model of PP where attacks of paralysis could be simulated. I used barium in combination with reduced potassium in order to simulate PP associated depolarisation in neonatal Sprague Dawley rat myotube cultures. Both the patient derived, and the *ex vivo* models of PP do not display spontaneous depolarisations. This drug model may help to identify effects of PP that are specifically a result of hypokalaemia associated depolarisations. Findings include some indication that spontaneous calcium release was potentiated by the drug treatment, but peak cytosolic calcium levels remained unaffected.

Gramicidin has been used to simulate the aberrant pore present in hypoPP in rat diaphragm sections (Jurkat-Rott et al, 2009) where it had the effect of shifting the tendency for paradoxical depolarisation towards more physiological extracellular potassium concentrations (around 2.5mM compared to 1.5mM for controls; see figure 3, introduction section 1.1.4). Gramicidin is a linear pentadecapeptide antibiotic that acts by creating a pore allowing the passage of monovalent cations across the plasma membrane, similar to the aberrant pore found in HypoPP. Barium has also been used to simulate HypoPP as described in the introduction (section 1.16.4). Barium acts by blocking potassium channels and thereby induces the paradoxical depolarisation characteristic of HypoPP (Struyk et al, 2008). I explored the use of both gramicidin and barium as simulators of HypoPP in neonatal Sprague Dawley rat myotube cultures.

In single fibres, reducing extracellular potassium concentration to 2mM barium did not have a discernible effect, but reducing it to 1mM potassium in the presence of 50µM barium was sufficient to cause paradoxical depolarization. Further reducing extracellular potassium to 0.5mM resulted in depolarization, even in the absence of barium. This effect is explained in introduction section 1.8 (see also Struyk et al, 2008). I initially tested the direct effects of these treatments on the neonatal cultures both electrophysiologically and using membrane potential sensitive dyes. I then focussed on the use of barium to simulate PP and studied the direct and the downstream effects of such a challenge on calcium handling and mitochondrial bioenergetics.

In addition I tested the possibility of using gramicidin to simulate HypoPP in neonatal cultures. Results from these tests were primarily negative. The use of barium as a drug model of HypoPP is thus the focus in this chapter of the results.

4.3.1 The direct effects of barium challenge on membrane potential - electrophysiology

Both whole cell and sharp electrode patch clamping were used to observe direct effects of the barium challenge. I initially used the method of whole cell patch-clamping in order to determine whether or not a paradoxical depolarisation would be observed if sufficiently low concentrations of potassium were applied. 1mM extracellular potassium has been shown elsewhere to produce depolarisation in dissociated fibres from interosseus muscle (Struyk & Cannon, 2008). I thus tried this concentration in my own investigations with the neonatal myotube cultures. I left cells to equilibrate for five minutes before taking measurements. Of the four cells that I successfully patched in this trial period, two did not show any response to the challenge of reduced extracellular potassium, one became marginally depolarized and one became marginally hyperpolarised (data not shown). This range of responses suggests that the experimental set up did not provide an appropriate approach for detecting subtle changes in the membrane potential such as those that were being sought. Although dialysation due to the whole cell patch configuration does not normally affect whole cell patching before 10 minutes have elapsed, it may be that readings were affected by minor dialysation such that more subtle changes were not detectable.

Tests were then carried out by sharp electrode patch clamping (see methods, section 3.10). This protects the cell from dialysis as the sharp electrode limits the passage of ions in and out of the intracellular fluid. The sharp electrode technique was carried out with a colleague of mine, Michael Thor (UCL, London). Results obtained by sharp electrode patch clamping indicate that 1mM potassium did not produce paradoxical depolarisation on its own, nor in the presence of gramicidin. Cells tested with 1mM potassium in the presence of 50µM barium did become depolarised, see table 6.

Mean V_{REST} for fibres exposed to different $[K]_{extra}$ with or without $BaCl_2$ or gramicidin			
$[K+]_{extra}$	Drugs	V_{REST} (mV)	Number of fibres
4mM	none	62.2 ±6.8	11
2mM	50µM Ba^{2+}	60.7 ±6.6	8
1mM	none	59.1 ±7.7	11
1mM	50µM Ba^{2+}	53.2 ±8.9	3
Errors represent ± SEM			

Table 6: Resting membrane potential at different external potassium concentrations. *The average values of resting membrane potentials were recorded for fibres exposed to 4mM, 2mM or 1mM extracellular potassium, with or without 50µM barium (Ba^{2+}). Fibres were allowed to stabilize for 15 minutes at 4mM and then to re-equilibrate for 5 minutes at each condition before recordings were taken.*

4.3.2 The direct effects of barium challenge on membrane potential – membrane potential sensitive dyes

Membrane potential can also be estimated using voltage sensitive dyes. I used these to determine the effect that the barium treatment had on membrane potential. Although patch clamping should be more accurate for these purposes, using a dye allows for many more cells to be observed at once.

I used two such dyes. Initially I used Fluovolt (Thermo Fisher) which is a fluorescent sensor. It acts by modulating photo-induced electron transfer via a synthetic molecular wire to a fluorophore (Miller et al, 2012) as described in methods (section 3.4.4, I.). It is characterised by fast kinetics making it appropriate for investigating responses to electrical stimulation. Fluovolt exhibits approximately 25% change in fluorescence in response to a depolarising voltage step of 100mV. The paradoxical depolarisation in response to potassium reduction on the other hand should result in a change in membrane potential of approximately 25mV and thus in an increase in dye fluorescence of approximately 5%. When tested on cells during depolarisation using 40mM potassium, there was a 20% increase in fluorescence – close to the predicted value of 25% (figure 44). However, smaller depolarisations were difficult to track by this fluorescence method because of the low signal to noise ratio. In particular challenge with 1mM potassium and 50µM barium should have resulted in a 5% increase in fluorescence but a change of only

0.2% was observed (figure 45). The effect of lowering external potassium to 2mM was not tested, having established that 1mM had such a marginal effect of FluoVolt fluorescence (figure 45).

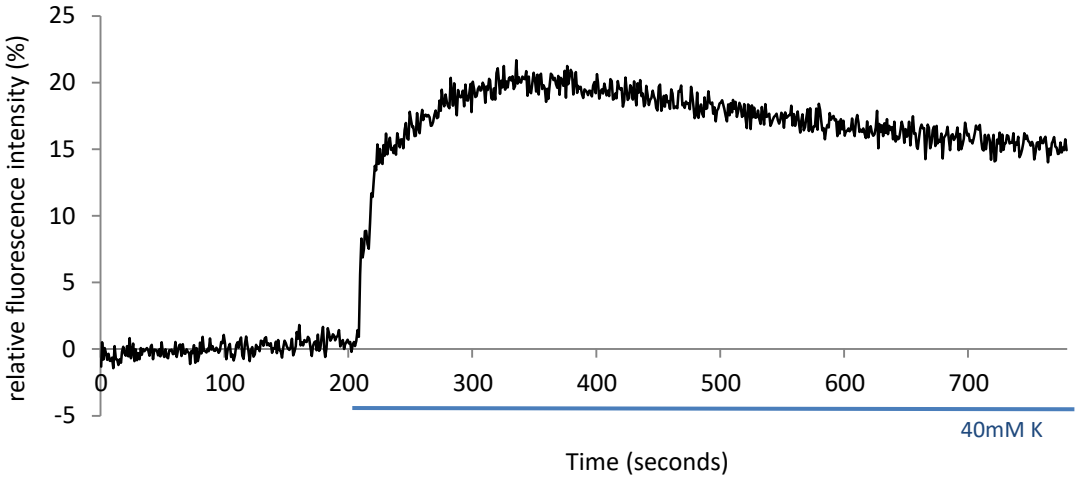

Figure 44: FluoVolt signal upon challenge with high potassium. Changes in FluoVolt fluorescence intensity upon challenging a neonatal culture with 40mM potassium. Values were collected from seven neonatal Sprague Dawley rat myotubes and are given relative to basal Fluovolt fluorescence.

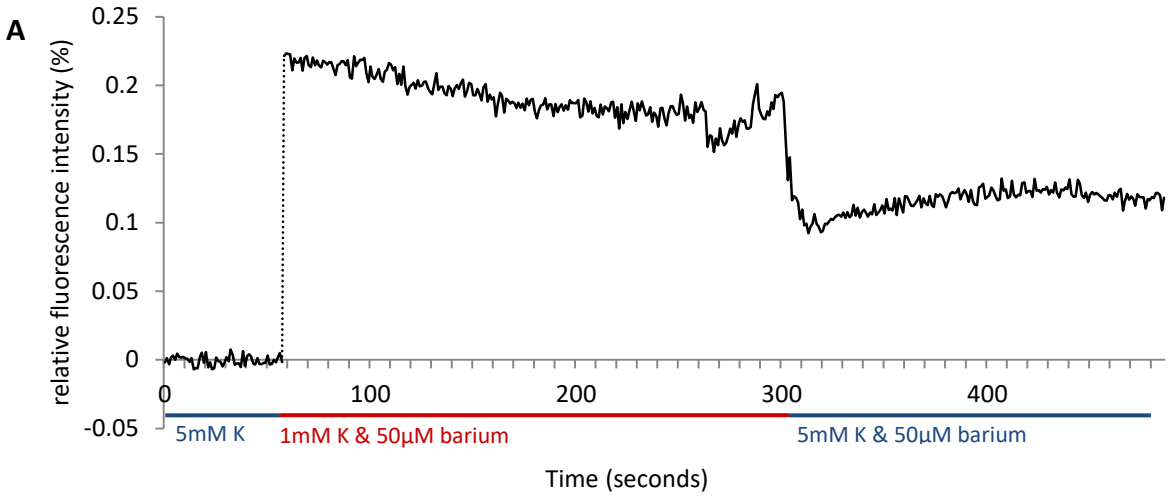

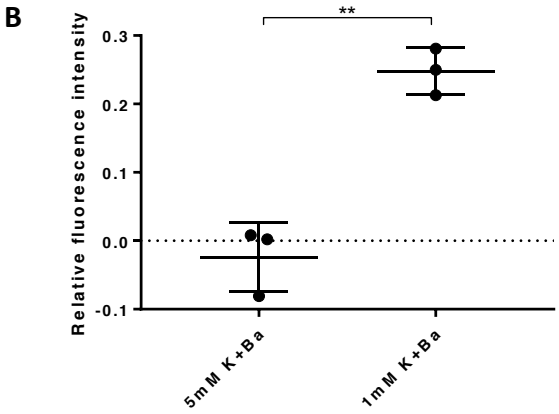

Figure 45: FluoVolt signal upon challenge with low potassium and barium. (**A**) Representative trace of typical changes in FluoVolt fluorescence intensity upon challenge with 1mM potassium in the presence of 50µM barium. Values are given relative to basal Fluovolt fluorescence. The average relative Fluovolt fluorescence was measured for 10 neonatal Sprague Dawley rat myotubes in culture before during and after challenge with 1mM potassium in the presence of 50µM barium. During removal of the standard recording solution and addition of the low potassium solution there was much fluctuation in signal. A dotted line is introduced to indicate that there was an interval between the lower fluorescence levels before challenge and the higher levels after challenge with low potassium. (**B**) Mean relative FluoVolt fluorescence ±SD upon treatment with control medium (0.0237 ± 0.0497) and upon treatment with low 1mM potassium (0.248 ± 0.034). N=3, three neonatal Sprague Dawley rat cultures each containing approximately 10 myotubes were analysed. Cultures were challenged with 1mM potassium in the presence of barium, and returned to control potassium levels. Relative Fluo-4 fluorescence increased upon challenge with low potassium. Unpaired Student's t-test, *P = 0.0015.

The second membrane potential dye that I used was part of a kit designed for high throughput investigations using a Fluorescent Imaging Plate Reader (FLIPR). This dye, the FLIPR Membrane Potential Assay Kit (Molecular Devices) has a negative charge and thus enters the cell upon depolarisation following an inflow of positive ions which create an inward current. Hyperpolarisation on the other hand results in a decrease in fluorescence as positive ions flow out creating an outward current, followed by an outflow of the dye. A quenching dye is also included in the kit to reduce background fluorescence. There are two versions of the quenching dye, a red quencher and a blue quencher, and thus two versions of the assay kit – the "red" kit and the "blue" kit. Results from the blue kit were more variable, both within each condition and when comparing the different conditions. This suggests that the blue kit was less suitable for the neonatal myotube cultures (as indicated by the manufacturer, both versions should be tested with each cell line, and in many cases one of the kits will be more appropriate). As a result only the red kit results are presented here (figure 46).

Paradoxical depolarization occurred in all cells that were treated with 0.5mM or 1mM potassium, it also occurred to some extent for the population treated with barium and 2mM potassium but not without barium (figure 46). This suggests that barium did promote paradoxical depolarization to some degree. Those treated with 5mM potassium did not display depolarization whether or not barium was present (figure 46).

Overall, results obtained using the membrane potential sensitive dyes support the hypothesis that low potassium will depolarise cells and that barium can contribute to such depolarisation. As with a study using a two electrode patch clamp technique carried out on dissociated muscle fibres (Struyk & Cannon, 2008) it appears that neonatal cultures challenged with 1mM extracellular potassium levels become depolarised (figure 46). This was the case for investigations carried out using the membrane potential sensitive dyes. However the sharp electrode patch clamp investigations did not display this effect. Reduction of extracellular potassium concentration did not alter the membrane potential in the 11 myotubes that where tested. Data from three further myotubes that were exposed to low extracellular potassium (1mM) with 50µM barium, did display paradoxical depolarisation as expected (see table 6). This suggests that the barium may have increased sensitivity to paradoxical depolarisation. It is not clear why reduction of extracellular potassium concentrations to 1mM was not sufficient to produce

paradoxical depolarisation (table 6). It may be that the interruption in membrane integrity caused by patch clamping affected sensitivity to the treatment.

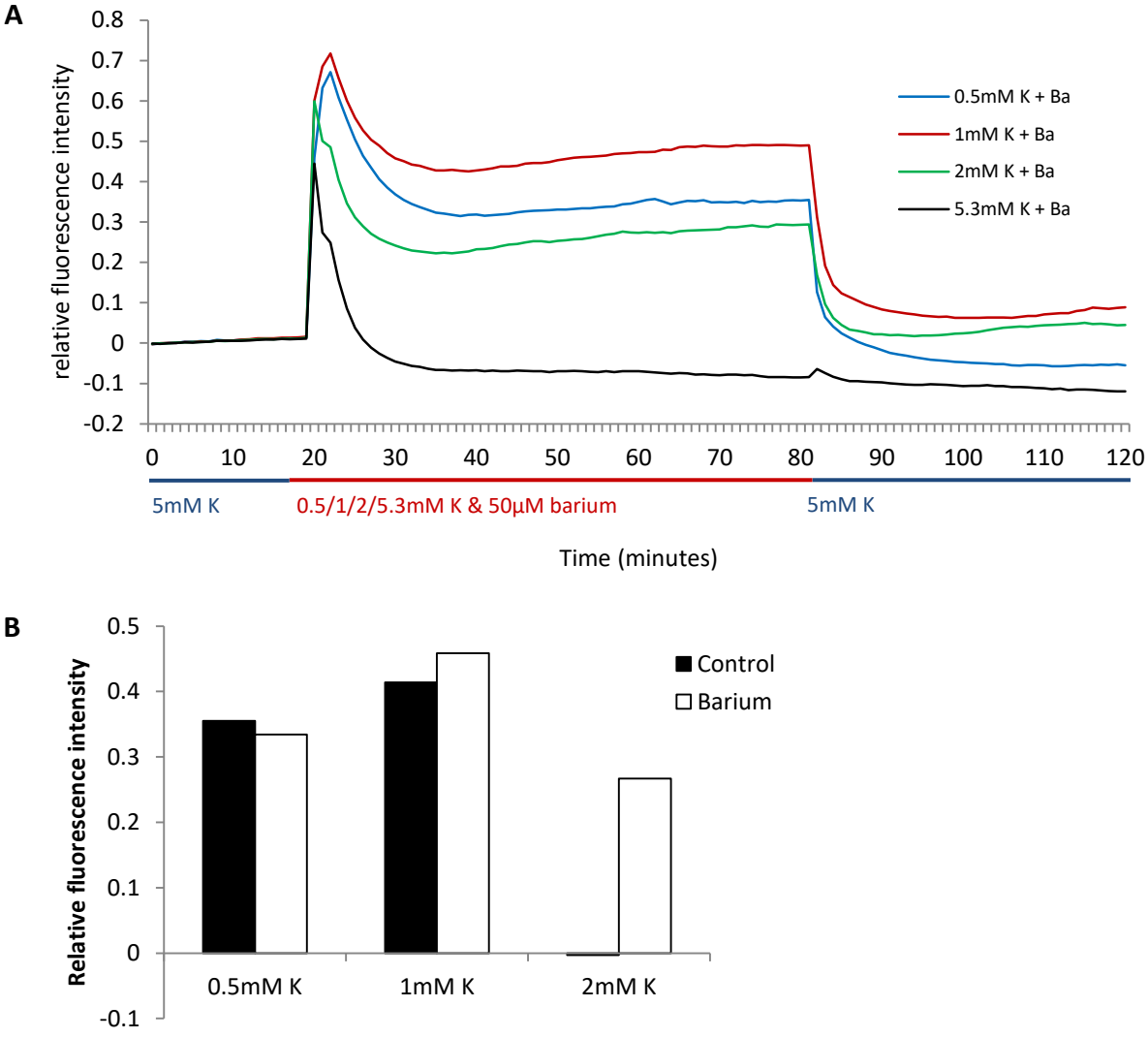

Figure 46: The Molecular Devices membrane potential "red" kit. *Values are given as fluorescence intensity levels during treatment relative to basal fluorescence levels before treatment. (**A**) Trace showing fluorescence levels before, during and after treatment. Cells were initially bathed in 5.3mM potassium, followed by 0.5mM, 1mM, 2mM or 5.3mM potassium in the presence of barium, and finally with 5.3mM potassium in the presence of barium. Treatments were applied at 20 minutes and removed at 80 minutes. The initial peak is an artefact due to solution changes in the FLIPR machine. (**B**) The mean relative fluorescence levels during treatment for cells treated with 0.5mM, 1mM or 2mM potassium. The chart suggests that reducing extracellular potassium levels below 2mM potassium causes increased cytosolic calcium, and that this increase is not affected by the presence of barium, however this investigation was only carried out once and statistical significance cannot be calculated.*

4.3.3 The effects of barium and gramicidin on spontaneous cytosolic calcium fluctuations

Having observed that barium has a direct effect on mitochondrial membrane potential, I went on to investigate effects of the barium and gramicidin treatments on calcium handling in the myotubes. Cultures were treated with Fluo4, AM and imaged by fluorescence microscopy.

I observed that the neonatal myotube cultures exhibited spontaneous calcium signals in culture upon reduction of extracellular potassium to 1mM (see figure 47A), but not at normal extracellular potassium levels, or even at 2mM extracellular potassium concentrations. I monitored these fluctuations in the presence and absence of both barium and gramicidin. A greater proportion of cells exhibited the calcium fluctuations in cultures treated with 50µM barium than in control cultures, and fewer exhibited such fluctuations upon treatment with gramicidin (figure 47B). Indeed in several cases the treatment with gramicidin resulted in cessation of all spontaneous calcium release as well as cessation of calcium signals in response to electrical stimulation. This may be related to the inhibitory effect of calcium ions on the gramicidin conductance (Gambale et al, 1987). Cells treated with a combination of 50µM barium and 0.1µM gramicidin did exhibit spontaneous calcium signals. Possibly due to the effects of barium in potentiating the calcium signals and despite the inhibitory effects observed when gramicidin was applied alone. Electrical stimulation was used as a positive control to ensure that cells were responsive.

The average time taken for cytosolic calcium levels to recover following each spontaneous fluctuation is compared in figure 47C for barium treated and control myotubes. These recovery times were not significantly difference.

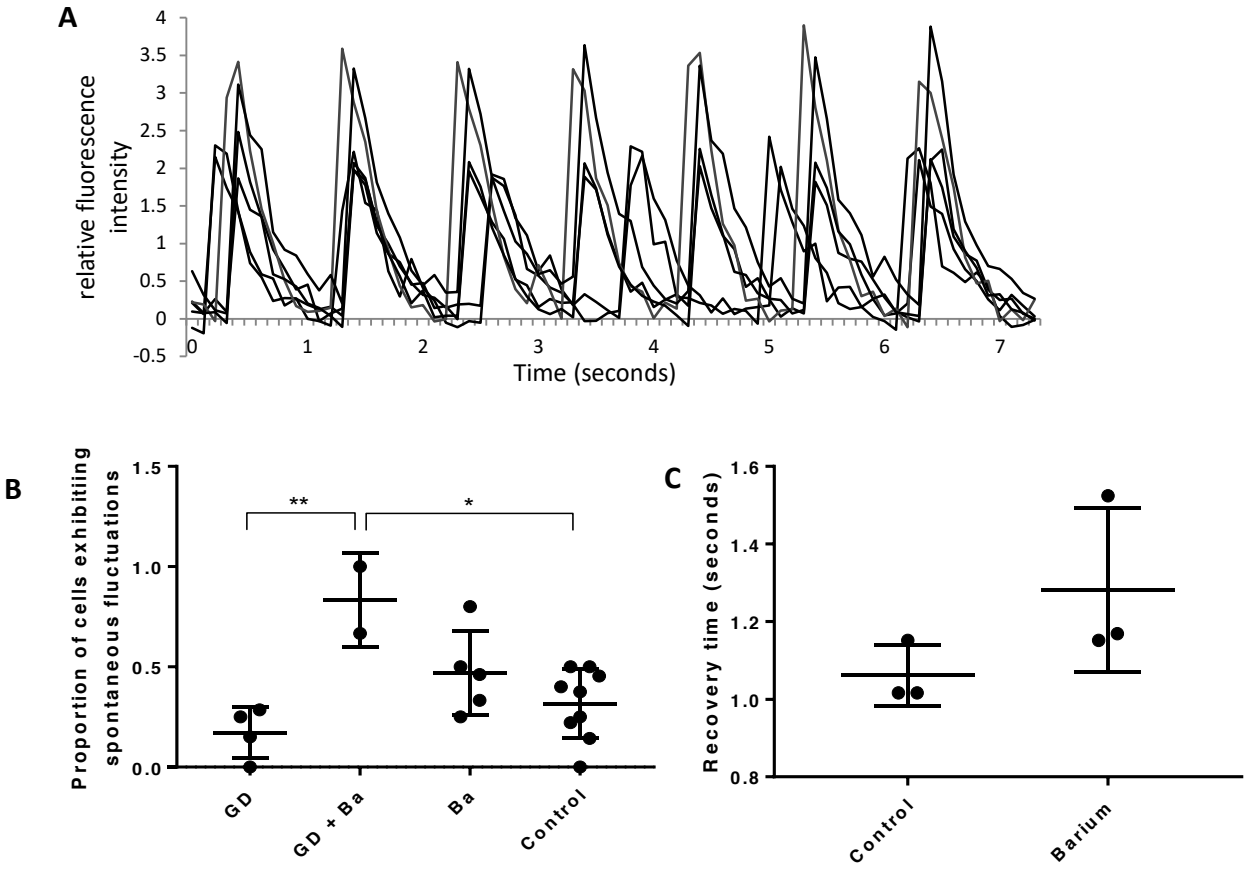

Figure 47: Drug models – spontaneous calcium fluctuations. *(**A**) A trace of six cells that exhibit spontaneous cytosolic calcium signals. Where there was contact between the cells in culture the signals were electrically coupled. (**B**) Scatter plot indicating the proportion of cells exhibiting calcium release upon treatment with low extracellular potassium (1mM) in presence of gramicidin (GD), gramicidin and barium (GD + Ba), barium (Ba), or with neither barium nor gramicidin (control). Mean ±SD is indicated for GD (0.171 ± 0.128) for GD + Ba (0.833 ± 0.236), Ba (0.469 ± 0.210) and for control (0.316 ± 0.173). None of the myotubes exhibited such fluctuations before reduction of the extracellular potassium concentration from 5.3mM to 1mM. N=4 for gramicidin treated cultures, n=2 for gramicidin and barium treated cultures, n=5 for barium treated cultures and n=9 for the controls. The proportion of cells exhibiting calcium fluctuations upon treatment with Barium and gramicidin is statistically significantly greater than that of cells upon treatment with gramicidin and that of untreated cells. One-way ANOVA followed by Tukey's post hoc test, **P = 0.0032 and *P = 0.0102, respectively. (**C**) Scatter plot of cytosolic calcium recovery times ±SD at the end of each transient calcium fluctuation. N=3, recovery times are compared for three barium treated myotubes (1.282 ± 0.210) and three control myotubes (1.062 ± 0.078). Recovery was typically slower in barium treated cultures. Unpaired Student's t-test, P = 0.1646.*

4.3.4 The effects of barium challenge on calcium handling and mitochondrial membrane potential

In conjunction with testing the direct effects of the low potassium/barium challenge on membrane potential, other effects on calcium handling and mitochondrial membrane potential were also investigated. The same model of neonatal Sprague Dawley rat cultures was used for these investigations. Calcium handling was monitored using Fluo-4. TMRM was used to investigate effects on mitochondrial membrane potential as well as for characterising mitochondrial structure.

Cultures were imaged both during treatment in order to monitor direct effects of the conditions, and following treatment in order to determine downstream effects. In addition cells were fixed for immunofluorescence assays and for Western blotting following treatment in order to better understand downstream effects of the treatment. Due to the inhibitory effects observed with use of gramicidin only barium was used for these downstream tests.

Fluo-4 fluorescence was monitored in cells while challenging the culture with 5 electrical pulses administered at 40 millivolts at a frequency of 0.1 Hertz (see figure 48A for sample response). 10, 20, 30 and 50 millivolts were also used but responses to pulses at 40 millivolts gave the most consistent results and are therefore considered here. I analysed the relative peak cytosolic calcium concentration reached following a set of 5 pulses (figure 48B). I compared cells that were pre-treated for an hour with 1mM, 2mM or 5.3mM potassium in the presence or absence of barium. Cells were imaged three hours after application of the different conditions. Peak cytosolic calcium levels reached in the myotubes were not affected by pre-treatment with low potassium, whether or not barium was added (figure 48B).

A

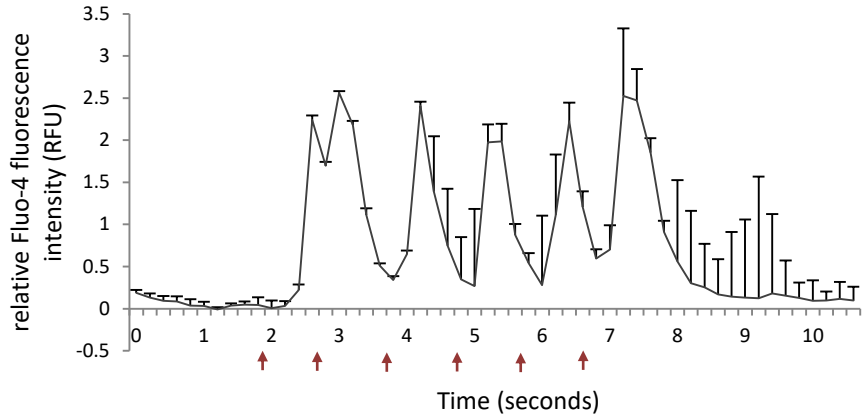

B

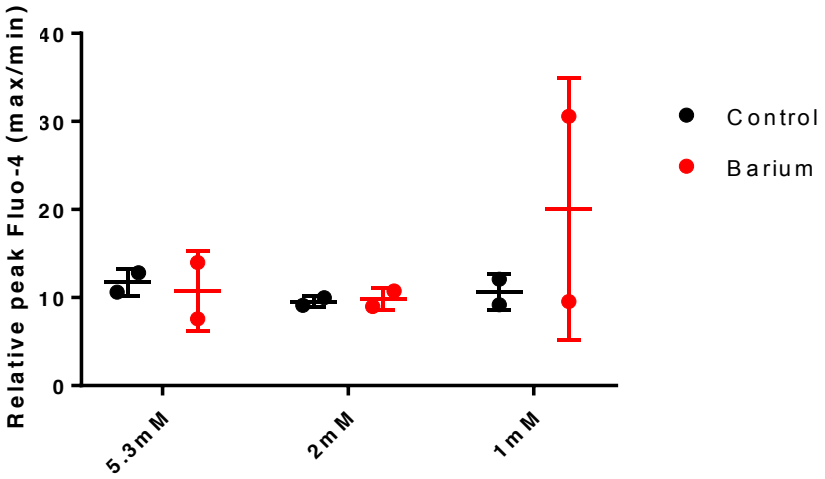

C

	5.3mM K	5.3mM K + Ba	2mM K	2mM K + Ba	1mM K	1mM K + Ba
Mean peak	11.73	10.77	9.553	9.865	10.62	20.06
SD of peak	1.556	4.525	0.6083	1.253	2.043	14.86
SEM of peak	1.101	3.199	0.4301	0.8861	1.445	10.51

Figure 48: Drug model – peak cytosolic calcium. *Neonatal* Sprague Dawley rat *myotube cultures were treated with medium containing 1mM, 2mM or 5.3mM potassium for one hour and imaged three hours after treatment. Relative Fluo-4 fluorescence intensity was measured while stimulating the cells electrically. Electrical stimulation was administered as 6 pulses of 40 millivolts at a frequency of 0.1 Hertz as indicated by arrows in A. (**A**) sample chart showing the fluctuations of Fluo-4 fluorescence in response to electrical stimulation in 3 cells from a single dish (pre-treated with 1mM potassium). (**B**) Peak cytosolic calcium levels in response to electrical stimulation. Relative peak cytosolic calcium levels were not affected by addition of barium in myotubes treated with 5.3mM, 2mM or 1mM extracellular potassium. Interaction P value = 0.5029 (two-way ANOVA test). (**C**) Table of mean and SD values from B, along with SEM. N=2, two neonatal myotubes cultures were tested per condition.*

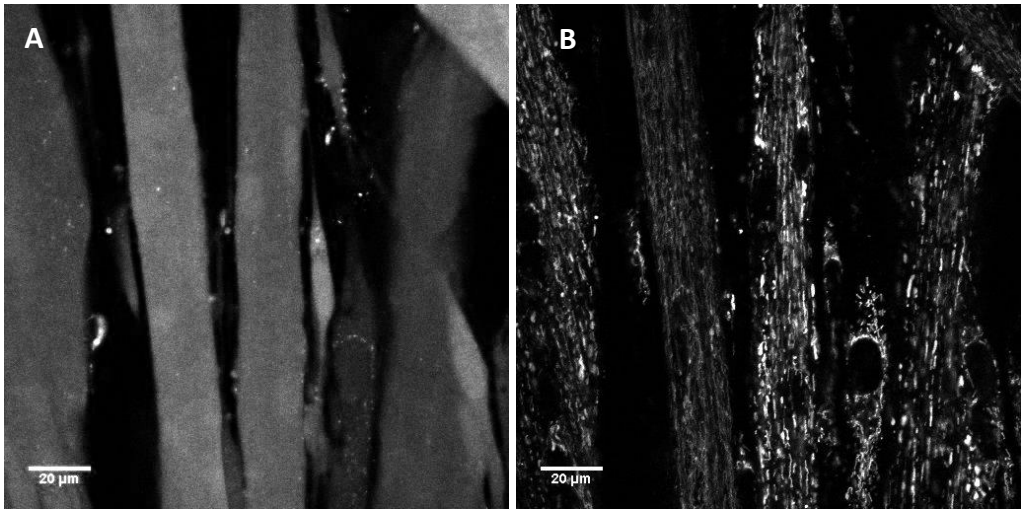

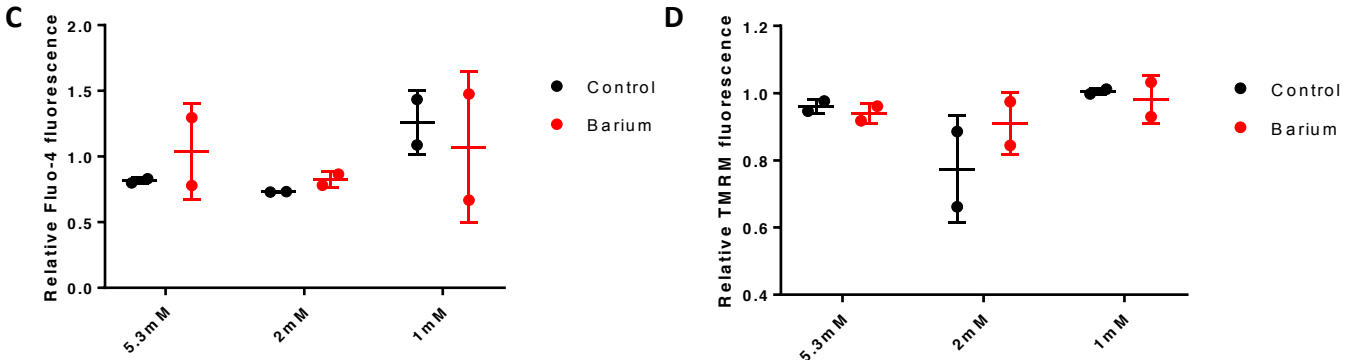

E

	5.3mM K	5.3mM K + Ba	2mM K	2mM K + Ba	1mM K	1mM K + Ba
Mean Fluo-4	0.8147	1.038	0.731	0.8241	1.26	1.071
SD of Fluo-4	0.02223	0.3655	0.002807	0.05999	0.2453	0.5721
SEM of Fluo-4	0.01572	0.2584	0.001985	0.04242	0.1735	0.4045
Mean TMRM	0.9613	0.9392	0.7739	0.9094	1.005	0.9813
SD of TMRM	0.02089	0.03067	0.1583	0.09235	0.00985	0.07259
SEM of TMRM	0.01477	0.02169	0.1119	0.0653	0.00697	0.05133

Figure 49: Drug model – mitochondrial membrane potential. *(**A**) Cytosolic calcium in neonatal myotube stained using Fluo-4. Myotubes were imaged three hours after treatment with low extracellular potassium (1mM) in the presence of barium for one hour. (**B**) Neonatal myotubes from figure A, stained with TMRM in order to visualise mitochondrial membrane potential. Imaged using a Zeiss 700 microscope with a 40x objective. (**C**) Cytosolic calcium levels were not affected by addition of barium in myotubes pre-treated with 5.3mM (control potassium levels), 2mM or 1mM extracellular potassium. Interaction P value = 0.6264 (two-way ANOVA test). (**D**) Mitochondrial membrane potential levels were not affected by addition of barium in myotubes pre-treated with 5.3mM (control potassium levels), 2mM or 1mM extracellular potassium. Interaction P value = 0.3535 (two-way ANOVA test). (**E**) Table of mean and SD values from C and D, along with SEM.N=2, two neonatal myotubes cultures were tested per condition.*

Relative Fluo-4 fluorescence was not affected by pre-treatment with 1mM extracellular potassium compared to those pre-treated with 5.3mM extracellular potassium ($p=0.01$). The addition of barium had no discernible effect on either calcium signalling or on mitochondrial membrane potential (figures 48c and 48d).

4.3.5 Barium challenge in single muscle fibres

This investigation was repeated with FDB fibres – fibres were exposed to 1mM, 2mM and 5.3mM potassium in the presence and absence of barium while imaging by fluorescence microscopy. TMRM was used to measure mitochondrial membrane potential during changes in extracellular potassium concentrations while cytosolic calcium concentration was measured with Fluo-4. No differences were detected in the mitochondrial membrane potential or in calcium handling in these fibres during treatment. Fibres were also treated with these conditions before imaging. Such pre-treatment did not affect mitochondrial membrane potential either (figure 50).

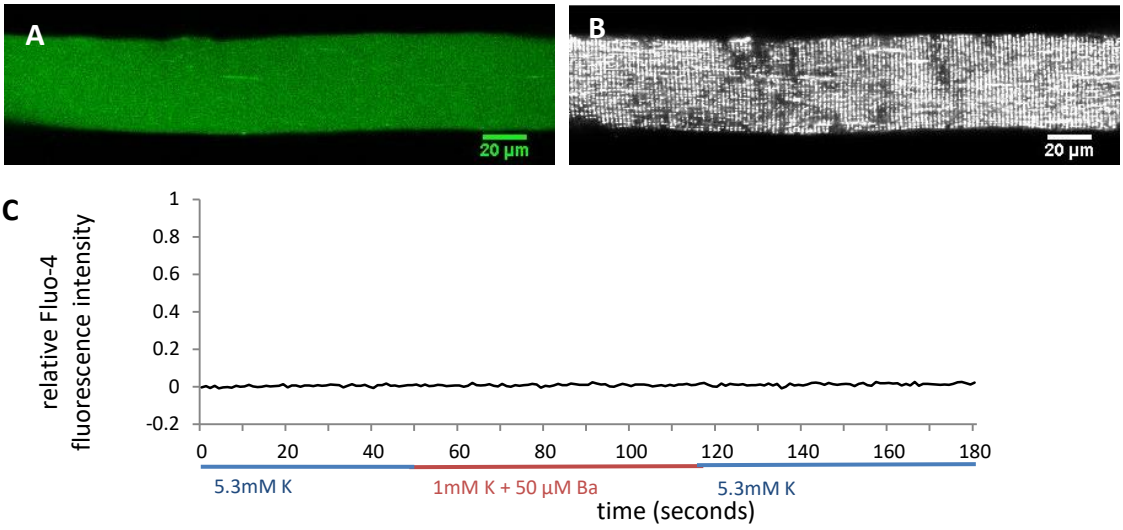

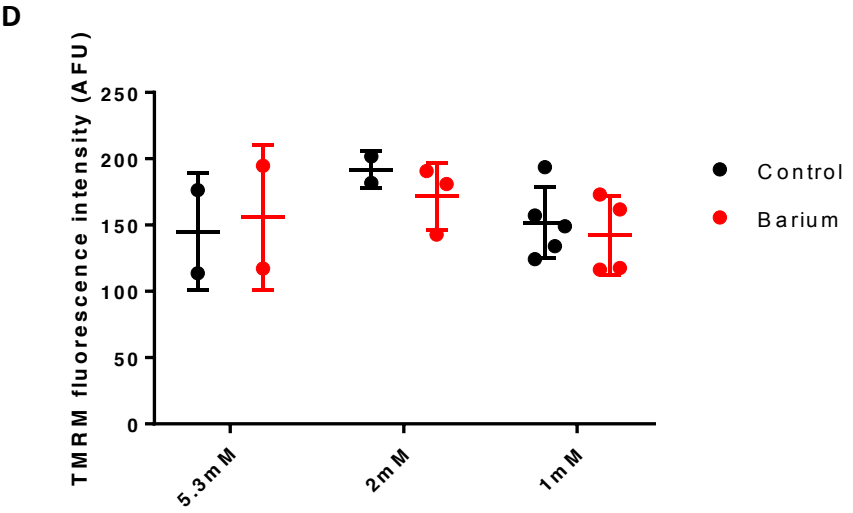

E

	5.3mM K	5.3mM K + Ba	2mM K	2mM K + Ba	1mM K	1mM K + Ba
Mean Fluo-4	145	156.1	191.8	171.5	151.7	142
SD of Fluo-4	44.27	54.54	14.14	25.36	26.73	29.59
SEM of Fluo-4	31.3	38.57	10	14.64	11.95	14.8

Figure 50: Drug model in single fibres – mitochondrial membrane potential. *(**A**) Cytosolic calcium in single FDB fibre stained using Fluo-4. Fibre was imaged three hours after treatment with low extracellular potassium (1mM) in the presence of barium for one hour. (**B**) Single fibre from figure A, stained with TMRM in order to visualise mitochondrial membrane potential. Imaged using a Zeiss 700 microscope with a 40x objective. (**C**) A sample chart of Fluo-4 fluorescence showing that levels of cytosolic calcium were unaffected by challenge with 1mM extracellular potassium and 50µM barium. (**D**) Mitochondrial membrane potential levels were not affected by addition of barium in fibres pre-treated with 5.3mM (control potassium levels), 2mM or 1mM extracellular potassium. Interaction P value = 0.7654 (two-way ANOVA test). (**E**) Table of mean and SD values from D, along with SEM.N=2, at least two fibres were tested per condition.*

4.3.6 The effects of the barium challenge on protein expression

The inward rectifier potassium (IRK-2.1) channels are essential for the occurrence of paradoxical depolarization. Their expression in the neonatal cultures was confirmed by immunofluorescence.

Cells that had been treated with low potassium (1mM) expressed more IRK-2.1 channels than controls that were treated with 5.3mM potassium (figure 51). Such upregulation of IRK-2.1 channels in treated cells may help to counter the inhibition of IRK-2.1 channels by barium (Standen & Stanfield, 1978).

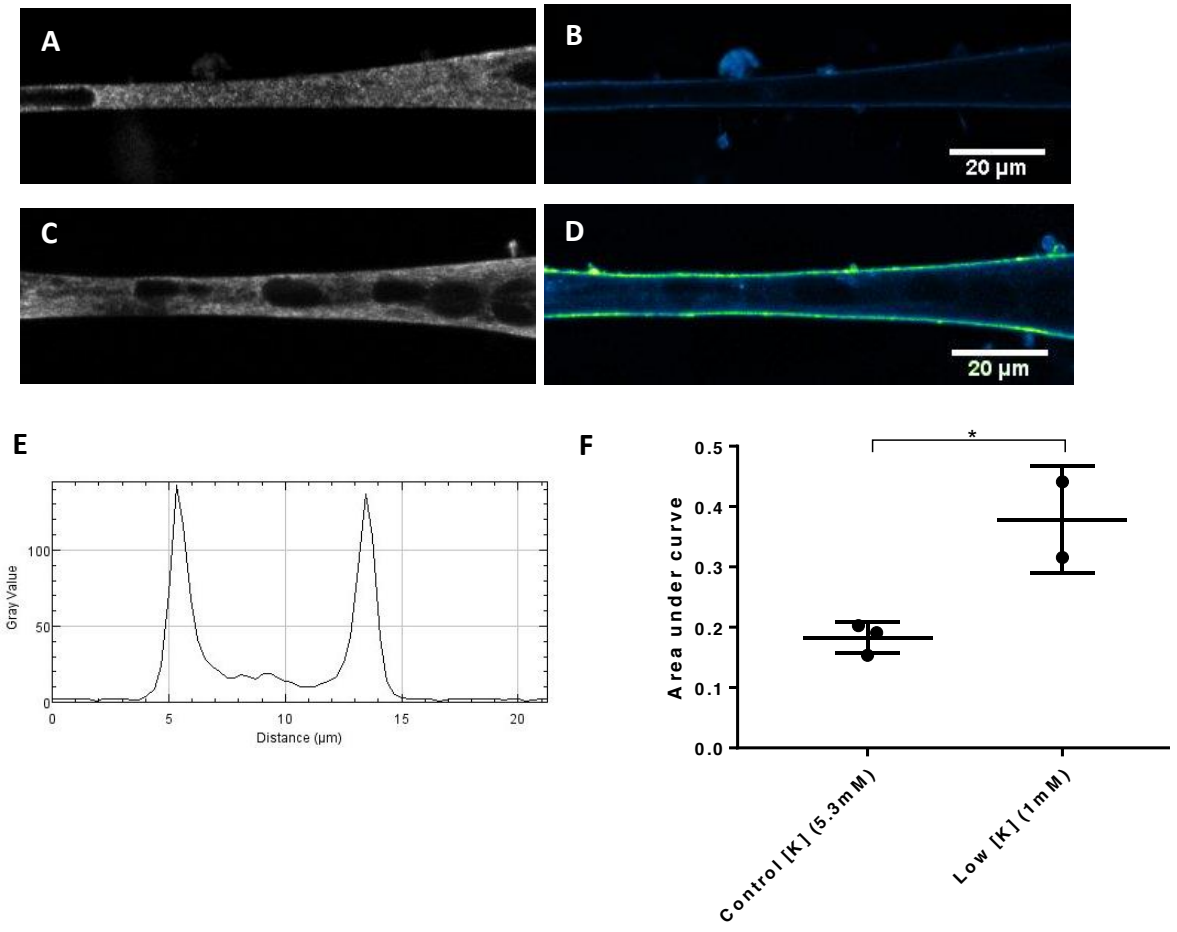

Figure 51: Drug model – IRK-2.1 expression. *Quantification of fluorescence signal from immunofluorescence analysis of IRK-2.1 channels. (**A-D**) Neonatal* Sprague Dawley rat *myotube fixed one day after treatment and stained with a desmin antibody (greys) and an IRK-2.1 antibody (green/blue). (**A-B**) Cells treated for one hour with 50µM barium and either 5.3mM potassium. (**C-D**) Cells treated for one hour with 50µM barium 1mM potassium. More IRK-2.1 staining can be seen following treatment with low potassium (D) than control (B). Cells were imaged using a Zeiss 700 microscope at a 40x objective. (**E**) A sample intensity plot used to quantify and compare levels of fluorescence. Antibody levels were quantified by measuring the area under the curve of each plot of fluorescence intensity across a single myotube, relative to equivalent plots of levels of desmin in the myotube (not shown). (**F**) The level of IRK-2.1 antibody detected in cells following one hour of treatment. Mean levels of IRK-2.1 expression ± SD are indicated. Greater levels of IRK-2.1 are expressed in myotubes treated with low potassium (0.378 ± 0.089) compared to controls(0.183 ± 0.026). Unpaired Student's t-test, *P < 0.0304. N=3 for control and N=2 for treated cultures, data were collected from three control cultures (treated with 5.3mM potassium), and from two cultures that had been treated with 1mM potassium.*

Although several myotubes were analysed, data were only collected from a single culture of each condition. In addition immunofluorescence assays are less quantitative than Western blot analysis. Consequently, while results presented in figure 51 may indicate a significant increase in expression of IRK-2.1 channels following challenge with low extracellular potassium in the presence of barium, it is not clear that such a difference would persists with further testing. I tested IRK-2.1 expression by Western blotting in order to confirm this trend however the antibody did not produce sufficiently clear bands and will not be considered here.

Western blotting analysis produced clearer results with TFAM and the mitochondrial respiratory complexes. TFAM is a regulator of mitochondrial transcription and also leads to increased oxidative phosphorylation. As demonstrated for the Dgn model of PP, affected fibres may shift toward a more oxidative phenotype. Such a shift could be detected in the drug model as an increase in TFAM levels or as an increase in levels of the mitochondrial respiratory complexes.

Effects of culture in 0.5mM, 1mM and 5.3mM potassium were compared, where the condition was applied for four hours, one hour or half an hour. All cultures included 50µM barium. Cells were fixed for analysis after overnight incubation in normal culture conditions. The TFAM test suggests that expression of TFAM was increased in cells that were treated for four hours with 0.5mM potassium, but not for treatment with higher potassium concentrations or shorter periods of time.

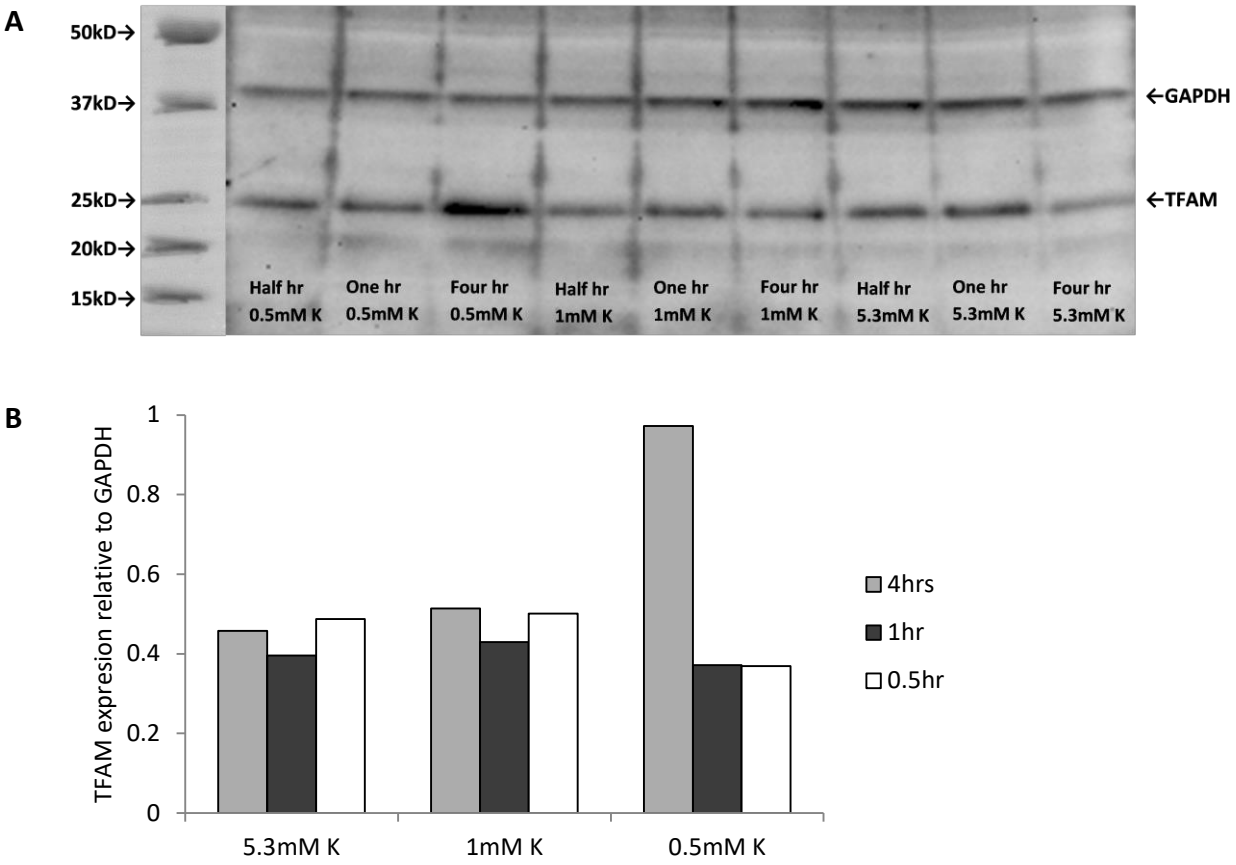

Figure 52: Drug model – TFAM expression. *(**A**) Western blot testing TFAM levels, relative to GAPDH. (**B**) Analysis of the Western blot. Values are given here relative to GAPDH expression. Cells were pre-treated with 50µM barium and 5.3mM (control), 1mM or 0.5mM extracellular potassium, for four hours, one hour or half an hour. Cells were then incubated under normal growth conditions overnight before fixing for analysis. N=1, data from a single Western blot are presented and each of the 9 conditions is represented by a single neonatal Sprague Dawley rat myotube culture.*

Expression of the mitochondrial respiratory complexes were likewise quantified following four hours, one hour or half an hour of treatment where cells were cultured in medium containing 5.3mM (control), 1mM or 0.5mM potassium. 50µM barium was present in all cultures. Cells were then incubated in normal growth conditions overnight before fixing for analysis. Having shown that TFAM expression was upregulated, an upregulation of the mitochondrial respiratory complexes might have been predicted as a further indication of a shift toward a more oxidative phenotype in treated cells. Complexes I, II, III, IV and V were all tested for, however the bands of complex II were not clear enough to be quantified.

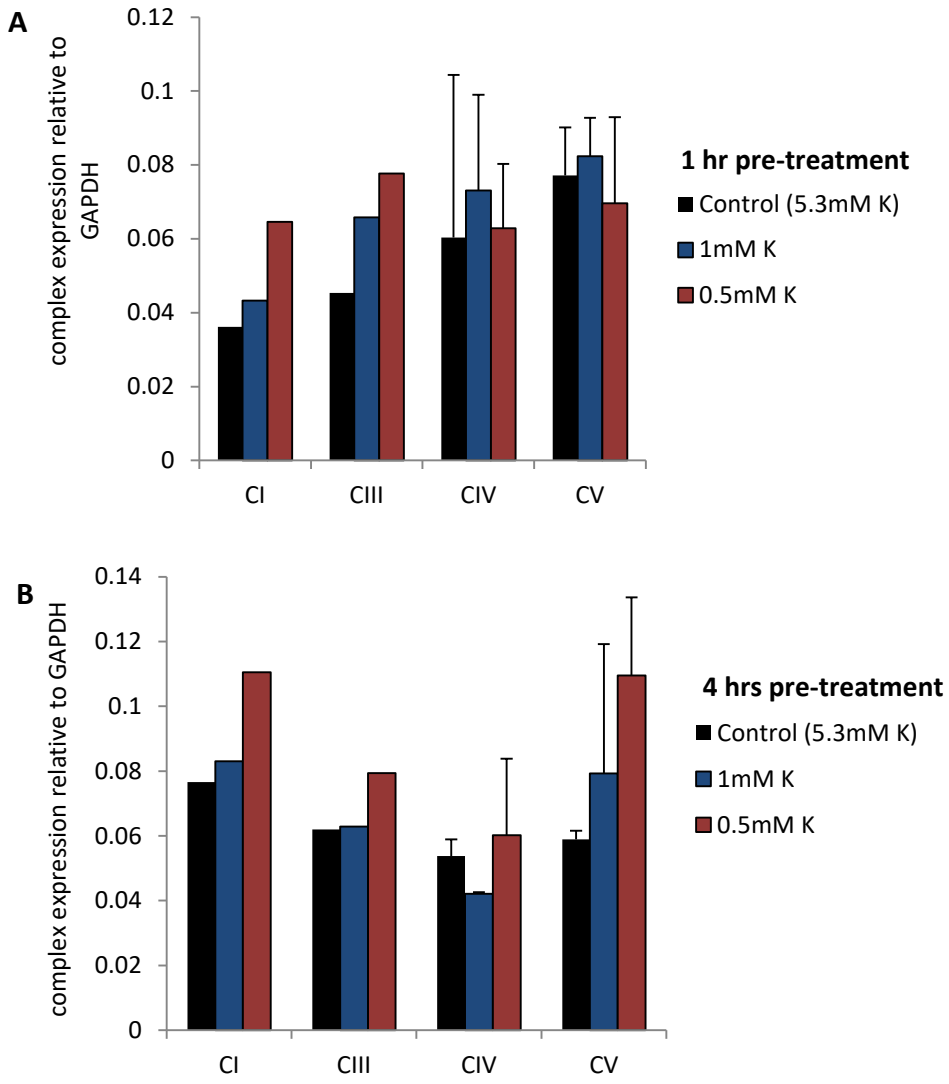

Figure 53: Drug model – mitochondrial complex expression. (A) *Expression of the mitochondrial complexes in neonatal cultures following pre-treatment for one hour. (**B**) Expression of the mitochondrial complexes in neonatal cultures following pre-treatment for four hours. Cells were pre-treated with 5.3mM (control) 1mM or 0.5mM extracellular potassium. Cells were then incubated under normal growth conditions overnight before fixing for analysis. Proteins from complexes I, III, IV and V were quantified by Western blot analysis. Complex I was detected as subunit NDUFB8 of 20kD, complex III as subunit core 2 of 47kDa, complex IV as subunit I of 39kDa and complex V as ATP synthase subunit alpha of 53kDa. GAPDH was used as a loading control, and values are given here relative to GAPDH expression. N= 1 for complexes I and III and N=2 for complexes IV and V; results for complexes I and III were produced using a single Western blot, whereas those for complexes IV and V were produced using data from two Western blots of two separate sets of cultures. Error bars for complexes IV and V indicate standard deviation.*

Results presented in figure 53 are highly variable, suggesting that the challenge with barium and low extracellular potassium does not have a large effect on expression of the mitochondrial complexes. Nevertheless expression of the complexes does appear to increase following four hours of treatment in 0.5mM extracellular potassium in the presence of barium. This may provide further evidence that a shift toward a more oxidative phenotype develops following challenge of cells with low extracellular potassium in the presence of barium.

4.3.7 Concluding remarks on part 3

The value of drug treatment as a model to simulate HypoPP was tested by studying cells both during and following treatment. During treatment, spontaneous calcium fluctuations occurred upon reduction of extracellular potassium to 1mM, whether in the presence or absence of barium. This effect was clearer in the presence of barium. The direct effects of treatment on membrane potential indicate that reducing extracellular potassium to 1mM results in membrane depolarisation (figure 46). Investigations using the FLIPR membrane potential dye suggest that 1mM potassium was sufficient to depolarise the membrane in the presence or in the absence of barium, as has been previously shown *in vivo* (Struyk & Cannon, 2008). Calcium handling was not affected by exposure to barium and low extracellular potassium levels.

Investigations were also performed following pre-treatment of the cultures with 1mM extracellular potassium. Such treatment did not affect basal calcium or basal mitochondrial membrane potential. There is some indication that treatment can lead to increased expression levels of TFAM and IRK-2.1. However these results are derived from a single Western blot in each case. Expression levels of the mitochondrial respiratory complexes were not affected at 1mM. The increase in TFAM may support the hypothesis that cells were shifting toward a more oxidative phenotype, as suggested by results from the animal model.

Treatment in preparation for Western blotting was applied the day before imaging. It may be that a stronger effect would have been observed nearer the time of treatment, for example if cultures were fixed several hours after treatment. The overnight culture in regular medium could result in recovery from the treatment.

5. DISCUSSION

The broad aim of this project was to explore the mechanisms by which PP progresses from intermittent attacks of paralysis into generalised muscle pathology. The work presented here sheds some light on this progression, primarily with regards to fibre type switching (see below - section 5.2, and results section 4.2.1). Data are presented from both cultured cells and animal work, and as well as being an investigation of PP progression, this project evolved into a comparative study of these different experimental models. I will discuss these below (section 5.1), evaluating their relevance to the study of PP progression as well as their limitations and potential follow-up investigations.

Work presented here also contributes a method of analysing mitochondrial structure in single FDB fibres using Fourier transform analysis (which I will discuss below in section 5.1.2), and possibly a method of monitoring cell fusion using flow cytometry (see section 5.1.1). Finally, I will discuss progress that is being made in the study of PP along with future directions of this research (section 5.3).

In vivo investigations focused on gross physiological effects of the PP mutations, while the spatiotemporal dynamics of calcium signals and mitochondrial structure and function were addressed in the *ex vivo* and *in vitro* investigations. The use of different experimental models in this study enabled me to look for common pathways leading to weakness and myopathy. If different models display the same phenotype it can be inferred that this phenotype results from a relevant feature of the disease progression. In PP this assumption is compounded if the same features are seen both in models of HypoPP and HyperPP, because of the distinct direct effect of their mutations and the common downstream pathological characteristics.

5.1 MODELS FOR THE INVESTIGATION OF PERIODIC PARALYSIS PROGRESSION

I used a range of different approaches to investigate periodic paralysis. The first model that I describe is a model prepared using fibroblasts from skin biopsies. These were acquired from control subjects and from patients. I generated myotubes from these fibroblasts by transfection with MyoD to produce myoblasts which I differentiated into myotubes. I tested

several different transfection and differentiation protocols in order to optimise this approach. I discuss this approach in section 5.1.1 below.

The second model that I describe is a mouse model of PP. I initially carried out *in vivo* investigations in order to validate the model, and once I had done so I used this model to explore PP progression *in vitro*. *In vivo* investigations included tension testing and motor neuron count, while *in vitro* investigations involved the isolation of single fibres which I characterised by confocal fluorescence microscopy.

The third model that I describe is a drug model of HypoPP, where treatment is applied to control neonatal cultures. In HypoPP, patients experience attacks of paralysis when their serum potassium levels are low, and in this model, such attacks are simulated by challenging the cultures with barium while reducing extracellular potassium concentrations.

5.1.1 Fibroblast derived myotubes

Due to the availability of a large cohort of patients, an attractive model for investigating PP was cultured cells derived from the patients. There are two major advantages to using myotubes derived from patient cells, compared to using animal or drug models of the disease. The first is that human physiology can be observed, rather than animal or cell line physiology. The second advantage is that the mutations in the model are identical to the mutations of interest in the patients and a range of such mutations can be investigated, according to the breadth of access to patients.

Specific mutations could also be investigated by generating knock-in mice expressing the mutations. However it takes many months as well as many resources to generate even a single such knock-in mouse. Furthermore, the presentation of patients with PP is frequently associated with factors other than the point mutations associated with PP. There are other influences that affect susceptibility to the disease, leading to phenotypic variability within families that express identical PP-associated mutations. The use of patient cells allows for each mutation to be investigated within the wider genotype of the patient. Furthermore, such investigations enable a comparative study of immediate effects of mutations and the way these manifest with progression of the disease in individual patients. Because PP constitutes a spectrum of disorders, novel mutations may lead to unique characteristics in

different patients stemming from distinct ionic interactions (Joshi et al, 2015; Yoshinaga et al, 2015).

Although patient cells have these advantages, investigations were carried out with fibroblasts from skin biopsies rather than using myoblasts from muscle biopsies. The lack of access to patient myoblasts is a major deterrent to the use of patient cells in the study of PP. The mutations found in PP are specific to skeletal muscle, and fibroblasts must therefore be converted to myotubes in order to make any comparative studies between patient and control cells. I therefore worked on optimising the conversion of fibroblasts to myotubes using different viral vectors and different growth and differentiation media.

I found that transducing cells with a lentiviral vector was more effective than with an adenoviral vector. There was also some indication that adding factors such as insulin, creatine and EGF to the medium during differentiation medium might increase levels of myosin expression in differentiated cells. Supplementing differentiation medium with araC also lead to the development of a higher proportion of myotubes in differentiated cultures (figure 23).

Other methods of improving fibroblast to myoblast transduction have been extensively investigated. A comparative genome wide analysis of fibroblast, myoblast and MyoD transduced fibroblast genes indicates that MyoD mediated transduction of fibroblasts does not produce cells with a complete myoblast genome. Many myoblast genes are expressed in transduced cells however some genes expressed in these cells resemble fibroblasts more closely than myoblasts (Manandhar et al, 2017). This is associated with reduced affinity of MyoD to MyoD binding sites. This study also found that the transduction process can be improved by increasing the expression of other factors including the SAND-domain proteins. The Sand-domain proteins are nuclear proteins involved in chromatin dependent transcription.

Although fibroblasts were the available patient derived cells for investigating PP, it is also possible to convert these to iPS cells prior to differentiating them into myotubes. This has been found to improve the proportion of myotubes in culture (Świerczek et al, 2015; Iovino et al, 2016). Iovino et al, used fibroblasts from patients with insulin resistance to generate iPS cells, and differentiated these to myotubes (2016). They did not find any differences in

cell viability or morphology in patient and control lines. This meant that differences arising from mutations could be investigated. While the myotube cultures produced by Iovino et al did not develop characteristic muscle striations, these have been produced using iPS cells in other studies (Skoglund et al, 2014). Although this technique is more demanding with regards to the time and resources it is likely to produce cultures that are more suitable for the investigation of muscle disease.

Once a myoblast culture is achieved, many different methods have been developed to aid the successful differentiation of myoblasts to myotubes and the production of mature skeletal muscle cultures. One approach toward making skeletal muscle cultures for the investigation of muscle disease is the 'tissue on a chip' approach. Growth on different surfaces can aid the differentiation of cell types, by mimicking the surfaces found *in vivo*. For example, soft substrates that are microplated in parallel lanes have been found to support the differentiation of myoblasts (Zatti et al, 2012). Such differentiation 'on a chip' has been used to study dystrophin production by mesangioblast and myoblast derived myotubes in a model of muscular dystrophy (Serena et al, 2016).

Because a primary focus was to improve myogenicity of cultures, I worked on several methods of assessing myogenicity. In particular, I investigated the options of using flow cytometry and protein expression. I tested the possibility of using flow cytometry to compare the efficiency of differentiation under different conditions. PI is routinely used to study cell cycle progression by flow cytometry, and I hoped to use this method of analysis to monitor the rate of cell fusion. I found that although flow cytometry may be useful for determining the proportion of cells with several nuclei, it is not a suitable tool for myoblast to myotube differentiation. Successfully differentiated myotubes are large and highly elongated, frequently reaching several hundred micrometres in length, such that it would only be able to pass through typical flow cytometry equipment lengthways. Particles of this size are also likely to become damaged and fragmented during the fixation and staining process. Myotubes and fragments of myotubes could also become aggregated and stuck in the flow cytometry equipment. Therefore, while the PI protocol may be a useful tool for analysing a limited degree of cell fusion, it is not appropriate for studying myoblast to myotube differentiation. A more appropriate method for studying such differentiation may be to stain with Hoechst and myosin. Although this method is more time consuming, it

would result in a more accurate estimation of fusion index. It may be that the PI protocol described here could be reserved for the initial stages of cell fusion, for example analysis on days one and two of differentiation could give an indication of the rate at which differentiation begins following transduction with MyoD and exposure to differentiation medium. In combination with microscopy it may be that this method could be used to determine the extent of myoblast fusion during the initial stages of differentiation.

As well as determining levels of multi-nucleation, myotube maturation stage was assessed by testing for proteins that are present in mature muscle but not in myoblasts and fibroblasts, such as myosin heavy chain (figure 16). Other markers of myotube maturation include expression of tropomyosin and the formation of triad junctions and striations. Such structural characteristics did not develop in the cultures described here. The development of structural likeness to muscle would enable a more thorough investigation of ionic interactions in patient and control tissue as such interactions may depend on proximity of ion channels to each other and to organelles. In particular, the effects of PP-associated CaV1.1 mutations are likely to be influenced by the formation of triad junctions, where T-tubule-bound CaV1.1 is associated with SR-bound RyRs. Due to the lack of striations, it is unclear whether triad junctions and other such structural characteristics developed.

Successful differentiation leads to the expression of skeletal muscle associated channels. NaV1.4 and CaV1.1 are expressed in all skeletal muscle, and were expressed in the fibroblast derived myotubes (see figure 23 for immunofluorescence of CaV1.1). Their expression can also be predicted by the spontaneous calcium fluctuations in the cultures, as these rely on interplay between inward currents through NaV1.4 and CaV1.1 channels and an outward current through Kir2.1 channels (Sciancalepore et al, 2005).

Patients of periodic paralysis express mutant NaV1.4, CaV1.1 or Kir2.1 in all their skeletal muscles, and expression can be even greater in muscle of affected patients than in control subjects (Cannon, 2015; Lucas et al, 2014). However not all skeletal muscles are affected by the condition. The diaphragm, for example, seems to be protected against features of periodic paralysis (Ammar & Renaud, 2015). It may be that the continuous activity of the diaphragm protects it, just as frequent moderate exercise can protect patients against attacks of PP. Alternatively, it may be that differences in the channelome, such as elevated

activity or expression of the sodium-calcium exchanger, protect the diaphragm (Ammar & Renaud, 2015). The diaphragm is more dependent on extracellular calcium for contraction than other skeletal muscles (Viires et al, 1988; Zavecz & Anderson, 1992). The sodium-calcium exchanger may work in reverse mode in muscle of HyperPP patients, as sarcoplasmic sodium ion concentrations are increased, leading to increased calcium influx and increased force during contractions (Lucas et al, 2014).

Similarly, pregnancy has a potassium lowering effect which can protect against HyperPP (Finsterer et al, 2017). Dynamics of potassium exchange across the plasma membrane of skeletal muscles are mediated by membrane transporters including the Na^+, K^+-ATPase and Kir2.1. Potassium uptake and release through these is regulated by circulating hormones, peptides and ions, as well as by muscle activity levels and changes in extracellular potassium concentration (Cheng et al, 2013).

These studies highlight a limitation of using the viral transduction of patient fibroblasts, or even iPS cells to form myotubes. Although such conversion leads to the production of myotubes that express mutant channels, ionic dynamics within the myotubes may protect against features of PP by a mechanism similar to that found in the diaphragm or during pregnancy.

5.1.2 Mouse Model of periodic paralysis

PP was studied in an animal model both *in vivo* and *ex vivo*. *In vivo* studies showed that skeletal muscle was affected in mutant compared to control mice. However the nervous system was not affected, as demonstrated by equal motor neuron counts.

As discussed in the results (section 4.2.1) female mice were used for *in vivo* characterisation of the model despite the greater penetrance and severity of the condition in males. This is because the extent of difference in presentation with features of PP in male and female mice was not yet established, and because the supply of males was low. Severely affected male mice were frequently killed by the mother at birth. A similar trend in gender segregation of disease severity has been found in patients, and although the cause is not clear, it has been hypothesised that oestrogen plays a protective role (Ke et al, 2013). Male mice were used for the *ex vivo* follow-up investigations.

The *in vivo* investigations that I carried out on females in contribution to the study by Corrochano et al (2014) indicate that EDL muscle of Dgn mice has a tendency to exhibit greater resistance to fatigue. Although these results did not reach statistical significance (p-value of 0.1; figure 32) they were consistent with results from investigations carried out by my colleague Pete Joyce on males, where mutant EDL showed significant resistance to fatigue (p-value of 0.001; figure 29; Corrochano et al, 2014). Resistance to fatigue is a hallmark of type I fibres and also a feature of type IIa fibres, suggesting that a switch in fibre type was taking place in Dgn mice, with type IIb fibres being downregulated and type I upregulated (this is further discussed below in section 5.2). I also helped to demonstrate in this study that female mice are less affected by the Dgn mutation than males. Muscle weakness, for example, was a feature in TA and EDL of male mice, but was not observed in females where the Dgn phenotype is less severe (Corrochano et al, 2014).

One advantage of using animals to study progressive diseases is that disease progression can be tracked with age and explored at different time points. Female mice were used at a late time point in disease progression, and earlier time points were subsequently not assessed in the females because even in the aged group the effects were modest. A follow up investigation using males of different age groups could help to illuminate how the disease progresses. Only males are currently being tested for this reason and as part of a study on sarcopenia, described below. Investigations presented here did indicate that mutants present with progressive changes associated with PP and thus validate the Dgn model.

Having established that the mutant mice displayed features of PP and that males were more severely affected than females, I ran further investigations *ex vivo* on single fibres of FDB muscle dissected from male mice. I monitored calcium handling and mitochondrial structure and function in these single fibres in order to determine whether or not these are affected in PP.

As indicated in figure 43, cytosolic calcium rise time was significantly faster in single fibres dissected from Dgn mice than in those from control mice (P=0.025). Cytosolic calcium recovery time was not affected (figure 43).

Changes in mitochondrial structure and membrane potential were also observed. The Dgn mice presented with reduced mitochondrial membrane potential (figure 35) and a reduced proportion of intermyofibrillar mitochondria (figure 34). A colleague is currently repeating these investigations on older male Dgn and control mice in order to confirm whether or not mitochondria are affected in mutants and to test whether such changes could be a feature of sarcopenia which is accelerated in mutants. As discussed in introduction (section 1.3.3, page 30) PP and sarcopenia are phenotypically similar, possibly reflecting a degree of accelerated aging in patients. I believe that in combination with these current investigations, this study can lead to a publication focussed on a possible change in the roles of IMF and SS mitochondria in skeletal muscles of Dgn mice and may contribute further evidence for a link between sarcopenia and PP.

The reduced mitochondrial membrane potential may be connected to the reduced proportion of intermyofibrillar mitochondria. It may be that subsarcolemmal mitochondria of affected muscle display higher activity levels in order to compensate for the lack of intermyofibrillar mitochondria. The subsequent increase in ATP turnover could reduce the mitochondrial membrane potential, due to the associated influx of protons through ATP-synthase.

Alternatively, it may be that increased ATP turnover leads to increased generation of ROS and to oxidative stress (Satoh et al, 1997). Such a process would likely be exacerbated in fibres of Dgn mice which have a higher proportion of subsarcolemmal mitochondria, because subsarcolemmal mitochondria are more sensitive to oxidative stress than intermyofibrillar mitochondria (Ayswarya and Kurian, 2016). However, oxidative stress is associated with reduced activity of the mitochondrial complexes, and activity levels of complexes I, II, III and IV were not affected in tissue from the Dgn mice (results section 4.2.4, figures 36, 37 and 38). This suggests that mitochondrial membrane potential was affected by increased ATP-turnover but not by oxidative stress.

Fourier transform analysis was used to distinguish between the subsarcolemmal and the intermyofibrillar mitochondria. This method allowed for several fibres to be tested per animal and revealed a significant difference between mutant and control groups despite a wide range in observations (figure 34). Fourier transform has been used to analyse TMRM

staining in muscle in other work, although this work was conducted in cardiac muscle using different methodology, and with different aims (Venable et al, 2013). This study therefore contributes a novel method of distinguishing between the different mitochondrial groups using Fourier transform analysis.

Advantages and limitations of using animal models in the study of human diseases have been widely discussed in the literature. As indicated above, an important advantage of using animal models is the ability to investigate PP as it progresses. Human and mouse genomes are 85% conserved (Chinwalla et al, 2002), and this similarity makes the mouse a valid experimental model for investigating human diseases. However there remain both physiological and metabolic differences between human and mouse tissue. Key differences between human and mouse tissue include differences in their circadian rhythms and their immunological defences (Mestas & Hughes, 2004). The oxidative metabolism of rodents and humans is also distinct; in humans the highest mitochondrial enzyme content is found in type I muscle fibres, but in rodents it is in type IIa muscle fibres (Fitts, 1994). Another major difference is that mice live for approximately 2 years and humans can live for more than 100. This is likely to be important in the study of progressive diseases, in particular PP which has a biphasic natural history. It is unclear whether the mice experience the second phase of PP, namely progressive weakness coupled with a reduction in attack frequency.

5.1.3 Drug model of periodic paralysis

Barium and low potassium were used to simulate the paradoxical depolarisation characteristic of HypoPP in cultures of myotubes from neonatal muscle. This method has been previously used to simulate key features of HypoPP in excised rat muscle fibres (Struyk & Cannon, 2007) and *in vivo* (Schott & McArdle, 1974). Struyk and Cannon found that paradoxical depolarisation could be initiated by reducing extracellular potassium levels to 1mM in the absence of barium or by reducing it to 2mM in the presence of barium (2007). Under normal physiological conditions extracellular potassium levels do not reach as low as 1mM, and this protects the muscle against paradoxical depolarisation. However in HypoPP, such depolarisation is potentiated and can occur at extracellular potassium concentrations as high at 2.5mM (Cheng et al, 2013).

Initial testing with a high throughput membrane potential sensitive dye (the FLIPR membrane potential assay kit) showed that in the presence of barium, membrane potential depolarises upon treatment with 1mM potassium, and to a lesser extent with 2mM potassium (see figure 46). Further testing of these treatments in the myotubes indicated that reducing extracellular potassium levels to 2mM did not have downstream effects whether in the presence or in the absence of barium.

In the myotubes, reducing the extracellular potassium concentration to 1mM led to spontaneous SR calcium release. Cells treated with 50µM barium and gramicidin displayed more spontaneous calcium fluctuations, however the level of spontaneous fluctuations was not affected in cells treated with 50µM barium without gramicidin (figure 47B). Furthermore, no changes in mitochondrial membrane potential or in basal calcium levels were observed following pre-treatment of the cultures, whether with 1mM or 2mM extracellular potassium (figures 49C and 49D for cultured myotubes and figures 50D for single fibres). Likewise, no changes in the expression of mitochondrial complexes were observed in such pre-treated cultured myotubes, even when pre-treatment of 0.5mM extracellular potassium concentration was used (figures 53A and 53B).

Pre-treatment of cultures with 1mM potassium in the presence of 50µM barium lead to higher expression levels of IRK2.1 (figures 51F). TFAM expression and peak cytosolic calcium levels reached upon electrical stimulation were not altered by pre-treated with 1mM or 2mM potassium in the presence or absence of 50µM barium (figures 52 and 48).

Overall these results show that treatment can accentuate calcium dynamics, but that downstream changes only occasionally occur in cultures exposed to more extreme and less physiological conditions (extracellular potassium concentrations lower than 2mM). Because such potassium levels are not physiological, they may have other effects on the ionic dynamics within the myotubes. This poses a major disadvantage of the model as it is unclear whether the effects of treating the myotubes with extracellular potassium concentrations of less than 2mM can be associated with PP progression.

Perhaps if cultures were exposed to treatment for longer, or if less time was allowed for recover from treatment before fixation, changes in TFAM expression would have been

detected following treatment with 2mM extracellular potassium. The overnight culture in regular medium may have resulted in recovery from the treatment.

There are several important advantages of using a drug model to study PP; it is readily available, the level as well as the frequency of “attacks of paralysis” can be controlled, and there is no genetic variability between models as the same cells are used for controls. A further advantage of using such a drug model is that it can be instrumental in clarifying pathways leading to any observed downstream effects associated with the disease. In models with a mutation, it is not always clear whether downstream observations are associated with direct effects of the mutation. For example, it is not clear whether muscle weakness observed in the Dgn model is associated with attacks of paralysis, or with some other effect of the mutation. Barium can also be used to simulate PP *in vivo* and investigations using single fibres from rats treated in this manner could provide a useful comparison to the single fibres that were used in the Dgn model.

However this experimental model has its limitations. For example a drug model can be designed to mimic what we know about a condition, but not other aspects thereof. It may be that a desired effect is achieved in a model, but that the mechanism leading to that effect is unrelated to the clinical process. In such a case, downstream effects in the model are unlikely to be related to the condition.

5.2 What do these results mean for periodic paralysis?

In vivo data indicate that the skeletal muscle of affected mice displayed resistance to fatigue. It may thus be deduced that fatigue resistance is a feature of PP. Fatigue develops during intense exercise when ATP demands can no longer be met. Metabolic by-products accumulate and interfere with actin-myosin interaction, thereby preventing hydrolysis of ATP and preserving any remaining ATP (Layzer, 1990). It may be that in the absence of this protective mechanism, excessive stimulation damages the skeletal muscle leading to the observed muscle weakness.

Several of the results presented here, including the resistance to fatigue in the male mice, suggest that skeletal muscle fibre type is affected by the progression of PP. EDL muscle is predominantly composed of fast twitch fibres (type IIa and IIb), but fatigue resistance is a hallmark of type I fibres (and is also a feature of type IIa fibres) due to their higher

mitochondrial content (Herbison et al, 1982; Fitts, 1994). The high fatigability of type IIb fibres results from low mitochondrial content, and dependence on anaerobic metabolism. The increased resistance to fatigue displayed by Dgn muscle suggests that the proportion of type IIb fibres was reducing in affected mice. In addition, immunostaining has shown that fibres switch from type IIb to type IIa in Dgn TA, displaying a more oxidative phenotype (see figure 54 below from Corrochano et al, 2014). The fibre characteristics changed whether or not the mice presented with attacks of paralysis (Corrochano et al, 2014).

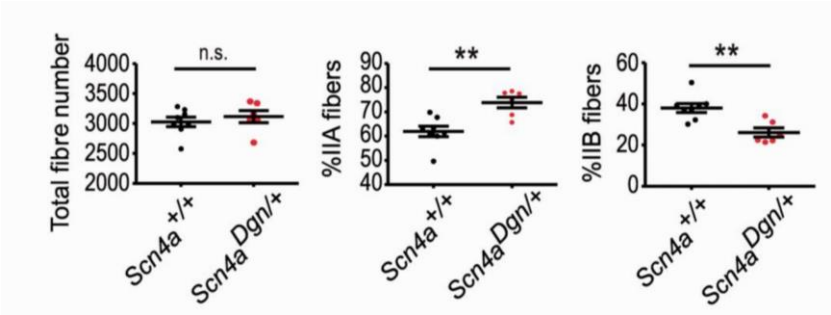

Figure 54: Muscle fibre type switch in Dgn fibres. *Reproduction of published figure (figure 4g in Corrochano et al, 2014), showing that fibres switch to a more oxidative phenotype in Dgn TA. The total number of fibres was quantified, as well as the total number and the percentage of type 1a (oxidative) and type IIb (glycolytic) fibres. (*$Scn4a^{+/+}$ n = *8;* $Scn4a^{Dgn/+}$ n = *6 mice,* P = *0.002 for both comparisons).*

This shift in fibre type may be connected to the increased muscle activity observed in affected animals. Increased muscle activity leads to activation of transcriptional regulators such as PGC1α. Moreover, acute exercise specifically increases levels of PGC1α and TFAM in subsarcolemmal mitochondria, and this population of mitochondria respond more efficiently to exercise training (Smith et al, 2013). PGC1α induces mitochondrial biogenesis and increased oxidative metabolism by co-activating Nrf1 and Nrf2 and by promoting the expression of TFAM. TFAM translocates to the mitochondria and promotes transcription of mtDNA encoded proteins (figure 55). Therefore PGC1α activation of TFAM promotes a shift toward a more oxidative phenotype (Lin et al, 2002b). PGC1-α co-activates Mef2 to promote the expression of type I fibrillar proteins. The promotion of metabolic and contractile properties of type I fibres is thereby coordinated (Lin et al, 2002b).

These interactions suggest that TFAM expression is increased following exposure to the drug treatment protocol. However results regarding TFAM expression are inconclusive.

Results from a single Western blot on TFAM expression (figure 52) suggest that exposure to 0.5mM potassium for four hours can lead to such an increase in expression levels of TFAM but not exposure for shorter time periods or higher extracellular potassium levels.

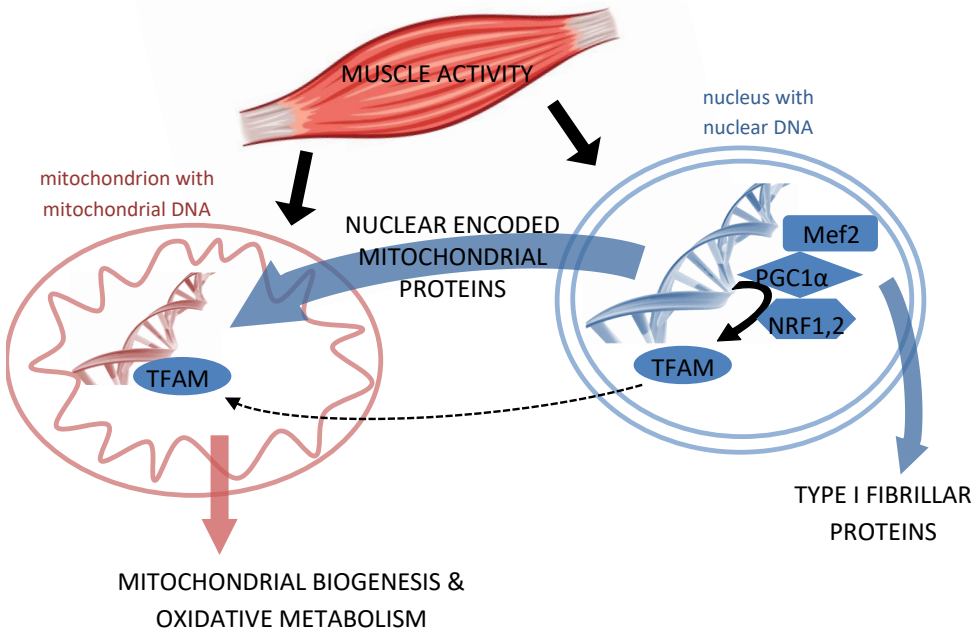

Figure 55: Muscle activity promotes a shift towards an oxidative phenotype. *Muscle activity initiates mitochondrial biogenesis and oxidative metabolism as well as promoting the expression of type I fibrillar proteins. PGC1-α co-activates NRF1 and 2 and promotes the expression of TFAM. TFAM translocates to the mitochondria and promotes mitochondrial biogenesis and oxidative metabolism. PGC1-α also co-activates Mef2 to promote the expression of type I fibrillar proteins.*

Type I and IIa fibres are more oxidative than type IIb fibres, and this may point toward mitochondrial involvement in progression of PP. However FDB muscle primarily expresses type IIa fibres, and very few type IIb fibres, such that downregulation of type IIb fibres is unlikely to have an impact. There is a high presence of type IIx myosin which is found in the type IIa fibres because the type IIa fibres of the FDB muscle contain a mixed population of type IIa and type IIx myosin (Lucas et al, 2014). Lucus et al showed that proportions of the different myosin isoforms were not affected in FDB muscle. It may be concluded that in other muscles such as TA and EDL that have higher proportions of type IIb muscle fibres, a shift in fibre composition takes place in order to deal with increased oxidative demands that develop during PP, as demonstrated by their resistance to fatigue, but that in FDB where the proportion of type IIb muscle fibres is low, any increase in oxidative demands

can already be met by the existing type IIa fibres. Lucas et al also suggest that fibre type changes do not occur in FDB due to a lower NaV1.4 content than other skeletal muscles, and reduced tetrodotoxin-sensitive sodium ion influx (2014).

A shift in mitochondrial sub-populations was observed in Dgn compared to control FDB single fibres – a reduced proportion of intermyofibrillar mitochondria was observed in fibres from Dgn mice. Crescenzo et al, show that intermyofibrillar mitochondria oxidise substrates at more than double the rate of subsarcolemmal mitochondria, in a study on rat skeletal muscle (2014). Protein synthesis, on the other hand, is more efficient in subsarcolemmal mitochondria (Hesketh et al, 2016). The shift from intermyofibrillar to subsarcolemmal mitochondria that was observed in FDB muscle may therefore be related to increased levels of protein synthesis and/or to lower oxidative demands. As discussed above in section 5.1.2, the reduced mitochondrial membrane potential in FDB fibres could result from increased ATP turnover in subsarcolemmal mitochondria as they compensate for reduced levels of intermyofibrillar mitochondria. This could dissipate the mitochondrial membrane potential because ATP turnover is associated with an influx of protons through ATP-synthase.

Calderon et al, show that during a calcium transient, the calcium release and recovery from type I fibres is slower than from type II fibres, and that peak cytosolic calcium is lower (2010). Since the resistance to fatigue described here indicates a shift towards a more oxidative phenotype with a switch in muscle fibre type from type II to type I, I would have expected calcium transients to display slower calcium dynamics and lower peak cytosolic calcium. However in FDB this may not be relevant as there is no evidence for a fast to slow switch in muscle fibre type in FDB.

The shift from fast to slow muscle fibre type is driven by calcineurin – a calcium/calmodulin-dependent protein phosphatase (Chin et al, 1998). Therefore, had an effect on calcium handling been observed, it would have been important to test whether cyclosporine, an inhibitor of calcineurin, could protect against the switch in fibre type. The calcium handling results obtained in these investigations were not significantly altered in the models of PP compared to the controls. Nevertheless in the drug model recovery was typically (but not significantly) slower in barium treated myotubes than in the control myotubes. In the FDB

fibres of Dgn mice there was a slight tendency toward faster calcium release, and as discussed above, this in unlikely to be related to a change in fibre type.

5.3 Current Progress in this field and future directions

Reduction in type II fibres and development of tubular aggregates are both features of PP and of aging (Chevessier et al, 2004). In addition, results presented here give some indication that TFAM expression could be increased in PP (figure 52), and this is also a feature in aged human skeletal muscle (Lee & Wei, 2005). It may be that other clinical features found in aging muscle also present in PP. One mouse model of PP, for example, presents with triad disruption and with a reduced number of skeletal calcium channels (Wu et al, 2012). Triad disruption is also a feature of aging (Boncompagni et al, 2006). Data from these studies thus suggest that there is some clinical similarity between normal aging and the progression of PP. A comparative study of PP and aging may help to illuminate the pathological process that leads to weakness in PP, and whether this presents as a form of accelerated aging (Suetterlin, unpublished work).

Fourier transform analysis was instructive in identifying a shift in mitochondrial populations resulting from the Dgn mutations. Skeletal intermyofibrillar mitochondria can also be distinguished from subsarcolemmal mitochondria by centrifugation, allowing for the subpopulations of mitochondria to be isolated (Ferreira et al, 2010). Centrifugation can be used to separate out particles of different mass in order to isolate mitochondria (Graham, 2002). Mitochondrial fractions can be sub-fractionated by a combination of protease and mechanical treatment and centrifugation in order to isolate SS and IMF mitochondria (Ferreira et al, 2010). In this way mitochondrial enzyme activity could be assessed (Ferreira et al, 2010; Krieger et al, 1980) and electron microscopy of the subpopulations performed (Ferreira et al, 2010). Such methods do not allow for localisation of the subpopulations to be viewed within skeletal muscle, which is an advantage of the Fourier transform method. Nevertheless these methods could help to identify further differences in the mitochondrial subpopulations resulting from PP. One might expect mitochondrial complexes from subsarcolemmal mitochondria of affected FDB muscle to display higher activity levels in order to compensate for the lack of intermyofibrillar mitochondria. Furthermore one might expect to see damage to intermyofibrillar mitochondria associated with their reduced abundance in affected tissue.

It would also be informative to repeat the TMRM imaging in single fibres from a different muscle. The FDB muscle is mainly composed of type IIa fibres (90%), but as discussed in section 5.2, type IIb fibres appear to be downregulated in PP. A muscle expressing a larger proportion of type IIb fibres is therefore likely to be more severely affected. FBD single fibres were used rather than TA or EDL fibres because they are shorter and less likely to be damaged by the isolation process. The first dorsal interosseus muscle, could be a suitable alternative, as it is also composed of short fibres, and it has equal proportions of type I and type II muscle fibres (Johnson et al, 1973).

One aspect of PP progression that was not addressed in the investigations presented here is that patients experience a reduction in attack frequency with age. This is a challenging problem to address. It is not clear whether the animal models could shed light on this feature of the disease, as they rarely present with any attacks at all. It could possibly be investigated by comparing age matched patient muscle biopsies from patients that have reached a stage of disease progression where their attacks subside and patients who regularly experience attacks. Mitochondrial complex activities from such samples could, for example, be compared. However this method would involve the extraction of a large number of biopsies from affected patients. Another approach could be a retrospective study of patients looking at other clinical features that develop or subside at the time when the frequency of their attacks reduces.

5.4 Concluding remarks

The models of PP that I used in this investigation can offer insight into different aspects and stages of development of the disease. I showed that fibroblasts from patients could be converted to myotubes expressing relevant disease associated channels. However these myotube cultures were not a useful tool for investigating the disease due to high levels of variability in their patterns of response to electrical and chemical stimulation, and due to the presence of fibroblasts. While myotube cultures derived from skin biopsies were not used to compare patient and control metabolism, there may be scope for using such biopsies if the fibroblasts are first converted to iPS cells. Muscle biopsies could likewise be used to compare patient and control, either by direct observation of the muscle biopsy histology or by producing myoblast cultures.

Using the Dgn mouse model of PP, I showed that mouse models of the disease can be used to highlight progressive features of the disease involving changes in oxidative metabolism. Although these investigations were carried out using a single age group, using animals of different ages could provide further insight into how changes in oxidative metabolism develop.

Drug models may also help to highlight the downstream effects of attacks of paralysis. I developed such a model where barium could be used to potentiate paradoxical depolarisation in cultures in order to mimic HypoPP. Investigations using this model only showed a difference between treatment and control groups where cultures were subjected to extremely low extracellular potassium levels. As such the model may not reflect changes that develop in patients. Nevertheless changes observed following the treatment did alter metabolism in a manner that is consistent with features observed in the mouse model.

Investigations using myotube cultures lacked structural characteristics of muscle. Further investigations into the progression of PP may be more informative if cultures with structural features of skeletal muscle are developed. In particular because of the differences found in the mitochondrial structure of fibres from Dgn and control mice.

Together my results from the drug model and from TA and EDL muscles of Dgn and control mice suggest that changes in oxidative phosphorylation occur during PP progression, and that this involves a shift in fibre type. Oxidative phosphorylation is enhanced and the composition of muscle shifts towards a more oxidative phenotype with fewer type IIb fibres. Results from the FDB muscles of Dgn and control mice indicate a reduction in intermyofibrillar mitochondria and in mitochondrial membrane potential.

6. BIBLIOGRAPHY

Acevedo-Arozena, A., Wells, S., Potter, P., Kelly, M., Cox, R.D. and Brown, S.D., 2008. ENU mutagenesis, a way forward to understand gene function. *Annu. Rev. Genomics Hum. Genet.*, *9*, pp.49-69.

Aitken, R.S., Abbott, E.N., Castleden, L.I.M. & Walker M., 1937. Observations on a case of familial periodic paralysis. *Clinical Science*, 3, pp.47-57.

Ammar, T. and Renaud, J.M., 2015. Diaphragm of Hyperkalemic Periodic Paralysis Mouse Has No Contractility Abnormality Compared to the Robust Abnormalities in EDL and Soleus. *The FASEB Journal*, *29*(1 Supplement), pp.947-8.

Ayswarya, A. and Kurian, G.A., 2016. Sensitivity of interfibrillar and subsarcolemmal mitochondria to cobalt chloride-induced oxidative stress and hydrogen sulfide treatment. *Indian journal of pharmaceutical sciences*, *78*(1), p.151.

Banerjee, A. and Saha, S.K., 2014. Tissue specific structural variations of mitochondria of fish ectoparasite Argulus bengalensis Ramakrishna, 1951 (Crustacea: Branchiura): functional implications. *Journal of advanced research*, *5*(3), pp.319-328.

Barazzoni, R., Short, K.R. and Nair, K.S., 2000. Effects of aging on mitochondrial DNA copy number and cytochromec oxidase gene expression in rat skeletal muscle, liver, and heart. *Journal of Biological Chemistry*, *275*(5), pp.3343-3347.

Barrientos, A., Casademont, J., Cardellach, F., Ardite, E., Estivill, X., Urbano-Márquez, A., Fernández-Checa, J.C. and Nunes, V., 1997. Qualitative and quantitative changes in skeletal muscle mtDNA and expression of mitochondrial-encoded genes in the human aging process. *Biochemical and molecular medicine*, *62*(2), pp.165-171.

Biswas, G., Adebanjo, O.A., Freedman, B.D., Anandatheerthavarada, H.K., Vijayasarathy, C., Zaidi, M., Kotlikoff, M. and Avadhani, N.G., 1999. Retrograde Ca2+ signaling in C2C12 skeletal myocytes in response to mitochondrial genetic and metabolic stress: a novel mode of inter-organelle crosstalk. *The EMBO journal*, *18*(3), pp.522-533.

Bladt, F., Riethmacher, D., Isenmann, S., Aguzzi, A. and Birchmeier, C., 1995. Essential role for the c-met receptor in the migration of myogenic precursor cells into the limb bud. *Nature*, *376*(6543), pp.768-771.

Blau, H.M., Pavlath, G.K., Hardeman, E.C., Chiu, C.P., Silberstein, L., Webster, S.G., Miller, S.C. and Webster, C., 1985. Plasticity of the Differentiated State. *Science*, *230*, pp.758-766.

Blaustein, M.P. and Lederer, W.J., 1999. Sodium/calcium exchange: its physiological implications. *Physiological reviews*, *79*(3), pp.763-854.

Boehning, D., Patterson, R.L., Sedaghat, L., Glebova, N.O., Kurosaki, T. and Snyder, S.H., 2003. Cytochrome c binds to inositol (1, 4, 5) trisphosphate receptors, amplifying calcium-dependent apoptosis. *Nature cell biology*, *5*(12), pp.1051-1061.

Boncompagni, S., d'Amelio, L., Fulle, S., Fanò, G. and Protasi, F., 2006. Progressive disorganization of the excitation–contraction coupling apparatus in aging human skeletal muscle as revealed by electron microscopy: a possible role in the decline of muscle performance. *The Journals of Gerontology Series A: Biological Sciences and Medical Sciences*, *61*(10), pp.995-1008.

Booth, F.W. and Thomason, D.B., 1991. Molecular and cellular adaptation of muscle in response to exercise: perspectives of various models. *Physiological reviews*, *71*(2), pp.541-585.

Bottinelli, R., 2001. Functional heterogeneity of mammalian single muscle fibres: do myosin isoforms tell the whole story?. *Pflügers Archiv European Journal of Physiology*, *443*(1), pp.6-17.

Bottinelli, R.Y.C.R. and Reggiani, C., 2000. Human skeletal muscle fibres: molecular and functional diversity. *Progress in biophysics and molecular biology*, *73*(2), pp.195-262.

Bradley, W.G., Taylor, R., Rice, D.R., Hausmanowa-Petruzewicz, I., Adelman, L.S., Jenkison, M., Jedrzejowska, H., Drac, H. and Pendlebury, W.W., 1990. Progressive myopathy in hyperkalemic periodic paralysis. *Archives of neurology*, *47*(9), pp.1013-1017.

Braun, T., Bober, E., Rudnicki, M.A., Jaenisch, R. and Arnold, H.H., 1994. MyoD expression marks the onset of skeletal myogenesis in Myf-5 mutant mice. *Development*, *120*(11), pp.3083-3092.

Bulman, D.E., Scoggan, K.A., Van Oene, M.D., Nicolle, M.W., Hahn, A.F., Tollar, L.L. and Ebers, G.C., 1999. A novel sodium channel mutation in a family with hypokalemic periodic paralysis. *Neurology*, *53*(9), pp.1932-1932.

Burge, J., Sansone, V., McDermott, M., Smith, P., Herr, B., Tawil, A., Pandya, S., Kissel, J., Ciafaloni, E., Shieh, P. and Ralph, J., 2016. Efficacy and Safety of Dichlorphenamide for the Treatment of Periodic Paralysis: a Phase 3 Randomized, Double-Blind, Parallel-Group, Placebo-Controlled Trial (PL02. 001). *Neurology*, *86*(16 Supplement), pp.PL02-001.

Buruma, O.J.S. and Bots, G.T.A.M., 1978. Myopathy in familial hypokalaemic periodic paralysis independent of paralytic attacks. *Acta neurologica Scandinavica*, *57*(2), pp.171-179.

Calderón, J.C., Bolaños, P. and Caputo, C., 2010. Myosin heavy chain isoform composition and Ca2+ transients in fibres from enzymatically dissociated murine soleus and extensor digitorum longus muscles. *The Journal of physiology*, *588*(1), pp.267-279.

Campiglio, M. and Flucher, B.E., 2015. The role of auxiliary subunits for the functional diversity of voltage-gated calcium channels. *Journal of cellular physiology*, *230*(9), pp.2019-2031.

Cannon, S.C., 2006. Pathomechanisms in channelopathies of skeletal muscle and brain. *Annu. Rev. Neurosci.*, *29*, pp.387-415.

Cannon, S.C., 2015. Channelopathies of skeletal muscle excitability. *Comprehensive Physiology*. 5(2), pp.761-790.

Cannon, S.C., Brown, R.H. and Corey, D.P., 1991. A sodium channel defect in hyperkalemic periodic paralysis: potassium-induced failure of inactivation. *Neuron*, *6*(4), pp.619-626.

Cannon, S.C., Hayward, L.J., Beech, J.I.L.L. and Brown, R.H., 1995. Sodium channel inactivation is impaired in equine hyperkalemic periodic paralysis. *Journal of neurophysiology*, *73*(5), pp.1892-1899.

Charles, G., Zheng, C., Lehmann-Horn, F., Jurkat-Rott, K. and Levitt, J., 2013. Characterization of hyperkalemic periodic paralysis: a survey of genetically diagnosed individuals. *Journal of neurology*, *260*(10), pp.2606-2613.

Cheng, C.J., Kuo, E. and Huang, C.L., 2013, May. Extracellular potassium homeostasis: insights from hypokalemic periodic paralysis. In *Seminars in nephrology*. 33(3), pp.237-247

Cheung, C.L., Lau, K.S., Ho, A.Y., Lee, K.K., Tiu, S.C., Lau, E.Y., Leung, J., Tsang, M.W., Chan, K.W., Yeung, C.Y. and Woo, Y.C., 2012. Genome-wide association study identifies a susceptibility locus for thyrotoxic periodic paralysis at 17q24. 3. *Nature genetics*, *44*(9), pp.1026-1029.

Chevessier, F., Marty, I., Paturneau-Jouas, M., Hantaı, D. and Verdiere-Sahuque, M., 2004. Tubular aggregates are from whole sarcoplasmic reticulum origin: alterations in calcium binding protein expression in mouse skeletal muscle during aging. *Neuromuscular Disorders*, *14*(3), pp.208-216.

Chin, E.R., Olson, E.N., Richardson, J.A., Yang, Q., Humphries, C., Shelton, J.M., Wu, H., Zhu, W., Bassel-Duby, R. and Williams, R.S., 1998. A calcineurin-dependent transcriptional pathway controls skeletal muscle fiber type. *Genes & development*, *12*(16), pp.2499-2509.

Chinwalla, A.T., Cook, L.L., Delehaunty, K.D., Fewell, G.A., Fulton, L.A., Fulton, R.S., Graves, T.A., Hillier, L.W., Mardis, E.R., McPherson, J.D. and Miner, T.L., 2002. Initial sequencing and comparative analysis of the mouse genome. *Nature*, *420*(6915), pp.520-562.

Choi, J., Costa, M.L., Mermelstein, C.S., Chagas, C., Holtzer, S. and Holtzer, H., 1990. MyoD converts primary dermal fibroblasts, chondroblasts, smooth muscle, and retinal pigmented epithelial cells into striated mononucleated myoblasts and multinucleated myotubes. *Proceedings of the National Academy of Sciences*, *87*(20), pp.7988-7992.

Cifelli, C., Bourassa, F., Gariépy, L., Banas, K., Benkhalti, M. and Renaud, J.M., 2007. KATP channel deficiency in mouse flexor digitorum brevis causes fibre damage and impairs Ca2+ release and force development during fatigue in vitro. *The Journal of physiology*, *582*(2), pp.843-857.

Conejo, R., Valverde, A.M., Benito, M. and Lorenzo, M., 2001. Insulin produces myogenesis in C2C12 myoblasts by induction of NF-κB and downregulation of AP-1 activities. *Journal of cellular physiology*, *186*(1), pp.82-94.

Conn, J.W., & Streeten, D.H.P., 1960. Periodic paralysis. *In*: J. B. Stanbury, J. B. Wyngaarden u. P. S. Fredrickson, The Metabolic Basis of Inherited Disease, New York: McGraw Hill Book Company,

Corrochano S, Männikkö R, Joyce PI, McGoldrick P, Wettstein J, Lassi G, Raja Rayan DL, Blanco G, Quinn C, Liavas A, Lionikas A, Amior N, Dick J, Healy EG, Stewart M, Carter S, Hutchinson M, Bentley L, Fratta P, Cortese A, Cox R, Brown SD, Tucci V, Wackerhage H, Amato AA, Greensmith L,

Koltzenburg M, Hanna MG, Acevedo-Arozena A. Novel mutations in human and mouse SCN4A implicate AMPK in myotonia and periodic paralysis. *Brain*, *137*(12), pp.3171-3185.

Cossu, G., Kelly, R., Tajbakhsh, S., Di Donna, S., Vivarelli, E. and Buckingham, M., 1996. Activation of different myogenic pathways: myf-5 is induced by the neural tube and MyoD by the dorsal ectoderm in mouse paraxial mesoderm. *Development*, *122*(2), pp.429-437.

Crescenzo, R., Bianco, F., Coppola, P., Mazzoli, A., Liverini, G. and Iossa, S., 2014. Subsarcolemmal and intermyofibrillar mitochondrial responses to short-term high-fat feeding in rat skeletal muscle. *Nutrition*, *30*(1), pp.75-81.

Csordás, G., Renken, C., Várnai, P., Walter, L., Weaver, D., Buttle, K.F., Balla, T., Mannella, C.A. and Hajnóczky, G., 2006. Structural and functional features and significance of the physical linkage between ER and mitochondria. *The Journal of cell biology*, *174*(7), pp.915-921.

Da, Y., Lei, L., Jurkat-Rott, K. and Lehmann-Horn, F., 2016. Successful treatment of periodic paralysis with coenzyme Q10: two case reports. *Acta Myologica*, *35*(2), p.107.

Damirchi, A., Babaei, P., Gholamali, M. and Ranjbar, K., 2012. Mitochondrial Biogenesis in Skeletal Muscle: Exercise and Aging. In *Skeletal Muscle-From Myogenesis to Clinical Relations*. InTech.

Deldicque, L., Theisen, D., Bertrand, L., Hespel, P., Hue, L. and Francaux, M., 2007. Creatine enhances differentiation of myogenic C2C12 cells by activating both p38 and Akt/PKB pathways. *American Journal of Physiology-Cell Physiology*, *293*(4), pp.C1263-C1271.

Delp, M.D. and Duan, C.H.A.N.G.P.I.N.G., 1996. Composition and size of type I, IIA, IID/X, and IIB fibers and citrate synthase activity of rat muscle. *Journal of applied physiology*, *80*(1), pp.261-270.

Dengler, R., Hofmann, W.W. and Rüdel, R., 1979. Effects of potassium depletion and insulin on resting and stimulated skeletal rat muscle. *Journal of Neurology, Neurosurgery & Psychiatry*, *42*(9), pp.818-826.

Duberley KE, Abramov AY, Chalasani A, Heales SJ, Rahman S, Hargreaves IP. Human neuronal coenzyme Q10 deficiency results in global loss of mitochondrial respiratory chain activity, increased mitochondrial oxidative stress and reversal of ATP synthase activity: implications for pathogenesis and treatment. Journal of inherited metabolic disease. 2013 Jan 1;36(1):63-73.

Ekstrand, M.I., Falkenberg, M., Rantanen, A., Park, C.B., Gaspari, M., Hultenby, K., Rustin, P., Gustafsson, C.M. and Larsson, N.G., 2004. Mitochondrial transcription factor A regulates mtDNA copy number in mammals. *Human molecular genetics*, *13*(9), pp.935-944.

Fan, C., Mao, N., Lehmann-Horn, F., Bürmann, J. and Jurkat-Rott, K., 2017. Effects of S906T polymorphism on the severity of a novel borderline mutation I692M in Nav1. 4 cause periodic paralysis. *Clinical genetics*, *91*(6), pp.859-867.

Ferreira, R., Vitorino, R., Alves, R.M., Appell, H.J., Powers, S.K., Duarte, J.A. and Amado, F., 2010. Subsarcolemmal and intermyofibrillar mitochondria proteome differences disclose functional specializations in skeletal muscle. *Proteomics*, *10*(17), pp.3142-3154.

Finsterer, J., Wakil, S.M. and Laccone, F., 2017. Pregnancy reduces severity and frequency of attacks in hyperkalemic periodic paralysis due to the mutation c. 2111C> T in the SCN4A gene. *Annals of Indian Academy of Neurology*, *20*(1), p.75.

Fitts, R.H., 1994. Cellular mechanisms of muscle fatigue. *Physiological reviews*, *74*(1), pp.49-94.

Folker, E. and Baylies, M., 2013. Nuclear positioning in muscle development and disease. *Frontiers in physiology*, *4*, p.363.

Foppen, R.J., Mil, H.V. and Heukelom, J.S., 2002. Effects of chloride transport on bistable behaviour of the membrane potential in mouse skeletal muscle. *The Journal of physiology*, *542*(1), pp.181-191.

Francis, G.L., 2010. Albumin and mammalian cell culture: implications for biotechnology applications. *Cytotechnology*, *62*(1), pp.1-16.

Gallant, E.M., 1983. Barium-treated mammalian skeletal muscle: similarities to hypokalaemic periodic paralysis. *The Journal of physiology*, *335*, p.577.

Gambale, F., Menini, A. and Rauch, G., 1987. Effects of calcium on the gramicidin A single channel in phosphatidylserine membranes. *European Biophysics Journal*, *14*(6), pp.369-374.

Gamstorp, I., Hauge, M., Helweg-Larsen, H.F., Mjönes, H. and Sagild, U., 1957. Adynamia episodica hereditaria. *The American journal of medicine*, *23*(3), pp.385-390.

Gerli, M.F., Maffioletti, S.M., Millet, Q. and Tedesco, F.S., 2014. Transplantation of induced pluripotent stem cell-derived mesoangioblast-like myogenic progenitors in mouse models of muscle regeneration. *Journal of visualized experiments: JoVE*, (83).

Girven, M., Dugdale, H.F., Owens, D.J., Hughes, D.C., Stewart, C.E. and Sharples, A.P., 2016. l-glutamine Improves Skeletal Muscle Cell Differentiation and Prevents Myotube Atrophy After Cytokine (TNF-α) Stress Via Reduced p38 MAPK Signal Transduction. *Journal of cellular physiology*, *231*(12), pp.2720-2732.

Gnaiger E. 2007. Mitochondrial Pathways and Respiratory Control, An Introduction to OXPHOS Analysis. Page 15. 3rd Edition [Online] Innsbruck: Oroboros MiPNet Publications 2012. www.bioblast.at/index.php/gnaiger_2012_MitoPathways

Gordeeva, A.V., Zvyagilskaya, R.A. and Labas, Y.A., 2003. Cross-talk between reactive oxygen species and calcium in living cells. *Biochemistry (Moscow)*, *68*(10), pp.1077-1080.

Graham, J., 2002. Preparation of crude subcellular fractions by differential centrifugation. *The Scientific World Journal*, *2*, pp.1638-1642.

Green, H.J., 1997. Mechanisms of muscle fatigue in intense exercise. *Journal of sports sciences*, *15*(3), pp.247-256.

Griggs, R.C., ENGEL, W.K. and Resnick, J.S., 1970. Acetazolamide treatment of hypokalemic periodic paralysis: prevention of attacks and improvement of persistent weakness. *Annals of Internal Medicine*, *73*(1), pp.39-48.

Grosson, C.L., Esteban, J., McKenna-Yasek, D., Gusella, J.F. and Brown, R.H., 1996. Hypokalemic periodic paralysis mutations: confirmation of mutation and analysis of founder effect. *Neuromuscular Disorders*, *6*(1), pp.27-31.

Györke, S., Stevens, S.C. and Terentyev, D., 2009. Cardiac calsequestrin: quest inside the SR. *The Journal of physiology*, *587*(13), pp.3091-3094.

Han, X., Tai, H., Wang, X., Wang, Z., Zhou, J., Wei, X., Ding, Y., Gong, H., Mo, C., Zhang, J. and Qin, J., 2016. AMPK activation protects cells from oxidative stress-induced senescence via autophagic flux restoration and intracellular NAD+ elevation. *Aging cell*, *15*(3), pp.416-427.

Handschin, C., Chin, S., Li, P., Liu, F., Maratos-Flier, E., LeBrasseur, N.K., Yan, Z. and Spiegelman, B.M., 2007. Skeletal muscle fiber-type switching, exercise intolerance, and myopathy in PGC-1α muscle-specific knock-out animals. *Journal of Biological Chemistry*, *282*(41), pp.30014-30021.

Hargreaves, I.P., Heales, S.J.R. and Land, J.M., 1999. Mitochondrial respiratory chain defects are not accompanied by an increase in the activities of lactate dehydrogenase or manganese superoxide dismutase in paediatric skeletal muscle biopsies. *Journal of inherited metabolic disease*, *22*(8), pp.925-931.

Hayashi, K., Miller, R.G. and Brownell, A.K.W., 1989. Central core disease: Ultrastructure of the sarcoplasmic reticulum and T-tubules. *Muscle & nerve*, *12*(2), pp.95-102.

Hayward, L.J., Kim, J.S., Lee, M.Y., Zhou, H., Kim, J.W., Misra, K., Salajegheh, M., Wu, F.F., Matsuda, C., Reid, V. and Cros, D., 2008. Targeted mutation of mouse skeletal muscle sodium channel produces myotonia and potassium-sensitive weakness. *The Journal of clinical investigation*, *118*(4), pp.1437-1449.

Herbison, G.J., Jaweed, M.M. and Ditunno, J.F., 1982. Muscle fiber types. *Archives of physical medicine and rehabilitation*, *63*(5), pp.227-230.

Hesketh, S., Srisawat, K., Sutherland, H., Jarvis, J. and Burniston, J., 2016. On the Rate of Synthesis of Individual Proteins within and between Different Striated Muscles of the Rat. *Proteomes*, *4*(1), p.12.

Hladky, S.B. and Haydon, D.A., 1972. Ion transfer across lipid membranes in the presence of gramicidin A: I. Studies of the unit conductance channel. *Biochimica et Biophysica Acta (BBA)-Biomembranes*, *274*(2), pp.294-312.

Hood, D., 2001. Plasticity in skeletal, cardiac, and smooth muscle: contractile activity-induced mitochondrial biogenesis in skeletal muscle. *J Appl Physiol*, 90(3), pp.1137 –*1157.*

Hopkins, P.M., 2006. Skeletal muscle physiology. *Continuing Education in Anaesthesia, Critical Care & Pain*, *6*(1), pp.1-6.

Horga, A., Rayan, D.L.R., Matthews, E., Sud, R., Fialho, D., Durran, S.C., Burge, J.A., Portaro, S., Davis, M.B., Haworth, A. and Hanna, M.G., 2013. Prevalence study of genetically defined skeletal muscle channelopathies in England. *Neurology*, *80*(16), pp.1472-1475.

Hoskins, B., Vroom, F.Q. and Jarrell, M.A., 1975. Hyperkalemic periodic paralysis: effects of potassium, exercise, glucose, and acetazolamide on blood chemistry. *Archives of neurology*, *32*(8), pp.519-523.

Huxley, A.F. and Niedergerke, R., 1954. Structural changes in muscle during contraction; interference microscopy of living muscle fibres. *Nature*, *173*(4412), p.971.

Huxley, H. and Hanson, J., 1954. Changes in the cross-striations of muscle during contraction and stretch and their structural interpretation. *Nature*, *173*(4412), p.973.

Hynes, T.R., Block, S.M., White, B.T. and Spudich, J.A., 1987. Movement of myosin fragments in vitro: domains involved in force production. *Cell*, *48*(6), pp.953-963.

Weber, Jurkat-Rott and Lehmann-Horn. Hyperkalemic Periodic Paralysis. *Gene Reviews [Internet].* Initial Posting: July 18, 2003; Last Update: January 28, 2016.

Iovino, S., Burkart, A.M., Warren, L., Patti, M.E. and Kahn, C.R., 2016. Myotubes derived from human-induced pluripotent stem cells mirror in vivo insulin resistance. *Proceedings of the National Academy of Sciences*, *113*(7), pp.1889-1894.

Jahnke, V.E., Sabido, O. and Freyssenet, D., 2009. Control of mitochondrial biogenesis, ROS level, and cytosolic Ca2+ concentration during the cell cycle and the onset of differentiation in L6E9 myoblasts. *American Journal of Physiology-Cell Physiology*, *296*(5), pp.C1185-C1194.

Johnson, M., Polgar, J., Weightman, D. and Appleton, D., 1973. Data on the distribution of fibre types in thirty-six human muscles: an autopsy study. *Journal of the neurological sciences*, *18*(1), pp.111-129.

Jornayvaz, F.R. and Shulman, G.I., 2010. Regulation of mitochondrial biogenesis. *Essays in biochemistry*, *47*, pp.69-84.

Joshi, M., Singh, N., Iqbal, M., Harijan, P., Saleem, R., Khan, A. and Hussain, N., 2015. P163–2479: Intra familial phenotypical variations in hypokalemic periodic paralysis. *European Journal of Paediatric Neurology*, *19*, pp.S139-S140.

Jurkat-Rott, K., Lehmann-Horn, F., Elbaz, A., Heine, R., Gregg, R.G., Hogan, K., Powers, P.A., Laple, P., Vale-Santos, J.E., Weissenbach, J. and Fontaine, B., 1994. A calcium channel mutation causing hypokalemic periodic paralysis. *Human Molecular Genetics*, *3*(8), pp.1415-1419.

Jurkat-Rott, K., Weber, M.A., Fauler, M., Guo, X.H., Holzherr, B.D., Paczulla, A., Nordsborg, N., Joechle, W. and Lehmann-Horn, F., 2009. K+-dependent paradoxical membrane depolarization and Na+ overload, major and reversible contributors to weakness by ion channel leaks. *Proceedings of the National Academy of Sciences*, *106*(10), pp.4036-4041.

Ke, Q., Luo, B., Qi, M., Du, Y. and Wu, W., 2013. Gender differences in penetrance and phenotype in hypokalemic periodic paralysis. *Muscle & nerve*, *47*(1), pp.41-45.

Khogali, S., Lucas, B., Ammar, T., Dejong, D., Barbalinardo, M., Hayward, L.J. and Renaud, J.M., 2015. Physiological basis for muscle stiffness and weakness in a knock-in M1592V mouse model of hyperkalemic periodic paralysis. *Physiological reports*, *3*(12), p.e12656.

Kim, I., Rodriguez-Enriquez, S. and Lemasters, J.J., 2007. Selective degradation of mitochondria by mitophagy. *Archives of biochemistry and biophysics*, *462*(2), pp.245-253.

Kimura, E., Han, J.J., Li, S., Fall, B., Ra, J., Haraguchi, M., Tapscott, S.J. and Chamberlain, J.S., 2008. Cell-lineage regulated myogenesis for dystrophin replacement: a novel therapeutic approach for treatment of muscular dystrophy. *Human molecular genetics*, *17*(16), pp.2507-2517.

Knudsen, K.A. and Horwitz, A.F., 1978. Differential inhibition of myoblast fusion. *Developmental biology*, *66*(2), pp.294-307.

Knudsen, K.A., McElwee, S.A. and Myers, L., 1990. A role for the neural cell adhesion molecule, NCAM, in myoblast interaction during myogenesis. *Developmental biology*, *138*(1), pp.159-168.

Kong, H., Jones, P.P., Koop, A., Zhang, L., Duff, H.J. and Chen, S.W., 2008. Caffeine induces Ca2+ release by reducing the threshold for luminal Ca2+ activation of the ryanodine receptor. *Biochemical Journal*, *414*(3), pp.441-452.

Kovács, M., Tóth, J., Hetényi, C., Málnási-Csizmadia, A. and Sellers, J.R., 2004. Mechanism of blebbistatin inhibition of myosin II. *Journal of Biological Chemistry*, *279*(34), pp.35557-35563.

Krieger, D.A., Tate, C.A., McMillin-Wood, J. and Booth, F.W., 1980. Populations of rat skeletal muscle mitochondria after exercise and immobilization. *Journal of Applied Physiology*, *48*(1), pp.23-28.

Krols, M., Van Isterdael, G., Asselbergh, B., Kremer, A., Lippens, S., Timmerman, V. and Janssens, S., 2016. Mitochondria-associated membranes as hubs for neurodegeneration. *Acta neuropathologica*, *131*(4), pp.505-523.

Kukat, C., Wurm, C.A., Spåhr, H., Falkenberg, M., Larsson, N.G. and Jakobs, S., 2011. Super-resolution microscopy reveals that mammalian mitochondrial nucleoids have a uniform size and frequently contain a single copy of mtDNA. *Proceedings of the National Academy of Sciences*, *108*(33), pp.13534-13539.

Layzer, R.B., 1990. 3 Muscle metabolism during fatigue and work. *Baillière's Clinical Endocrinology and Metabolism*, *4*(3), pp.441-459.

Lee, H.C. and Wei, Y.H., 2005. Mitochondrial biogenesis and mitochondrial DNA maintenance of mammalian cells under oxidative stress. *The international journal of biochemistry & cell biology*, *37*(4), pp.822-834.

Lee, H.C., Yin, P.H., Chi, C.W. and Wei, Y.H., 2002. Increase in mitochondrial mass in human fibroblasts under oxidative stress and during replicative cell senescence. *Journal of biomedical science*, *9*(6), pp.517-526.

Lehmann-Horn, F., Sipos, I., Jurkat-Rott, K., Heine, R., Brinkmeier, H., Fontaine, B., Kovacs, L. and Melzer, W., 1995. Altered calcium currents in human hypokalemic periodic paralysis myotubes expressing mutant L-type calcium channels. *Society of General Physiologists series*, *50*, pp.101-113.

Lin, J., Wu, H., Tarr, P.T., Zhang, C.Y., Wu, Z., Boss, O., Michael, L.F., Puigserver, P., Isotani, E., Olson, E.N. and Lowell, B.B., 2002. Transcriptional co-activator PGC-1α drives the formation of slow-twitch muscle fibres. *Nature*, *418*(6899), pp.797-801.

Lin, J., Puigserver, P., Donovan, J., Tarr, P., Spiegelman, B.M., 2002. Peroxisome proliferator-activated receptor gamma coactivator 1beta (PGC-1beta), a novel PGC-1-related transcription coactivator associated with host cell factor. *J Biol Chem.* 277(3), pp.1645-1648.

Links, T.P., Smit, A.J., Molenaar, W.M., Zwarts, M.J. and Oosterhuis, H.J., 1994. Familial hypokalemic periodic paralysis: clinical, diagnostic and therapeutic aspects. *Journal of the neurological sciences*, *122*(1), pp.33-43.

Links, T.P., Zwarts, M.J., Wilmink, J., Molenaar, W.M. and Oosterhuis, H.J., 1990. Permanent muscle weakness in familial hypokalaemic periodic paralysis. *Brain*, *113*(6), pp.1873-1889.

Lucas, B., Ammar, T., Khogali, S., DeJong, D., Barbalinardo, M., Nishi, C., Hayward, L.J. and Renaud, J.M., 2014. Contractile abnormalities of mouse muscles expressing hyperkalemic periodic paralysis mutant NaV1. 4 channels do not correlate with Na+ influx or channel content. *Physiological genomics*, *46*(11), pp.385-397.

MacLennan, D.H. and Wong, P.T.S., 1971. Isolation of a calcium-sequestering protein from sarcoplasmic reticulum. *Proceedings of the National Academy of Sciences*, *68*(6), pp.1231-1235.

Maffioletti, S.M., Gerli, M.F., Ragazzi, M., Dastidar, S., Benedetti, S., Loperfido, M., VandenDriessche, T., Chuah, M.K. and Tedesco, F.S., 2015. Efficient derivation and inducible differentiation of expandable skeletal myogenic cells from human ES and patient-specific iPS cells. *Nature protocols*, *10*(7), pp.941-958.

Maggi, L., Brugnoni, R., Colleoni, L., Kapetis, D., Ardissone, A., Pini, A., Ricci, G., Vercelli, L., Ravaglia, S., Moroni, I. and Pegoraro, E., 2014. GP 136: Muscle channelopathies: Clinical and genetic features in a large cohort of Italian patients. *Neuromuscular Disorders*, *24*(9), pp.841-842.

Mamchaoui, K., Trollet, C., Bigot, A., Negroni, E., Chaouch, S., Wolff, A., Kandalla, P.K., Marie, S., Di Santo, J., St Guily, J.L. and Muntoni, F., 2011. Immortalized pathological human myoblasts: towards a universal tool for the study of neuromuscular disorders. *Skeletal muscle*, *1*(1), p.34.

Manandhar, D., Song, L., Kabadi, A., Kwon, J.B., Edsall, L.E., Ehrlich, M., Tsumagari, K., Gersbach, C.A., Crawford, G.E. and Gordân, R., 2017. Incomplete MyoD-induced transdifferentiation is associated with chromatin remodeling deficiencies. *Nucleic Acids Research*, *45*(20), pp.11684-11699.

Maroto, M., Reshef, R., Münsterberg, A.E., Koester, S., Goulding, M. and Lassar, A.B., 1997. Ectopic Pax-3 activates MyoD and Myf-5 expression in embryonic mesoderm and neural tissue. *Cell*, *89*(1), pp.139-148.

Matthews, E., Labrum, R., Sweeney, M.G., Sud, R., Haworth, A., Chinnery, P.F., Meola, G., Schorge, S., Kullmann, D.M., Davis, M.B. and Hanna, M.G., 2009. Voltage sensor charge loss accounts for most cases of hypokalemic periodic paralysis. *Neurology*, *72*(18), pp.1544-1547.

Matthews, E., Portaro, S., Ke, Q., Sud, R., Haworth, A., Davis, M.B., Griggs, R.C. and Hanna, M.G., 2011. Acetazolamide efficacy in hypokalemic periodic paralysis and the predictive role of genotype. *Neurology*, *77*(22), pp.1960-1964.

McArdle, B., 1956. Familial periodic paralysis. *British medical bulletin*, *12*(3), pp.226-229.

McCarthy, T.V., Quane, K.A. and Lynch, P.J., 2000. Ryanodine receptor mutations in malignant hyperthermia and central core disease. *Human mutation*, *15*(5), p.410.

McMahon, D.K., Anderson, P.A., Nassar, R.A.S.H.I.D., Bunting, J.B., Saba, Z., Oakeley, A.E. and Malouf, N.N., 1994. C2C12 cells: biophysical, biochemical, and immunocytochemical properties. *American Journal of Physiology-Cell Physiology*, *266*(6), pp.C1795-C1802.

Merrell, A.J. and Kardon, G., 2013. Development of the diaphragm–a skeletal muscle essential for mammalian respiration. *The FEBS journal*, *280*(17), pp.4026-4035.

Mestas, J. and Hughes, C.C., 2004. Of mice and not men: differences between mouse and human immunology. *The Journal of Immunology*, *172*(5), pp.2731-2738.

Miglio, G., Rosa, A.C., Rattazzi, L., Collino, M., Lombardi, G. and Fantozzi, R., 2009. PPARγ stimulation promotes mitochondrial biogenesis and prevents glucose deprivation-induced neuronal cell loss. *Neurochemistry international*, *55*(7), pp.496-504.

Miller, E.W., Lin, J.Y., Frady, E.P., Steinbach, P.A., Kristan, W.B. and Tsien, R.Y., 2012. Optically monitoring voltage in neurons by photo-induced electron transfer through molecular wires. *Proceedings of the National Academy of Sciences*, *109*(6), pp.2114-2119.

Miller, T.M., Da Silva, M.D., Miller, H.A., Kwiecinski, H., Mendell, J.R., Tawil, R., McManis, P., Griggs, R.C., Angelini, C., Servidei, S. and Petajan, J., 2004. Correlating phenotype and genotype in the periodic paralyses. *Neurology*, *63*(9), pp.1647-1655.

Miranda, S., Foncea, R., Guerrero, J. and Leighton, F., 1999. Oxidative stress and upregulation of mitochondrial biogenesis genes in mitochondrial DNA-depleted HeLa cells. *Biochemical and biophysical research communications*, *258*(1), pp.44-49.

Moretti, I., Ciciliot, S., Dyar, K.A., Abraham, R., Murgia, M., Agatea, L., Akimoto, T., Bicciato, S., Forcato, M., Pierre, P. and Uhlenhaut, N.H., 2016. MRF4 negatively regulates adult skeletal muscle growth by repressing MEF2 activity. *Nature communications*, *7*.

Narici, M.V. and Maffulli, N., 2010. Sarcopenia: characteristics, mechanisms and functional significance. *British medical bulletin*, *95*(1), pp.139-159.

Naya, F.J., Mercer, B., Shelton, J., Richardson, J.A., Williams, R.S. and Olson, E.N., 2000. Stimulation of slow skeletal muscle fiber gene expression by calcineurin in vivo. *Journal of Biological Chemistry*, *275*(7), pp.4545-4548.

Neki, N.S., Singh, M. and Shah, D.M., 2013. Hyperkalemic Periodic Paralysis. *RGUHS Journal of Medical Sciences*, *3*(4), pp.251-254.

Nolan, P.M., Hugill, A. and Cox, R.D., 2002. ENU mutagenesis in the mouse: application to human genetic disease. *Briefings in functional genomics & proteomics*, *1*(3), pp.278-289.

Oh, M., Rybkin, I.I., Copeland, V., Czubryt, M.P., Shelton, J.M., van Rooij, E., Richardson, J.A., Hill, J.A., De Windt, L.J., Bassel-Duby, R. and Olson, E.N., 2005. Calcineurin is necessary for the maintenance but not embryonic development of slow muscle fibers. *Molecular and cellular biology*, *25*(15), pp.6629-6638.

Olguín, H.C. and Pisconti, A., 2012. Marking the tempo for myogenesis: Pax7 and the regulation of muscle stem cell fate decisions. *Journal of cellular and molecular medicine*, *16*(5), pp.1013-1025.

Olson, E.N., 1992. Interplay between proliferation and differentiation within the myogenic lineage. *Developmental biology*, *154*(2), pp.261-272.

Olson, EN., 1990. MyoD family: a paradigm for development? Genes & development, 4(9), pp.1454-1461.

Parsons, S.A., Millay, D.P., Wilkins, B.J., Bueno, O.F., Tsika, G.L., Neilson, J.R., Liberatore, C.M., Yutzey, K.E., Crabtree, G.R., Tsika, R.W. and Molkentin, J.D., 2004. Genetic loss of calcineurin blocks mechanical overload-induced skeletal muscle fiber type switching but not hypertrophy. *Journal of Biological Chemistry*, *279*(25), pp.26192-26200.

Porta, M., Zima, A.V., Nani, A., Diaz-Sylvester, P.L., Copello, J.A., Ramos-Franco, J., Blatter, L.A. and Fill, M., 2011. Single ryanodine receptor channel basis of caffeine's action on Ca 2+ sparks. *Biophysical journal*, *100*(4), pp.931-938.

Proenza, C., O'Brien, J., Nakai, J., Mukherjee, S., Allen, P.D. and Beam, K.G., 2002. Identification of a region of RyR1 that participates in allosteric coupling with the α1S (CaV1. 1) II–III loop. *Journal of Biological Chemistry*, *277*(8), pp.6530-6535.

Ptáček, L.J., George, A.L., Griggs, R.C., Tawil, R., Kallen, R.G., Barchi, R.L., Robertson, M. and Leppert, M.F., 1991. Identification of a mutation in the gene causing hyperkalemic periodic paralysis. *Cell*, *67*(5), pp.1021-1027.

Puigserver, P. and Spiegelman, B.M., 2003. Peroxisome proliferator-activated receptor-γ coactivator 1α (PGC-1α): transcriptional coactivator and metabolic regulator. *Endocrine reviews*, *24*(1), pp.78-90.

Rajan, S., Dang, H.C.P., Djambazian, H., Zuzan, H., Fedyshyn, Y., Ketela, T., Moffat, J., Hudson, T.J. and Sladek, R., 2011. Analysis of early C2C12 myogenesis identifies stably and differentially expressed transcriptional regulators whose knock-down inhibits myoblast differentiation. *Physiological genomics*.

Rawls, A., Valdez, M.R., Zhang, W., Richardson, J., Klein, W.H. and Olson, E.N., 1998. Overlapping functions of the myogenic bHLH genes MRF4 and MyoD revealed in double mutant mice. *Development*, *125*(13), pp.2349-2358.

Rizzuto, R., Pinton, P., Brini, M., Chiesa, A., Filippin, L. and Pozzan, T., 1999. Mitochondria as biosensors of calcium microdomains. *Cell calcium*, *26*(5), pp.193-200.

Rojas, C.V., Neely, A., Velasco-Loyden, G., Palma, V. and Kukuljan, M., 1999. Hyperkalemic periodic paralysis M1592V mutation modifies activation in human skeletal muscle Na+ channel. *American Journal of Physiology-Cell Physiology*, *276*(1), pp.C259-C266.

Rojas, C.V., Wang, J. and Schwartz, L.S., Hoffman, E.P., Powell, B.R., & Brown, R.H., 1991. A Met-to-Val mutation in the skeletal muscle Na+ channel-subunit in hyperkalaemic periodic paralysis. *Nature*, *354*, pp.387-389.

Royer, L. and Ríos, E., 2009. Deconstructing calsequestrin. Complex buffering in the calcium store of skeletal muscle. *The Journal of physiology*, *587*(13), pp.3101-3111.

Rudnicki, M.A., Braun, T., Hinuma, S. and Jaenisch, R., 1992. Inactivation of MyoD in mice leads to up-regulation of the myogenic HLH gene Myf-5 and results in apparently normal muscle development. *Cell*, *71*(3), pp.383-390.

Rudnicki, M.A., Schnegelsberg, P.N., Stead, R.H., Braun, T., Arnold, H.H. and Jaenisch, R., 1993. MyoD or Myf-5 is required for the formation of skeletal muscle. *Cell*, *75*(7), pp.1351-1359.

Rudolph, J.A., Spier, S.J., Byrns, G. and Hoffman, E.P., 1992. Linkage of hyperkalaemic periodic paralysis in quarter horses to the horse adult skeletal muscle sodium channel gene. *Animal genetics*, *23*(3), pp.241-250.

Russell, J. M., 2000. Sodium-Potassium-Chloride Cotransport. *Physiological Reviews*, 80(1), pp.211-276

Sandow, A., 1952. Excitation-contraction coupling in muscular response. *The Yale journal of biology and medicine*, *25*(3), p.176-201.

Sansone, V., Meola, G., Links, T., Panzeri, M. and Rose, M.R., 2008. Treatment for periodic paralysis. *The Cochrane Library*.

Satoh, T., Enokido, Y., Aoshima, H., Uchiyama, Y. and Hatanaka, H., 1997. Changes in mitochondrial membrane potential during oxidative stress-induced apoptosis in PC12 cells. *Journal of neuroscience research*, *50*(3), pp.413-420.

Scarpulla, Richard C. "Nuclear activators and coactivators in mammalian mitochondrial biogenesis." *Biochimica et Biophysica Acta (BBA)-Gene Structure and Expression* 1576.1 (2002): 1-14.

Schiaffino, S. and Reggiani, C., 2011. Fiber types in mammalian skeletal muscles. *Physiological reviews*, *91*(4), pp.1447-1531.

Schott, G.D. and McArdle, B., 1974. Barium-induced skeletal muscle paralysis in the rat, and its relationship to human familial periodic paralysis. *Journal of Neurology, Neurosurgery & Psychiatry*, *37*(1), pp.32-39.

Sciancalepore, M., Afzalov, R., Buzzin, V., Jurdana, M., Lorenzon, P. and Ruzzier, F., 2005. Intrinsic ionic conductances mediate the spontaneous electrical activity of cultured mouse myotubes. *Biochimica et Biophysica Acta (BBA)-Biomembranes*, *1720*(1), pp.117-124.

Selak, M.A., de Chadarevian, J.P., Melvin, J.J., Grover, W.D., Salganicoff, L. and Kaye, E.M., 2000. Mitochondrial activity in Pompe's disease. *Pediatric neurology*, *23*(1), pp.54-57.

Serena, E., Zatti, S., Zoso, A., Lo Verso, F., Tedesco, F.S., Cossu, G. and Elvassore, N., 2016. Skeletal Muscle Differentiation on a Chip Shows Human Donor Mesoangioblasts' Efficiency in Restoring Dystrophin in a Duchenne Muscular Dystrophy Model. *Stem cells translational medicine*, *5*(12), pp.1676-1683.

Shefer, G. and Yablonka-Reuveni, Z., 2005. Isolation and culture of skeletal muscle myofibers as a means to analyze satellite cells. *Basic Cell Culture Protocols*, pp.281-304.

Shieh, R.C., Chang, J.C. and Arreola, J., 1998. Interaction of Ba 2+ with the pores of the cloned inward rectifier K+ channels Kir2. 1 expressed in Xenopus oocytes. *Biophysical journal*, *75*(5), pp.2313-2322.

Shields IV, C.W., Reyes, C.D. and López, G.P., 2015. Microfluidic cell sorting: a review of the advances in the separation of cells from debulking to rare cell isolation. *Lab on a Chip*, *15*(5), pp.1230-1249.

Short, K.R., Bigelow, M.L., Kahl, J., Singh, R., Coenen-Schimke, J., Raghavakaimal, S. and Nair, K.S., 2005. Decline in skeletal muscle mitochondrial function with aging in humans. *Proceedings of the National Academy of Sciences of the United States of America*, *102*(15), pp.5618-5623.

Skoglund, G., Lainé, J., Darabi, R., Fournier, E., Perlingeiro, R. and Tabti, N., 2014. Physiological and ultrastructural features of human induced pluripotent and embryonic stem cell-derived skeletal myocytes in vitro. *Proceedings of the National Academy of Sciences*, *111*(22), pp.8275-8280.

Smith, B.K., Mukai, K., Lally, J.S., Maher, A.C., Gurd, B.J., Heigenhauser, G.J., Spriet, L.L. and Holloway, G.P., 2013. AMP-activated protein kinase is required for exercise-induced peroxisome proliferator-activated receptor γ co-activator 1α translocation to subsarcolemmal mitochondria in skeletal muscle. *The Journal of physiology*, *591*(6), pp.1551-1561.

Spier, S.J., Carlson, G.P., Holliday, T.A., Cardinet 3rd, G.H. and Pickar, J.G., 1990. Hyperkalemic periodic paralysis in horses. *Journal of the American Veterinary Medical Association*, *197*(8), pp.1009-1017.

Spudich, J.A., 2001. The myosin swinging cross-bridge model. *Nature Reviews Molecular Cell Biology*, *2*(5), pp.387-392.

Standen, N.B. and Stanfield, P.R., 1978. A potential-and time-dependent blockade of inward rectification in frog skeletal muscle fibres by barium and strontium ions. *The Journal of Physiology*, *280*(1), pp.169-191.

Steiss, J.E. and Naylor, J.M., 1986. Episodic muscle tremors in a quarter horse: resemblance to hyperkalemic periodic paralysis. *The Canadian Veterinary Journal*, *27*(9), p.332.

Sternberg, D., Maisonobe, T., Jurkat-Rott, K., Nicole, S., Launay, E., Chauveau, D., Tabti, N., Lehmann-Horn, F., Hainque, B. and Fontaine, B., 2001. Hypokalaemic periodic paralysis type 2 caused by mutations at codon 672 in the muscle sodium channel gene SCN4A. *Brain*, *124*(6), pp.1091-1099.

Struyk, A.F. and Cannon, S.C., 2007. A Na+ channel mutation linked to hypokalemic periodic paralysis exposes a proton-selective gating pore. *The Journal of general physiology*, *130*(1), pp.11-20.

Struyk, A.F. and Cannon, S.C., 2008. Paradoxical depolarization of BA2+-treated muscle exposed to low extracellular K+: Insights into resting potential abnormalities in hypokalemic paralysis. *Muscle & nerve*, *37*(3), pp.326-337.

Struyk, A.F., Scoggan, K.A., Bulman, D.E. and Cannon, S.C., 2000. The human skeletal muscle Na channel mutation R669H associated with hypokalemic periodic paralysis enhances slow inactivation. *Journal of Neuroscience*, *20*(23), pp.8610-8617.

Suzuki, A., Scruggs, A. and Iwata, J., 2015. The temporal specific role of WNT/β-catenin signaling during myogenesis. *Journal of nature and science*, *1*(8), p.e143.

Świerczek, B., Ciemerych, M.A. and Archacka, K., 2015. From pluripotency to myogenesis: a multistep process in the dish. *Journal of muscle research and cell motility*, *36*(6), pp.363-375.

Tajbakhsh, S., Rocancourt, D., Cossu, G. and Buckingham, M., 1997. Redefining the genetic hierarchies controlling skeletal myogenesis: Pax-3 and Myf-5 act upstream of MyoD. *Cell*, *89*(1), pp.127-138.

Talbott, J.H., 1941. Periodic paralysis. *Medicine*, *20*(1), pp.85-143.

Tanaka, K., Sato, K., Yoshida, T., Fukuda, T., Hanamura, K., Kojima, N., Shirao, T., Yanagawa, T. and Watanabe, H., 2011. Evidence for cell density affecting C2C12 myogenesis: possible regulation of myogenesis by cell–cell communication. *Muscle & nerve*, *44*(6), pp.968-977.

Tawil, R., McDermott, M.P., Brown, R., Shapiro, B.C., Ptacek, L.J., McManis, P.G., Dalakas, M.C., Spector, S.A., Mendell, J.R., Hahn, A.F. and Griggs, R.C., 2000. Randomized trials of dichlorphenamide in the periodic paralyses. *Annals of neurology*, *47*(1), pp.46-53.

Tedesco, F.S., Dellavalle, A., Diaz-Manera, J., Messina, G. and Cossu, G., 2010. Repairing skeletal muscle: regenerative potential of skeletal muscle stem cells. *The Journal of clinical investigation*, *120*(1), p.11.

Tedesco, F.S., Gerli, M.F., Perani, L., Benedetti, S., Ungaro, F., Cassano, M., Antonini, S., Tagliafico, E., Artusi, V., Longa, E. and Tonlorenzi, R., 2012. Transplantation of genetically corrected human iPSC-derived progenitors in mice with limb-girdle muscular dystrophy. *Science translational medicine*, *4*(140), pp.140ra89-140ra89.

Tombola, F., Pathak, M.M. and Isacoff, E.Y., 2005. Voltage-sensing arginines in a potassium channel permeate and occlude cation-selective pores. *Neuron*, *45*(3), pp.379-388.

Torres, C.F., Griggs, R.C., Moxley, R.T. and Bender, A.N., 1981. Hypokalemic periodic paralysis exacerbated by acetazolamide. *Neurology*, *31*(11), pp.1423-1423.

Tricarico, D., Mele, A. and Camerino, D.C., 2006. Carbonic anhydrase inhibitors ameliorate the symptoms of hypokalaemic periodic paralysis in rats by opening the muscular Ca 2+-activated-K+ channels. *Neuromuscular Disorders*, *16*(1), pp.39-45.

Venable, P.W., Taylor, T.G., Sciuto, K.J., Zhao, J., Shibayama, J., Warren, M., Spitzer, K.W. and Zaitsev, A.V., 2013. Detection of mitochondrial depolarization/recovery during ischaemia–reperfusion using spectral properties of confocally recorded TMRM fluorescence. *The Journal of physiology*, *591*(11), pp.2781-2794.

Venance, S.L., Cannon, S.C., Fialho, D., Fontaine, B., Hanna, M.G., Ptacek, L.J., Tristani-Firouzi, M., Tawil, R. and Griggs, R.C., 2005. The primary periodic paralyses: diagnosis, pathogenesis and treatment. *Brain*, *129*(1), pp.8-17.

Viires, N., Murciano, D., Seta, J.P., Dureuil, B.E.R.T.R.A.N.D., Pariente, R. and Aubier, M., 1988. Effects of Ca2+ withdrawal on diaphragmatic fiber tension generation. *Journal of Applied Physiology*, *64*(1), pp.26-30.

Virbasius, J.V. and Scarpulla, R.C., 1994. Activation of the human mitochondrial transcription factor A gene by nuclear respiratory factors: a potential regulatory link between nuclear and mitochondrial gene expression in organelle biogenesis. *Proceedings of the National Academy of Sciences*, *91*(4), pp.1309-1313.

Vroom, F.Q., Jarrell, M.A. and Maren, T.H., 1975. Acetazolamide treatment of hypokalemic periodic paralysis: probable mechanism of action. *Archives of neurology*, *32*(6), pp.385-392.

Wang, Y. and Pessin, J.E., 2013. Mechanisms for fiber-type specificity of skeletal muscle atrophy. *Current opinion in clinical nutrition and metabolic care*, *16*(3), p.243.

Webb, J., Wu, F.F. and Cannon, S.C., 2009. Slow inactivation of the NaV1. 4 sodium channel in mammalian cells is impeded by co-expression of the β1 subunit. *Pflügers Archiv-European Journal of Physiology*, *457*(6), p.1253.

Wei-LaPierre, L., Carrell, E.M., Boncompagni, S., Protasi, F. and Dirksen, R.T., 2013. Orai1-dependent calcium entry promotes skeletal muscle growth and limits fatigue. *Nature communications*, *4*, pp2805

Wu, F., Mi, W. and Cannon, S.C., 2013. Beneficial effects of bumetanide in a CaV1. 1-R528H mouse model of hypokalaemic periodic paralysis. *Brain*, *136*(12), pp.3766-3774.

Wu, F., Mi, W. and Cannon, S.C., 2013. Bumetanide prevents transient decreases in muscle force in murine hypokalemic periodic paralysis. *Neurology*, *80*(12), pp.1110-1116.

Wu, F., Mi, W., Burns, D.K., Fu, Y., Gray, H.F., Struyk, A.F. and Cannon, S.C., 2011. A sodium channel knockin mutant (NaV1. 4-R669H) mouse model of hypokalemic periodic paralysis. *The Journal of clinical investigation*, *121*(10), p.4082.

Wu, F., Mi, W., Hernández-Ochoa, E.O., Burns, D.K., Fu, Y., Gray, H.F., Struyk, A.F., Schneider, M.F. and Cannon, S.C., 2012. A calcium channel mutant mouse model of hypokalemic periodic paralysis. *The Journal of clinical investigation*, *122*(12), pp.4580-4591.

Wu, Z., Puigserver, P., Andersson, U., Zhang, C., Adelmant, G., Mootha, V., Troy, A., Cinti, S., Lowell, B., Scarpulla, R.C. and Spiegelman, B.M., 1999. Mechanisms controlling mitochondrial biogenesis and respiration through the thermogenic coactivator PGC-1. *Cell*, *98*(1), pp.115-124.

Yoshinaga, H., Sakoda, S., Shibata, T., Akiyama, T., Oka, M., Yuan, J.H., Takashima, H., Takahashi, M.P., Kitamura, T., Murakami, N. and Kobayashi, K., 2015. Phenotypic variability in childhood of skeletal muscle sodium channelopathies. *Pediatric neurology*, *52*(5), pp.504-508.

Zatti, S., Zoso, A., Serena, E., Luni, C., Cimetta, E. and Elvassore, N., 2012. Micropatterning topology on soft substrates affects myoblast proliferation and differentiation. *Langmuir*, *28*(5), pp.2718-2726.

Zavecz, J.H. and Anderson, W.M., 1992. Role of extracellular Ca2+ in diaphragmatic contraction: effects of ouabain, monensin, and ryanodine. *Journal of Applied Physiology*, *73*(1), pp.30-35.

Zheng, J., Liang, Z., Hou, Y., Liu, F., Hu, Y., Lin, P. and Yan, C., 2016. A novel Kir2. 6 mutation associated with hypokalemic periodic paralysis. *Clinical Neurophysiology*, *127*(6), pp.2503-2508.